Maria Pia Ciocci Structural Analysis of the Timber Structure of Ica Cathedral, Peru

Portugal | 2015

ADVANCED MASTERS IN STRUCTURAL ANALYSIS
OF MONUMENTS AND HISTORICAL CONSTRUCTIONS

Master's Thesis

Maria Pia Ciocci

Structural Analysis of the Timber Structure of Ica Cathedral, Peru

University of Minho

UNIVERSITAT POLITÈCNICA DE CATALUNYA

Education and Culture

Erasmus Mundus

ADVANCED MASTERS IN STRUCTURAL ANALYSIS
OF MONUMENTS AND HISTORICAL CONSTRUCTIONS

Master's Thesis

Maria Pia Ciocci

Structural Analysis of the Timber Structure of Ica Cathedral, Peru

This Masters Course has been funded with support from the European Commission. This publication reflects the views only of the author, and the Commission cannot be held responsible for any use which may be made of the information contained therein.

Portugal | 2015

DECLARATION

Name: Maria Pia Ciocci

Email: mariapiaciocci@gmail.com

Title of the Msc Dissertation: Structural Analysis of the Timber Structure of Ica Cathedral, Peru

Supervisor(s): Paulo B. Lourenço, Elisa Poletti

Year: 2015

I hereby declare that all information in this document has been obtained and presented in accordance with academic rules and ethical conduct. I also declare that, as required by these rules and conduct, I have fully cited and referenced all material and results that are not original to this work.

I hereby declare that the MSc Consortium responsible for the Advanced Masters in Structural Analysis of Monuments and Historical Constructions is allowed to store and make available electronically the present MSc Dissertation.

University: University of Minho

Date: 07 / 09 / 2015

Signature:

_____

This page is left blank on purpose.

Acknowledgements

I would like to express my great appreciation to my supervisors.
My sincere gratitude to Prof. Paulo Lourenço for this exceptional challenge. His inspiring guidance and enthusiasm to discuss every single idea were essential in each step of this work.
I would like to acknowledge Elisa for her continuous help and patience.

I would like to profusely thank the European Commission for the financial support without which this fulfilling experience would not have been possible.

I am very grateful to everyone who ran this great SAHC marathon with me.
A special thanks to *who* discussed FEM while I was brushing my teeth, to *who* helped me day by day and to *who* made me feel at home.

Thanks to the special friend *who* has shared this entire journey with me, for all the discussions and for all the smiles shared.

A special thanks to *who* has encouraged me since the first day of this experience.

As usual, my deepest gratitude to my family and my friends who always supports me without any hesitation.

To my dad, who showed me the way.

This page is left blank on purpose.

Abstract

The Cathedral of Ica, built in 1759 and damaged by the 2007 Pisco earthquake, is one of the most representative of the churches built in coastal cities of Peru. Declared as national monument in 1982, Ica Cathedral is part of the Seismic Retrofitting Project of the Getty Conservation Institute.

Two structural systems are present in Ica Cathedral. At the exterior, a massive and stable load–bearing masonry envelope surrounds the cathedral consisting of the fired brick front façade with two bell towers and thick mud brick lateral walls. On the other hand, the internal space of Ica Cathedral is divided by a series of pillars that support a complex vaulted roof framing system constructed with the quincha technique. In particular, the latter is the main object of this thesis.

The important influence of timber connections on the global behaviour of timber structures is investigated by modelling a timber frame wall, analytically and numerically. The architecture, the structural systems and recent damage of Ica Cathedral are presented in details with the construction of 3D–architectural models in AutoCAD. Performing linear elastic analyses on the model of the representative bay in SAP 2000 software, the compliance with the criteria specified by Eurocode is evaluated. Finally, the elastic behaviour of the complete timber structure is investigated by constructing a model in MIDAS FX+ for DIANA software.

The results obtained from this thesis represent a starting point for the further research on the numerical model of the combined timber and masonry structures of Ica Cathedral.

This page is left blank on purpose.

Resumo

A Catedral de Ica, construída em 1759 e danificada pelo terremoto de Pisco em 2007, é uma das mais representativas igrejas construídas nas cidades costeiras do Peru. Declarada como monumento nacional em 1982, a Catedral de Ica é parte do projeto Seismic Retrofitting Project do Getty Conservation Institute.

Dois sistemas estruturais estão presentes na Catedral de Ica. No exterior, uma massiva e estável alvenaria estrutural envolve a catedral, consistindo numa fachada frontal em tijolo com duas torres e as paredes laterais de elevada espessura compostas por alvenaria de adobe. Por outro lado, o espaço interno da catedral é dividido por uma série de pilares que suportam a estrutura da cobertura que é composta por um complexo sistema abobadado construído com a técnica de quincha. Em particular, este último é o principal objeto desta tese.

A importante influência das ligações de madeira no comportamento global das estruturas de madeira é investigada através da modelação de uma parede de estrutura de madeira, analiticamente e numericamente. A arquitetura, os sistemas estruturais e os danos recentes observados na catedral são apresentados em detalhe com modelos arquitetónicos 3D executados em AutoCAD. Foram realizadas análises elásticas lineares de um modelo representativo da estrutura através do software SAP 2000, avaliando a conformidade com os critérios especificados pelo Eurocode. Finalmente, o comportamento elástico de toda a estrutura de madeira é investigado através da construção de um modelo em MIDAS +FX para o software Diana.

Os resultados obtidos com esta tese representam um ponto de partida de um modelo combinado de madeira e alvenaria para a Catedral de Ica.

This page is left blank on purpose.

Contents

List of Figures

List of Tables

Chapter 1

Introduction

Efficient restoration and conservation studies of architectural heritage cannot be carried out without a proper evaluation of the structural behaviour. The aim of this thesis is to investigate the complex and unique timber structure of Ica Cathedral in Peru.

In the interior, Ica Cathedral is divided by a series of pillars, pilasters and piers that support a complex roof framing system. These structural parts are essentially hollow structures constructed by applying the *quincha* technique. The technique of *quincha*, or *bahareque*, construction is common in Central America and the South American countries. Although in each country the process varies because of the types of local materials available, the fundamentals of the method are the same (Carbajal, et al., 2005): connected timber elements are covered with cane or small branches forming a single or double–stuffed mesh. The mesh is made of mud, earth, plaster (mixture of lime and water), or a combination of such materials. Timber elements made of different wood species (cedar, sapele and huarango) and connected by various timber connections (mainly, mortise and tenon and half–lap joints) are used to construct the hollow structures that are present in Ica Cathedral. C*aña chancada* (wrap with flattened cane reeds) and *caña brava (*cane reeds) are the particular covering layers used for these elements (Cancino, et al., 2012). This timber structure of Ica Cathedral represents an extraordinary example of the application of *quincha* technique. It should be mentioned

that while many examples of timber frame walls constructed with *quincha* technique exist, its application to the curved roof framing system represents an exception that must be preserved.

The main objective of this work is to assess the structural performance of the timber structure with a proper investigation of the architecture and the structural systems that are present in Ica Cathedral. The structural behaviour of the timber structure is studied considering different load configurations and assumptions for the modelling of the timber joints. The compliance of the criteria specified by the modern building standards, such as *Eurocode*, represents another task for a general evaluation of the performance of structures constructed with *quincha* technique. In particular, the nonlinear behaviour of the timber joints would be studied by applying the approach obtained from the preliminary study on the model of a timber frame wall. Parametric analyses are carried out to investigate the influence of the timber connections and to select the most critical joints to introduce the nonlinearity in the model. Finally, the numerical model of the complete timber structure is constructed in order to study the global structural response and to provide the starting point for the research on the numerical model of the combined timber and masonry structures of Ica Cathedral.

In order to fulfil the objective of this thesis, the work is organized into the following six chapters:

- **Chapter 1** introduces the motivation, the objectives and the organization of this thesis;
- **Chapter 2** presents the analytical and numerical models of the timber frame wall in order to simulate the experimental tests and investigate the modelling approaches for timber connections;
- **Chapter 3** provides upgraded information concerning the architecture, the structural systems and the recent damage present in Ica Cathedral with the help of 3D–architectural models of the representative bay and of the transept;
- **Chapter 4** presents the results obtained from the linear analysis on a representative bay performed in SAP 2000 software and the compliance with the criteria specified by Eurocode is carried out;
- **Chapter 5** presents the results obtained from the linear analysis on the complete timber structure performed in DIANA software;
- **Chapter 6** presents conclusions from this thesis and few recommendations for further work.

Chapter 2

Modelling of a timber frame wall

2.1 Traditional carpentry joints

The complexity of timber structures depends mainly on the connections, which are often characteristic of a region, a period of time and even the carpenters' know-how. The conception and execution of joints have always been the most complex task to be carried out on timber structures.

Traditional practice and empirical experience were the rules of thumb used to construct traditional carpentry connections in the past. Nowadays joints are usually verified and designed with simplified methods that assume either hinges or full moment transmitting connections, while the real semi–rigid behaviour of the structure is somewhere in–between (Palma & Cruz, 2007). The incorrect evaluation of strength and stiffness can lead to: (1) non-compliance of the connections with the safety factors imposed by codes; and (2) dangerous fragile behaviour in seismic conditions (Parisi & Piazza, 2008).

The structural assessment and morpho–chronology of traditional timber connections represent a great challenge for several reasons, as summarized by Descamps (2009):

- a huge variability of typologies due to their widespread use all over the world, as given by the overview in terms of geometry, efficiency and technology provided by Ercüment (2002);

- the use of a natural material, which leads to decay and a great variability in the same frame;
- the structural complexity of the global geometry and of the connections;
- the lack of technical data regarding cross sections, strength classes or joints (contact areas, nodes, cracks);

The carpentry joints of traditional timber construction usually work by contact pressure and friction depending on the cutting shape. When metal connectors are present, they are only used to safeguard the connection against the separation of parts during exceptional actions. For these reasons, the mechanical characteristics of traditional connections are difficult to understand, such as cyclic and post-elastic behaviour in seismic conditions (Parisi & Piazza, 2008).

In literature, engineering methods, which are typically used for the examination and repair of historic timber structures, were presented by Feio (2005). The structural behaviour and the realistic simulation of historical timber structures were discussed by Holzer & Köck (2009), while different authors studied more in detail selected configurations. As a first example, mortise and tenon joints were examined by Bulleit et al. (1999) and design considerations were presented by Schmidt & Daniels (1999). Pegged mortise and tenon joints were investigated by Miller & Schmidt (2004). Experimental and numerical investigations into the rounded dovetail connection and the skew joint can be found in Rautenstrauch et al. (2010) and Tannert et al. (2011). The load–displacement behaviour of halved joints in historical timber structures was examined by Kock & Holzer (2010). Experimental and numerical modelling were carried out for tapered tenon joints to back up the basic understanding of failure modes and strength by Koch et al. (2013). Some research on birdsmouth connections was carried out by Tomasi et al. (2007) and connections in timber roof trusses were investigated by Branco (2008) and Palma et al. (2012).

Different modern–type connections are also available and several research projects are devoted to developing and improving them, so that they comply with seismic principles and regulations. In this case, timber elements are kept within the elastic range and the seismic response highly relies on the post–elastic dissipation capabilities of the connections – if they are suitably designed (Parisi & Piazza, 2008). The situation in historical timber structures is significantly different: more research is needed for sufficient experimental and analytical evidence so that reliable models can be performed and useful recommendations can be provided for upgrading or strengthening interventions.

2.2 Experimental studies

An extensive experimental campaign on real scale specimens was carried out at the University of Minho in order to study the seismic performance of traditional half–timbered walls (Poletti, 2013). Based on the results obtained in this investigation for the timber frame wall without infill, numerical and analytical studies will be carried out in **Section 3.2** and **Section 0**.

2.2.1 Geometry

A real scale specimen of a timber frame wall was constructed taking into account the common dimensions of existing buildings. The timber frame wall – that has a total width of 2.42 m and a total height of 2.36 m – was composed by four braced cells with the dimensions of 840 x 860 mm^2. The top and the bottom beams of the main frame had a cross section of 160 x 120 $mm^{2,}$ while all the other elements were of 80 x 120 mm^2. The geometry of the test specimen is shown in **Figure 1.**

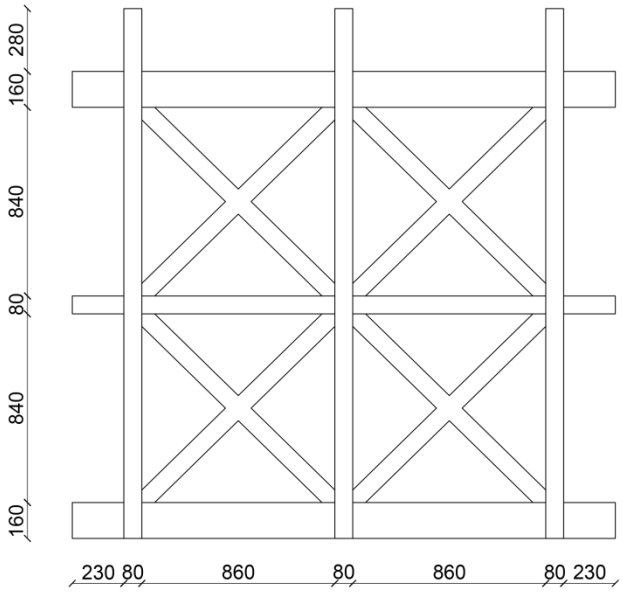

Figure 1. Geometry of the timber frame wall specimen.

The timber joints of the wall can be divided as follows:

- **Half–lap tee halving connection** between the post and the beam of the main frame;
- **Half–lap halving connection** between the diagonal elements;
- **Connection by contact** between the diagonal elements and the main frame.

In all the connections, a modern nail with a square cross section is inserted. For all the half–lap connections, the nail has a side of 4 mm and a length of 10 cm. For the connection by contact, the nail has a side of 6 mm and a length of 15 cm.

It has to be mentioned that several clearances were present in the connections influencing the shear behaviour of the wall, such as a gap of about 2 mm in the half–lap joints.

2.2.2 Material properties

The timber used in the tests was Maritime Pine (*Pinus pinaster*). The material properties that were not derived from experimental tests were obtained using the probabilistic model code (Poletti, 2013). The material properties used for timber are shown in **Table 1**.

Table 1. Timber material properties (Poletti, 2013).

$f_{t,0}$	15	MPa	G_v	700	MPa	γ	9	-
$f_{t,90}$	5	MPa	ν	0.3		$G_{ft,0}$	70	Nmm/mm^2
E_0	11000	MPa	ρ	590	kg/m^3	$G_{ft,90}$	50	Nmm/mm^2
E_{90}	5000	MPa	α_τ	1	-	$G_{fc,0}$	130	Nmm/mm^2
$f_{c,0}$	25	MPa	α_h	1	-	$G_{fc,90}$	70	Nmm/mm^2
$f_{c,90}$	3	MPa	β	-1	-	κ_p	0.001	-

It should be mentioned that the timber used was already dry and drying fissures were present in the timber elements, influencing the onset of cracking propagation and failure in the wall during testing.

2.2.3 Test setup

The specimen was arranged on top of a steel profile that was connected to the three posts and the reaction floor. The top beam of the wall was confined by two steel plates connected through sufficiently stiff steel rods in such a way that cyclic displacements could be imposed to the top of the wall. A guide created by means of punctual steel rollers was provided in the top timber beam in order to avoid out–of–plane displacements. The bottom timber beam was connected to the steel profile in 6 points and was confined laterally in order to prevent any kind of movement of this element.

The application of the vertical load was done by means of vertical hydraulic actuators applied directly on the three posts of the wall. The horizontal displacement was applied to the top timber beam through a hydraulic servo–actuator. Further details on their set-up can be found in (Poletti, 2013).

The displacements were controlled by 16 linear voltage displacements transducers (LVDTs) placed in order to capture the global and local behaviour of the wall – particularly, the local opening of the connections.

The experimental campaign on the seismic behaviour of the timber frame wall was composed by:

- **Preliminary monotonic tests** in order to validate the prevention of the out–of–plane movement of the wall and to calculate the displacement capacity of the wall;
- **Quasi–static in–plane cyclic tests** divided into the following steps:
  - **Pre–application of vertical load** with two different levels of 25 kN and 50 kN on top of each post of the wall;
  - **Cyclic application of a horizontal displacement history** on the top timber beam.

Both the preliminary monotonic tests and the cyclic tests were carried out by adopting the procedure according to ISO 21581 (2010). In particular, an ultimate displacement of around 101 mm was obtained in the monotonic test considering a pre–compression load of 25 kN. This value will be used in order to perform the numerical analyses in **Section 0.**

2.2.4 Test results

The timber frame – tested as a cantilever – showed a shear resisting mechanism as presented by the force–displacement hysteresis diagrams, see **Figure 2**. Besides, the flat trend of the hysteretic curves – that was not only at the origin where the load was inverted – is associated with a severe pinching effect for the timber frame wall. The evolution of the vertical displacements pointed out that there was an uplift of the posts which conditioned the shape of the hysteretic loops – 13.8 mm and 17.5 mm for the lower and higher values of the load. However, the unloading branch of the various loops was quite regular.

In general, the experimental tests showed that when a higher pre–compression vertical load was applied, the load capacity and the stiffness were higher: an increase in the lateral resistance of 105% with a loss of ultimate displacement of only 3% was noticeable. In particular, in the wall with the lower pre–compression vertical load the failure occurred at an applied displacement of 30.4 mm, while for the higher pre–compression vertical load failure occurred at an applied displacement of 70.8 mm.

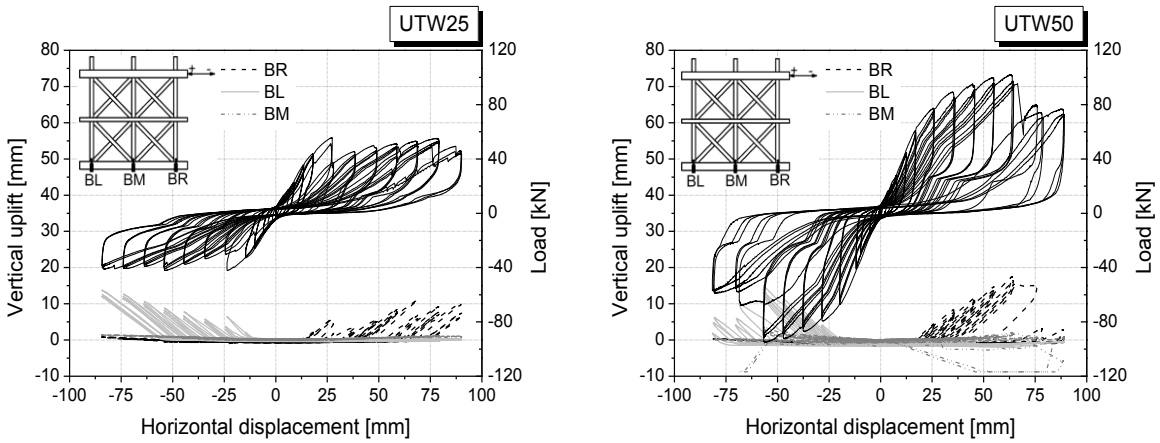

Figure 2. Timber frame wall with lower (left) and higher (right) vertical load levels (Poletti, 2013).

Regarding the main deformation features and failure modes of the timber frame walls, a significant deformation capacity was observed until failure. As the diagonal elements were able to move independently from the posts, they induced great damage and a high shear concentration on the central connection. Complete failure occurred in this connection in both cases. The cracking of the central connection promoted the elongation of the diagonals. This meant that they were detaching in one direction, while they were cutting the connections in the other one. In other words, when tensile forces were applied along the diagonals, the posts separated from them – in particular, this was more evident near the failure. After failure, the diagonals started opening with a higher rate and all the connections moved freely.

It is worth noting that stress redistribution between all the connections was noticeable when the failure of the central connection occurred under the pre–compression vertical load of 25 kN. This allowed the timber frame wall to regain strength even though the stiffness decreased and this was possible because of the low value of the displacement. In fact, the timber frame wall was not able to show the same behaviour when the applied displacement was of 70.8 mm.

The damage pattern of the timber frame wall was characterized by the significant bending experienced by the posts and the trend of pulling-out of the nails from the connections, see **Figure 3**. Regarding the half–lap connections, as previously mentioned, the damage was concentrated in the central connection that crushed due to the lateral compression applied by the diagonals. The redistribution of stresses that was observed after the failure of the central connection in the case of the lower pre–compression vertical load level led to the failure of the right connection after that of

the central one. In general, the damage was more severe when the timber frame wall was subjected to the higher pre–compression vertical load level.

Finally, it is important to underline that the results obtained for the timber frame walls were significantly different from those obtained for half–timbered walls – that were considered in the same experimental campaign. The presence of the infill changed the response to cyclic actions showing a prevalent rocking behaviour with a higher value of uplift, an increase in terms of capacity load and stiffness, a less evident pinching effect and a more progressive damage and opening of the connections.

Figure 3. Typical damage of the connections.

2.2.5 Envelope curves and stiffness

The *monotonic envelope curves* – i.e. the curve connecting the points of the maximum load in the hysteresis plot in each displacement level (ISO 21581, 2010) – were defined for both cases. The envelope curves presented a low initial stiffness, low lateral strength and softening behaviour. The maximum load, the maximum displacement and the ultimate displacement are showed in

Table 2. It can be seen that the variation between the initial cycle and the two stabilizing cycles was minimal. In general, the increase in the pre–compression vertical load led to higher values of maximum load and lower values of ultimate displacement.

In order to obtain the *equivalent bilinear diagrams* – perfectly elasto–plastic representations of the response of the timber frame wall specimens – the yield displacement was calculated by applying the approach provided by Tomaževic (1999). The failure load was considered as 80% of the maximum load and the yield displacement was calculated by considering the equivalent area.

Table 2. Significant values for the envelope curves (Poletti, 2013).

		F_{max} [kN]		d_{max} [mm]		d_u [mm]	
WALL		**UTW25**	**UTW50**	**UTW25**	**UTW50**	**UTW25**	**UTW50**
1st envelope curve	**P**	55.73	102.06	27.44	63.89	89.89	88.71
	N	-42.11	-95.22	-23.65	-56.73	-84.2	-80.75
2nd envelope curve	**P**	52.87	97.36	79.18	64.49	90.16	89.05
	N	-40.91	-91.62	-54.15	-56.82	-84.22	-81.20
3rd envelope curve	**P**	52.02	94.65	79.17	64.58	90.15	89.09
	N	-39.57	-89.92	-54.24	-56.91	-84.27	-81.61
avg	**P**	53.54	98.02	61.93	64.32	90.07	88.95
	N	-40.86	-92.25	-44.01	-56.82	-84.23	-81.19
C.O.V. [%]	**P**	3.63	3.82	48.23	0.58	0.17	0.23
	N	3.11	2.93	40.07	0.16	0.04	0.53

The initial stiffness and the secant stiffness of the timber frame walls were calculated for the initial cycle according to ISO 21581 (2010). In particular, the latter was considered as an initial nonlinear behaviour observed at a very small value of the lateral drift, which was likely due to the initial adjustment of the connections.

The lateral initial stiffness $\mathrm{K}_{1,\mathrm{in}+}$ was calculated by applying the following formula

$$\mathrm{K}_{1,\mathrm{in}+} = \frac{0.4 \cdot \mathrm{F}_{\max}}{\delta_{40\%\mathrm{Fmax}} - \delta_{10\%\mathrm{Fmax}}}, \quad (1)$$

where:

- $\delta_{40\%\mathrm{Fmax}}$ is the displacement value obtained in the envelope curve at 40% of the maximum load $\mathrm{F}_{\max}$;
- $\delta_{10\%\mathrm{Fmax}}$ is the displacement value obtained in the envelope curve at 10% of the maximum load $\mathrm{F}_{\max}$.

On the other hand, the secant stiffness $\mathrm{K}_{1,+}$ was calculated by taking into account the origin and the point corresponding to 40% of the maximum load. For the lower pre–compression load level, average values of 2.14 kN/mm and 2.60 kN/mm were obtained for the initial and secant stiffness, respectively. Higher values of the initial and secant stiffness – 3.16 kN/mm and 3.60 kN/mm respectively – were obtained when the higher pre–compression vertical load was considered. It was

noticeable that the vertical pre–compression influenced the lateral stiffness in agreement with previous results (Vasconcelos & Lourenço, 2009).

Further details regarding the degradation of the stiffness, the evaluation of ductility, energy dissipation and equivalent viscous damping can be found in (Poletti, 2013).

2.3 Analytical model

In order to derive an analytical model of the joints behaviour of the timber frame wall subjected to quasi–static in–plane cyclic tests described in **Section 2.2.3,** the component method is applied by following the approach suggested by Drdácký et al. (1999), and Descamps (2009). The axial and shear stiffness are computed for the connection between the diagonal elements and the main frame, while the rotational stiffness is evaluated for the half–lap connections of the main frame.

2.3.1 Component method

When the structure is not statically determined, stiffness properties of the members and the joints are extremely important. The component method provides a quick and efficient technique used for the assessment of axial, shear and rotational stiffness of timber joints under combined loads. This is even more useful in the case of traditional carpentry connections for which the lack of background information does not allow for the investigation of the influence on the structural deformability, as previously explained.

A clear understanding of the behaviour of the connection under study is crucial right from the beginning in order to properly apply the component method and to proceed with (1) the identification of the components, (2) the evaluation of the mechanical properties for each component and (3) the assembling of the active components to form a mechanical spring model.

The general approach of the component method consists of the following steps:

- Definition of a **statically equivalent model;**
- Identification of the k–couple of **surfaces in contact** i, j that transmit the forces between timber elements according to the application of the load;
- Calculation of the **total displacement** δ_k of the k–couples of surfaces in contact i, j as follows:

$$\delta_k = \delta_i + \delta_j = \frac{F_k}{k_i} + \frac{F_k}{k_j} = \frac{F_k}{k_k}, \quad (2)$$

where F_k is the compression force acting between the surfaces i, j and k_i, k_j the respective elastic stiffness.

- Calculation of the **elastic stiffness of each k–couple k_k** by considering the equivalent spring constant of the stiffness k_i, k_j acting in series as follows:

$$k_k = \frac{1}{\sum_{i,j} \frac{1}{k_i}}, \quad (3)$$

where k_i is the elastic stiffness for each surface i, j.

- Calculation of the **elastic stiffness for each surface k_i** by means of the elastic soil mechanics equation (4) giving settlements under a rectangular footing on a semi-rigid half-space,

$$k_i = \frac{E_\alpha \sqrt{b \cdot d}}{C} \quad (4)$$

where b, d are the dimensions of the contact area, E_α is the modulus of elasticity according to the direction α to the grain, C is a coefficient depending on the ratio between b, d and the coefficient of Poisson – values to be found in Lambe & Whitman (1969) and Drdácký et al. (1999). The evaluation of the value of the **modulus of elasticity** E_α is possible by using Hankinson's relation,

$$E_\alpha = \frac{E_0 \cdot E_{90}}{E_0 \cdot (\sin \alpha)^2 + E_{90} \cdot (\cos \alpha)^2} \quad (5)$$

where E_0 and E_{90} are the parallel and perpendicular moduli of elasticity and α is the grain direction.

It is important to point out that the elastic definition of the stiffness given by (4) is obtained by assuming the deformation of an elastic half space. However, the contact areas of timber connections are rather small and proper boundary conditions of the free surface surrounding them should be taken into account. A cut factor $C_{m,E}$ is proposed to enhance the component method by Descamps (2009). In particular, the values of the cut factor are defined by numerical modelling depending on the grain slope and the slenderness of the contact area. Chang et al. (2006) provide another possible approach by considering an additional length effect.

The experimental tests pointed out that the behaviour of the timber frame wall was mainly influenced by two joints: (1) the connection between the diagonal elements and the main frame; (2) the half–lap connection between the elements of the main frame. As described in **Section 2.2.1,** both connections were nailed.

2.3.2 Evaluation of the axial and shear stiffness

Following the procedure presented previously, the component method is applied to calculate the axial and shear stiffness of the connections between the diagonal elements and the main frame. As shown in **Figure 4**, the following stiffness are considered:

- The stiffness $\mathbf{k_c}$ provided by the contact areas;
- The stiffness $\mathbf{k_e}$ and the stiffness $\mathbf{k_{sp}}$ provided by the nail.

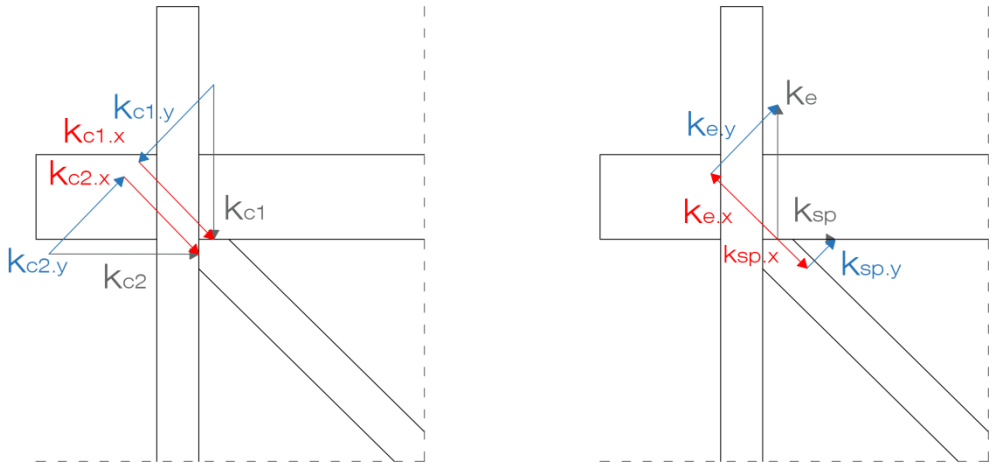

Figure 4. Axial and shear stiffness for the connection between the diagonals and the main frame.

Considering the stiffness by contact k_c, two contact areas, A_1 and A_2, are identified for each connection as shown in **Figure 5.** In turns, the compression stiffness k_{ck} is calculated for the k–couple of surfaces in contact i, j by considering their elastic stiffness, $k_{ck.1}$ and $k_{ck.2}$. Each elastic stiffness was evaluated by applying (4) and considering the slope of grain of each timber element: $E_\alpha = 1.66 \cdot 10^6$ kN/m^2 ($\alpha = 45°$) and $E_{90} = 9 \cdot 10^5$ kN/m^2 are the moduli of elasticity considered for the diagonals and the main frame elements, respectively.

Finally, the axial stiffness $k_{c.x}$ and shear stiffness $k_{c.y}$ in compression are calculated considering the projection of the elastic stiffness for the k–couple of surfaces, $k_{ck.x}$ and $k_{ck.y}$. The obtained values are summarized in **Table 3.**

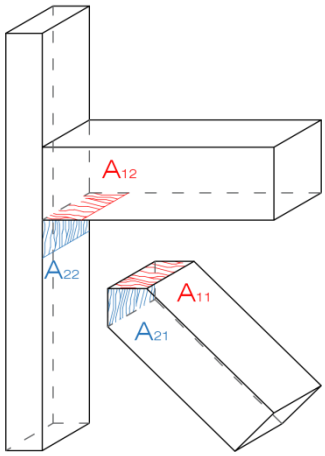

Figure 5. Contact areas of the connections by contact.

Table 3. Axial and shear stiffness for the connection by contact.

A_1 [m^2]	k_{c11} [kN/m]	k_{c12} [kN/m]	k_{c1} [kN/m]	$k_{c1.x}$ [kN/m]	$k_{c1.y}$ [kN/m]
$6.84 \cdot 10^{-4}$	$1.15 \cdot 10^{5}$	$6.20 \cdot 10^{4}$	$4.02 \cdot 10^{4}$	$2.85 \cdot 10^{4}$	$2.85 \cdot 10^{4}$
A_2 [m^2]	**k_{c21}** [kN/m]	**k_{c22}** [kN/m]	**k_{c2}** [kN/m]	**$k_{c2.x}$** [kN/m]	**$k_{c2.y}$** [kN/m]
$6.84 \cdot 10^{-4}$	$1.15 \cdot 10^{5}$	$6.20 \cdot 10^{4}$	$4.02 \cdot 10^{4}$	$2.85 \cdot 10^{4}$	$2.85 \cdot 10^{4}$

As shown in **Figure 4,** two contributions are considered to estimate the stiffness of the nail: (1) the extraction stiffness k_e and (2) the ultimate shear plane stiffness k_{sp}. The extraction stiffness k_e can be calculated by considering the axial strain of a linear elastic isotropic material, as follows

$$k_e = \frac{E_s \cdot A_s}{l_{pen}} = 8.48 \cdot 10^4 \text{ kN/m} \qquad (6)$$

where E_s = 210 GPa is the modulus of elasticity of steel, A_s= 28.27 mm^2 is the cross sectional area of the nail and l_{pen} = 7 cm is the penetration length. In particular, the penetration length is calculated as the length of the nail piercing the timber element excluding the possible gap present in the connection.

Concerning the ultimate shear plane stiffness k_{sp}, the formula provided by Eurocode 5 (2004) for nails without pre–drilling is used:

$$k_{sp} = \frac{2}{3} \cdot \left[\frac{\rho_m^{1.5} \cdot d^{0.8}}{30}\right] = 1.34 \cdot 10^3 \text{ kN/m} \quad (7)$$

where ρ_m = 590 kg/m^3 is the mean density of the wood and d = 6 mm is the diameter of the nail.

Hence, by considering the projections of the stiffness values found, the axial and the shear stiffness are calculated on the parallel and perpendicular directions. The values obtained are summarized in Table 4**.** However, the value calculated for the nail that results to be pushed–out from the connection seems to be rather high.

Table 4. Axial and shear stiffness for the connection by contact.

$\mathbf{k_e}$ [kN/m]	$\mathbf{k_{e.x}}$ [kN/m]	$\mathbf{k_{e.y}}$ [kN/m]	$\mathbf{k_{sp}}$ [kN/m]	$\mathbf{k_{sp.x}}$ [kN/m]	$\mathbf{k_{sp.y}}$ [kN/m]
$8.48 \cdot 10^4$	$6 \cdot 10^4$	$6 \cdot 10^4$	$1.34 \cdot 10^3$	944	944

2.3.3 Evaluation of the rotational stiffness

The component method presented in **Section 3.2.1** is applied to calculate the elastic rotational stiffness of the half–lap connections between the elements of the main frame. As shown in **Figure 6**, four contact areas are identified and the corresponding elastic stiffness values are calculated taking into account the slope of grain. If M is the applied bending moment and ϑ is the relative rotation between the connected members, the rotational stiffness of the half–lap joints can be written as (Descamps & Guerlement, 2009):

$$k_{rot} = \frac{M}{\vartheta} = \frac{\sum_k F_k \cdot z_k}{\vartheta} = \frac{\sum_k k_k \cdot \delta_k \cdot z_k}{\vartheta} = \frac{\sum_k k_k \cdot (z_k \cdot \vartheta) \cdot z_k}{\vartheta} = \sum_k k_k \cdot z_k^2 \quad (8)$$

where k_k is the elastic stiffness of each k–couple of surfaces and z_k is the distance between the point of application of each stiffness k_k and the instantaneous centre of rotation (ICR). In this case, the ICR is assumed to be fixed and located where the nail of the half–lap joint is placed. Enhancement of the ICR definition is provided by Descamps (2009) considering its movement during loading. The value of 477 kNm/rad can be assumed for the rotational stiffness k_{rot}. A summary of the obtained results is shown in **Table 5**.

Table 5. Rotational stiffness for the half–lap connection.

A_1 [m^2]	k_{11} [kN/m]	k_{12} [kN/m]	k_1 [kN/m]	z_1 [m]
$9.60 \cdot 10^{-3}$	$1.04 \cdot 10^{6}$	$7.84 \cdot 10^{4}$	$1.15 \cdot 10^{4}$	0.05
A_3 [m^2]	**k_{31}** [kN/m]	**k_{32}** [kN/m]	**k_3** [kN/m]	**z_3** [m]
$6.80 \cdot 10^{-4}$	$5.18 \cdot 10^{5}$	$4.24 \cdot 10^{4}$	$3.92 \cdot 10^{4}$	0.02

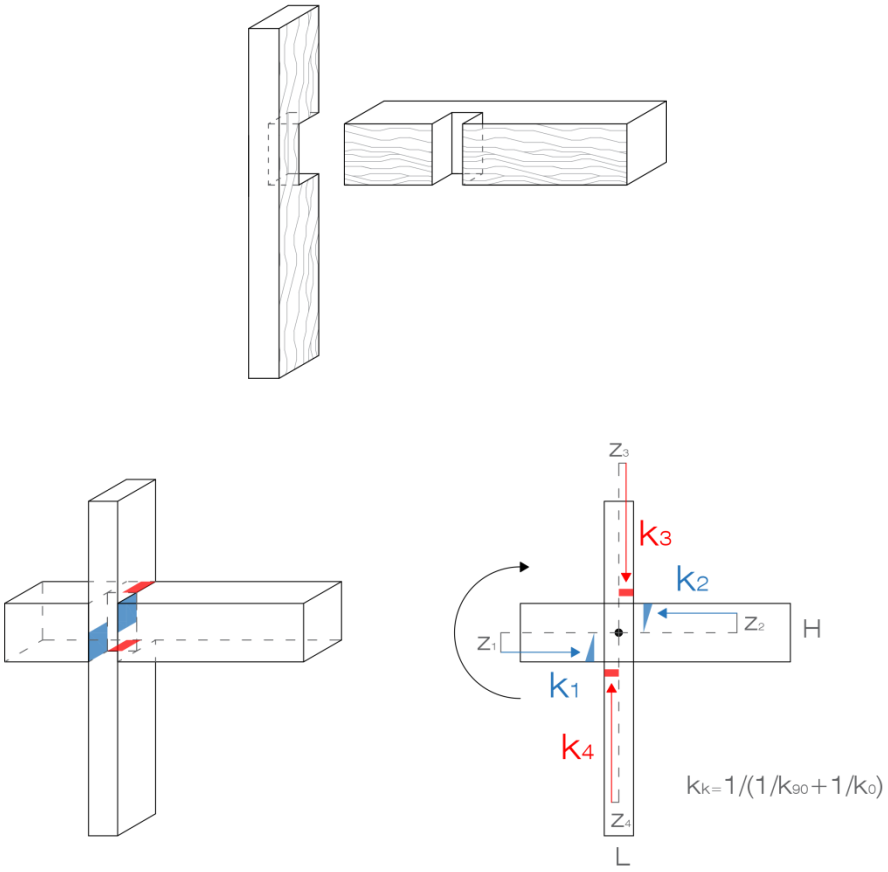

Figure 6. Rotational stiffness for the half–lap connection.

2.4 Numerical model

In order to simulate the mechanical behaviour that was observed for the pre–compression load of 25 kN in the experimental tests described in **Section 2.2,** the timber frame wall is modelled by using *Frame* and *Link* elements in SAP2000 structural and earthquake engineering software. The calibration of the model is performed by comparing the numerical and the experimental capacity curves. It should to be noted that only the positive values of the experimental diagram are taken into account. This is due to the fact that the load was applied only on one side during testing and this provoked an asymmetrical response.

2.4.1 Geometry and material properties

Timber is modelled as a linear elastic isotropic homogeneous material. According to the experimental results, the value of the modulus of elasticity is $1 \cdot 10^7$ KN/m^2 and the Poisson's ratio is 0.3. Geometrically, the model consists of four cells that are assumed to have the same dimensions of 0.95 x 0.95 m^2, as shown in **Figure 7**.

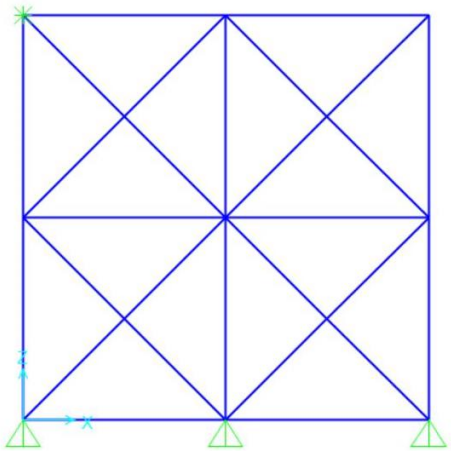

Figure 7. Schematic of the numerical model.

Figure 8 presents four different models that depend on the assumptions made for the timber connections:

- **MOD 0** : Rigid connection for each joint;
- **MOD 1** : Hinged connection between the diagonal elements and the main frame;
- **MOD 2** : Semi–rigid connections between the diagonal elements and the main frame:

- **MOD 3** : Semi–rigid connections between (1) the diagonal elements and the main frame, and (2) the elements of the main frame.

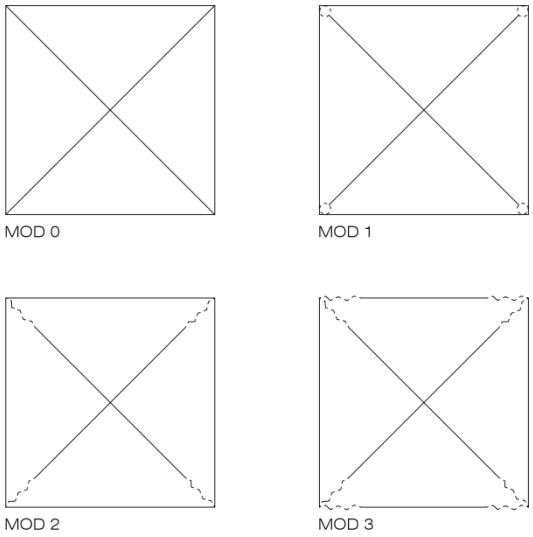

Figure 8. Typical cell for each numerical model.

It should be noted that the half-lap connections in the diagonals are not modelled, as it was observed during the experimental campaign that they have little influence on the behaviour of the wall (Poletti, 2013). Each element of the main frame is modelled as *Frame element* – a straight line connecting two points. In order to model the semi–rigid connection, *Link element* – two joint connecting link – is used with multi–linear elasticity property. Each link element is assumed to be composed of six separate springs, one for each deformational degree of freedom. The link element is assumed to have zero length. This is performed by setting the distance between the two connected joints as the value in the Auto Merge Tolerance. The *Advanced local coordinate system* is used to define the orientation of local 1 axis coincident with the longitudinal axis of the element that is connected to the link element. For the *link element deformational degree of freedom (DOF)*, three options are available:

- **Option unchecked**: any contributing stiffness is kept to the direction specified for the link;
- **Fixed option:** the link does not experience any deformation in the direction specified;
- **Nonlinear option**: the link contributes the specified stiffness.

It is possible to fix either all or none of the link element deformational DOF. However, link elements with fixed element deformational DOFs should not be connected to constrained joints as these might result to be multiply–constrained. As it will be described in the following sections, the left corner of

the top beam needs to be restrained in order to apply a horizontal displacement. Moreover, the link elements that will be used are present at the same location. For this reason, it is necessary that all the element deformational DOFs are not fixed. Reasonable large stiffness values are considered in order to specify a stiff behaviour, as recommended by CSI (2014).

For each internal deformation – that does not affect the behaviour of any other – a multi–linear elastic *force–deformation relationship* can be specified. A multi–linear curve can be defined by a set of points respecting some restrictions given by CSI (2014) in order to describe a nonlinear elastic behaviour for the timber connections.

In this study, two link elements are considered: *Link 1* and *Link 2*. *Link 1* is located at each connection between the main frame and the diagonal elements in MOD 2 and MOD 3. In MOD 3, *Link 2* is located at each beam–post connection. Because of the planar nature of the problem, only the axial u_1, shear u_2 and pure bending r_3 stiffness are considered for the element deformational DOFs. While the axial and the shear stiffness are specified for *Link 1*, the rotational one is defined for *Link 2*. Linear elastic force–deformation relationships are used for *Link 1* in MOD 2 (**Figure 9**); linear and nonlinear elastic force–deformation ones are introduced for *Link 1* and *Link 2* in MOD 3 (**Figure 10**).

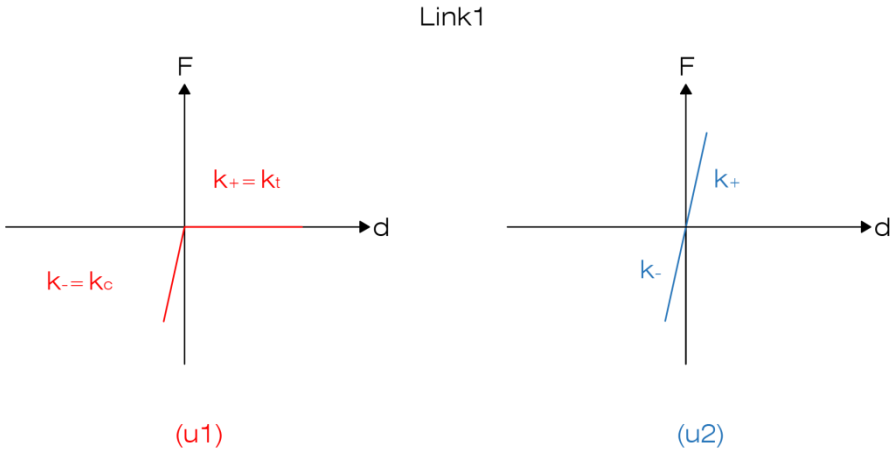

Figure 9. Linear elastic force–deformation for *Link 1* in MOD 2.

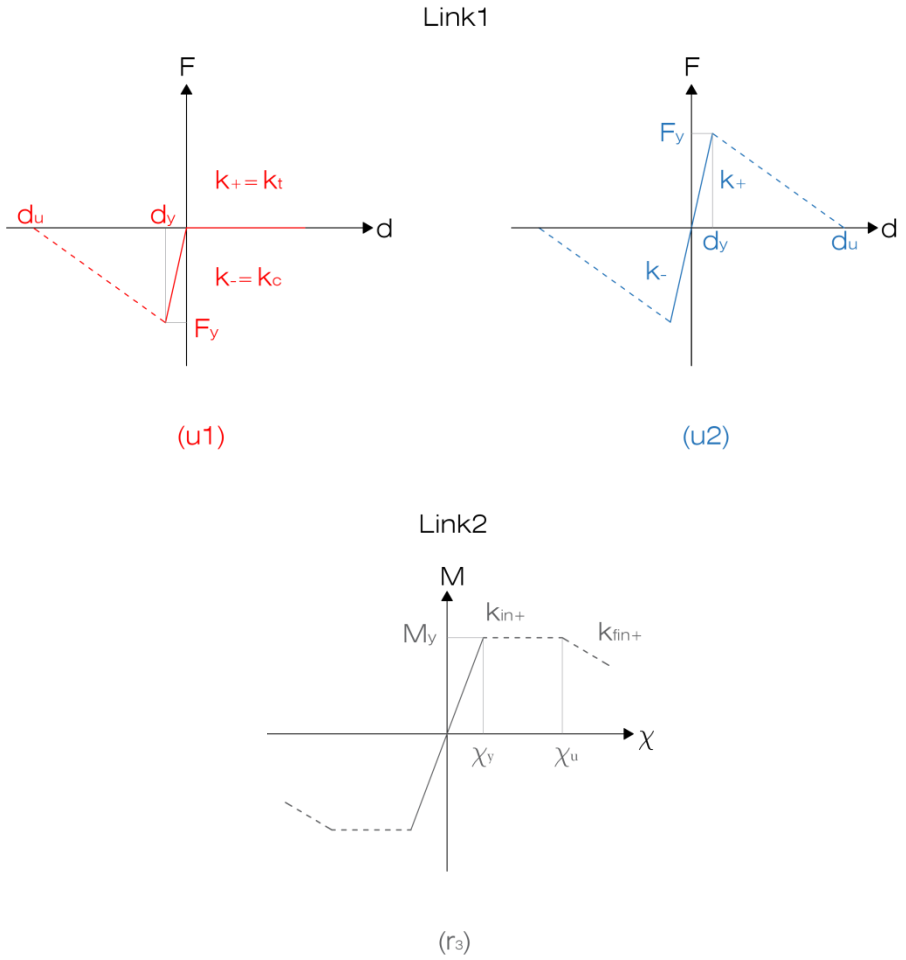

Figure 10. Linear and nonlinear elastic force–deformation for *Link 1* and *Link 2* in MOD 3.

2.4.2 Loading condition

In order to simulate the experimental tests described in **Section 2.2**, the following load conditions are considered for the model of the timber frame wall:

- **Vertical load of 25 kN** applied downwards at the three nodes intersecting the top beam and the posts;
- **Horizontal displacement of 0.10 m** applied on the left corner of the top beam.

2.4.3 Restraints

For the full wall, as shown next, the three nodes of the bottom beam are restrained in the vertical and horizontal directions. Besides, the left corner of the top beam is restrained in the horizontal

direction in order to apply the prescribed displacement. In MOD 1, all the rotational DOFs of each diagonal element are released at one end in in order to model the connection as a hinge.

2.4.4 Structural analysis

In order to obtain the capacity curve of the structural system, the following two steps of a nonlinear static analysis are performed:

- **Full load application** of the dead and vertical loads;
- **Displacement control** of the applied horizontal displacement.

The capacity curve is constructed by considering the base shear and the applied horizontal displacement at each step of the nonlinear analysis. As expected, when no non–linearity is present in the model in terms of geometry, material, loading and boundary condition – such as in MOD 0, MOD 1 and MOD 2 – the results are the same of those obtained by performing a linear static analysis. Nonlinearity is only introduced in MOD 3, considering the capacity for both timber connections under study.

2.5 Calibration of the model

As explained in **Section 2.2.5**, the secant stiffness of the timber wall was calculated and a value of $2.60 \cdot 10^3$ kN/m was obtained for the lower pre–compression load. In order to calibrate the numerical model, the following study was performed considering the four different models described in **Section 2.4.1**.

2.5.1 Model with rigid connections (MOD 0)

Firstly, MOD 0 is considered with rigid connections for all joints. By observing the deformed shape in **Figure 11**, it is noted that the deformation is mostly due to the application of the horizontal displacements. Moreover, all the nodes behave rigidly as expected. As observed in the axial forces diagram, the diagonal elements that are inclined along (against) the applied displacement are in tension (compression). The value of the stiffness of the timber frame wall is $39.94 \cdot 10^3$ kN/m, which is much higher than the experimental value.

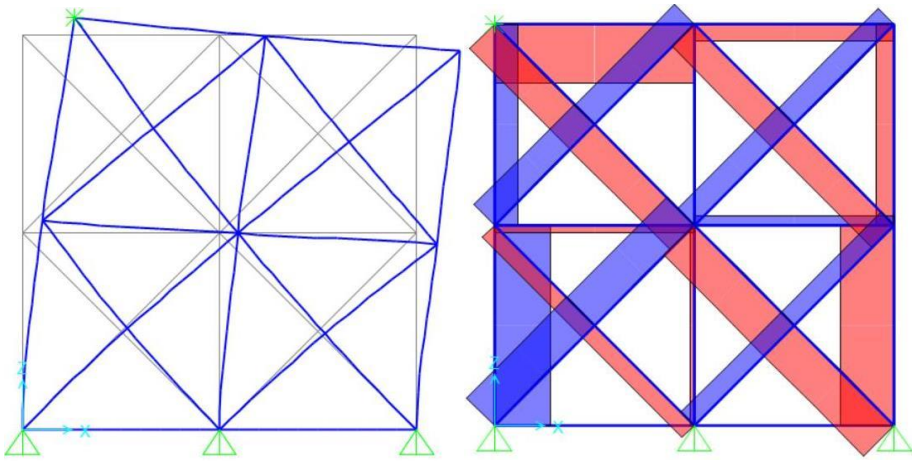

Figure 11. Deformed shape (left) and axial force diagram (right) of MOD 0.

2.5.2 Model with hinged connections of the diagonal elements (MOD 1)

In MOD 1, all the diagonal elements are released at one end in all the rotational DOFs. The value of the stiffness obtained is $39.87 \cdot 10^3$ kN/m. As this is slightly lower than that obtained in MOD 0, the rotational stiffness between the diagonals and the main frame appears not to be significant, which is expected in timber structures due to the low bending stiffness and the almost rigid triangular configuration of the structure. By eliminating one of the diagonal elements for each cell of the wall, the stiffness of the structure is $22.17 \cdot 10^3$ kN/m, almost the half of the original value (MOD 1_BIS). This is also expected because, elastically, all diagonals work similarly, independently of the connection being in tension or compression.

2.5.3 Model with semi–rigid connections of the diagonal elements (MOD 2)

In order to provide more flexibility in MOD 2, all the connections between the diagonal elements and the main frame are modelled as *Link 1* described in Section **2.4.1**. In particular, the axial and shear deformational DOFs of *Link 1* are modelled with a linear elastic force–deformation relationship. Let k_{1-} and k_{1+} be the axial stiffness of *Link 1* in compression and in tension, respectively **(Figure 10**). By assuming $k_{1-} = k_{1+}$ and applying the *inverse fitting method*, the stiffness of the structure reaches the experimental value when the stiffness of the connection results to be $k_{1-} = k_{1+} = 4.15 \cdot 10^3$ kN/m. In particular, an almost linear relationship is observed between the stiffness of the connection and that of the structure. This confirms that the rotational stiffness of the connection between the diagonals and the main frame appears to be negligible. Assuming $k_{1-} = 4.15 \cdot 10^3$ kN/m and $k_{1+} = 0$ kN/m - and vice versa – the value of the stiffness of the structure is halved. This is equivalent to

removing one diagonal element – and all its link elements – for each cell of the wall, as shown in MOD 2_O. Moreover, taking the value of the stiffness in compression as the double of the previous one and zero stiffness in tension, as shown in MOD 2_A, the value of the stiffness of the structure is slightly lower than the experimental one. The exact experimental value is reached by considering the stiffness in tension of the connection as $k_{1+} = 1/100\, k_{1-}$ in MOD 2_B. Note that the shear stiffness does not seem to affect the result when linear elastic properties are applied, as shown by comparing MOD_2_A with MOD_2_C in **Table 6.**

Table 6. Results of the numerical model MOD 2.

			MOD 2	MOD 2_0	MOD_2_A	MOD 2_B	MOD 2_C
LINK 1	u_1	k_{1+} [KN/m]	$4.15 \cdot 10^3$	0	0	85	0
		k_{1-} [KN/m]	$4.15 \cdot 10^3$	$4.15 \cdot 10^3$	$8.50 \cdot 10^3$	$8.50 \cdot 10^3$	$8.50 \cdot 10^3$
	u_2	k_{2+} [KN/m]	∞	∞	∞	∞	$8.50 \cdot 10^3$
		k_{2-} [KN/m]	∞	∞	∞	∞	$8.50 \cdot 10^3$
	r_3	k_{3+} [KNm/rad]	0	0	0	0	0
		k_{3-} [KNm/rad]	0	0	0	0	0
Global stiffness K [kN/m]			$2.60 \cdot 10^3$	$1.65 \cdot 10^3$	$2.58 \cdot 10^3$	$2.60 \cdot 10^3$	$2.58 \cdot 10^3$

2.5.4 Model with semi–rigid connections of the diagonal elements and elements of the main frame (MOD 3)

As previously explained, *Link 1* and *Link 2* are used in MOD 3: while the axial u_1 and the shear u_2 stiffness are specified for the former, the rotational r_3 one is defined for the latter. Initially, linear elastic force–deformation relationships are considered for the link elements. The results on in–plane cyclic tests on half-lap joints with a pre–compression vertical load of 25 kN obtained by Poletti (2013) are used to define the deformational DOF of *Link 2*. The average force–displacement diagram is calculated from the experimental curves and a tri–linear curve is assumed for the numerical model, as shown in **Figure 12**. The corresponding tri–linear moment–rotation diagram shown in **Figure 13** is obtained. The mean values of the initial and the final rotational stiffness are calculated as k_{in} = 171 kNm/rad and k_{fin} = 47 kNm/rad, respectively.

As the axial stiffness of *Link 1* in tension is not influencing the structural behaviour significantly, it is assumed to be zero. By applying the *inverse fitting method*, the axial stiffness of the connection in compression is calculated as $10 \cdot 10^3$ kN/m (MOD 3_A). By assuming the axial stiffness in tension of the connection as $k_{1+} = 1/100\, k_{1-}$ (MOD 3_B), the value of the stiffness is $2.56 \cdot 10^3$ kN/m, slightly lower than the experimental one. Finally, it is noticeable that the shear stiffness does not seem to

affect the result when linear elastic properties are applied (MOD 3_C). A summary of all the results is presented in **Table 7.**

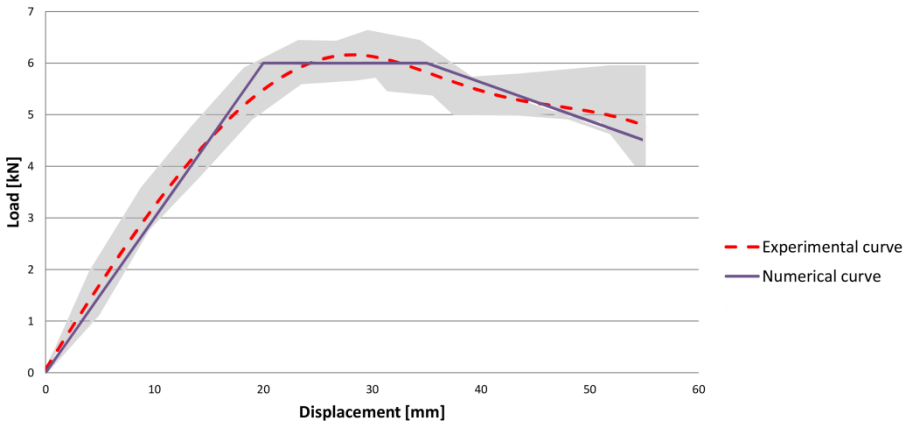

Figure 12. Force–displacement for the half–lap connection.

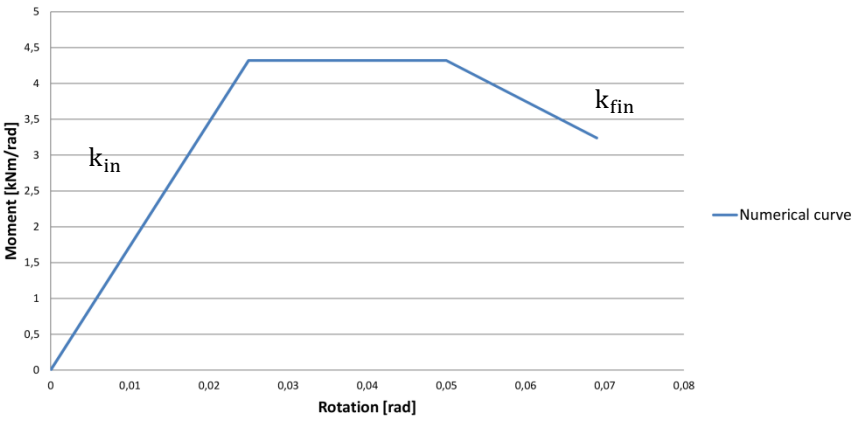

Figure 13. Moment–rotation for the half–lap connection.

Table 7. Results of the linear elastic analysis on MOD 3.

			MOD 3_A	MOD 3_B	MOD 3_C
LINK 1	u_1	k_{1+} [KN/m]	0	100	0
		k_{1-} [KN/m]	$10{\cdot}10^3$	$10{\cdot}10^3$	$10{\cdot}10^3$
	u_2	k_{2+} [KN/m]	∞	∞	$10{\cdot}10^3$
		k_{2-} [KN/m]	∞	∞	$10{\cdot}10^3$
	r_3	k_{3+} =k_{3-} [KNm/rad]	0	0	0
LINK 2	u_1	k_{1+} =k_{1-} [KN/m]	∞	∞	∞
	u_2	k_{2+} =k_{2-} [KN/m]	∞	∞	∞
	r_3	k_{in3+} = k_{in3-} [kNm/rad]	171	171	171
		k_{fin3+} = k_{fin3-} [kNm/rad]	47	47	47
Global Stiffness K [kN/m]			$2.53{\cdot}10^3$	$2.56{\cdot}10^3$	$2.56{\cdot}10^3$

Subsequently, nonlinear elastic force–deformation relationships are introduced by considering the capacity of the two timber connections, as shown in **Figure 10**. The tri–linear moment–rotation diagram described previously is used to define the multi–linear curve for the deformational DOF of *Link 2*. An initial linear behaviour followed by a linear softening is considered as the multi–linear curve to define the axial and shear deformational DOFs of *Link 1*. The capacity of the connection F_y is calculated by considering the compressive strength perpendicular to the grain f_{c90} and the contact areas for each connection by applying (9). In particular, only one contact area is considered due to the presence of initial clearances and the development of damage during the experimental tests. Hence, also the yield displacement d_y needs to be defined by applying (10).

$$F_y = f_{c90} \cdot A \quad (9)$$

$$d_y = F_y/k \quad (10)$$

The ultimate displacement d_u is assumed to be the same of that of half–lap connections: when the failure occurs for the half–lap connection, the connection between the diagonal and the main frame no longer works. When the ultimate displacement is reached (d_u = 50 mm), the capacity of the connection between the diagonals and the main frame is assumed to be zero (F_u = 0 kN). This is assumed for both the axial and shear stiffness of *Link 1*.

Due to the absence of experimental tests, parametric analyses have been carried out to better understand the influence of the capacity and of the stiffness of the connection between the diagonals and the main frame on the timber frame wall, as shown in **Table 8.** Different compressive strength values perpendicular to the grain are considered as this value was not directly derived from experimental tests described in previous section and it can vary greatly. Hence, different capacity values are considered. As shown in **Figure 14**, changing the compressive strength perpendicular to the grain f_{c90} affects mostly the initial behaviour. For a fixed value of the connection stiffness, an increase in the compressive strength leads to higher values of capacity and of yield displacement of the timber frame wall, as expected. As the displacement increases, the effect fades out. Considering the value of f_{c90} = 5 MPa (

Table 2) – that corresponds to a capacity value of 23.9 kN – C_1 reaches a capacity of less than 4kN. The capacity value obtained considering C_5 (f_{c90} = 6 MPa) can be assumed to approximate reasonably well the experimental curve. On the other hand, changing the stiffness affects significantly the initial stiffness of the structure, while the capacity changes slightly, as shown in

Figure 15. The value obtained previously by applying the inverse fitting method in the elastic analysis is assumed as the initial stiffness of the connection between the diagonal and the main frame.

Table 8. Parametric analysis on the connection between the diagonals and the main frame.

			CAPACITY					STIFFNESS		
			C_1	C_2	C_3	C_4	C_5	S_4	S_5	S_6
LINK 1	u1	k_{1+}[KN/m]	0	0	0	0	0	0	0	0
		k_{1-}[KN/m]	10000	10000	10000	10000	10000	10000	20000	50000
		F_y [KN]	23.9	25.7	27.4	29.1	30.8	30.8	30.8	30.8
	u2	k_{2+} =k_{2-} [KN/m]	10000	10000	10000	10000	10000	10000	20000	50000
		F_y [KN]	23.9	25.7	27.4	29.1	30.8	30.8	30.8	30.8
	r3	k_{3+} =k_{3-} [KNm/rad]	0	0	0	0	0	0	0	0
LINK 2	u1	k_{1+}= k_{1-}[KN/m]	∞	∞	∞	∞	∞	∞	∞	∞
	u2	k_{2+} =k_{2-} [KN/m]	∞	∞	∞	∞	∞	∞	∞	∞
	r3	k_{in3+} = k_{in3-} [kNm/rad]	171	171	171	171	171	171	171	171
		k_{fin3+} = k_{fin3-} [kNm/rad]	47	47	47	47	47	47	47	47

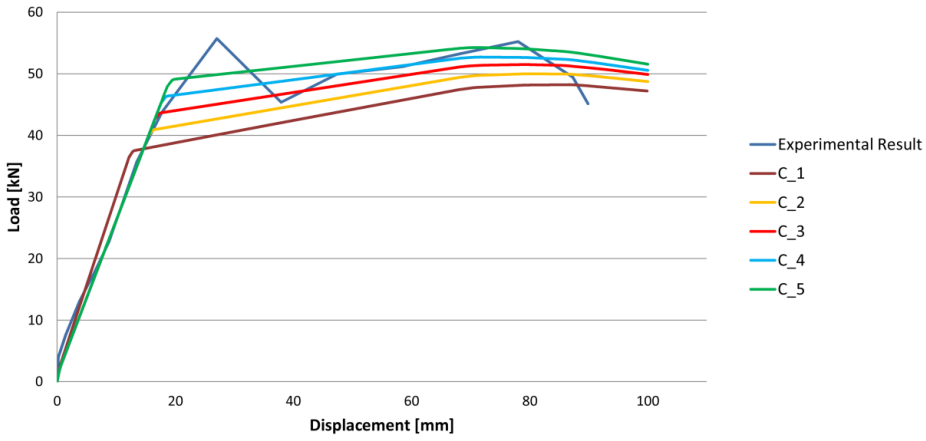

Figure 14. Parametric analysis on the capacity of the connection between the diagonals and the main frame.

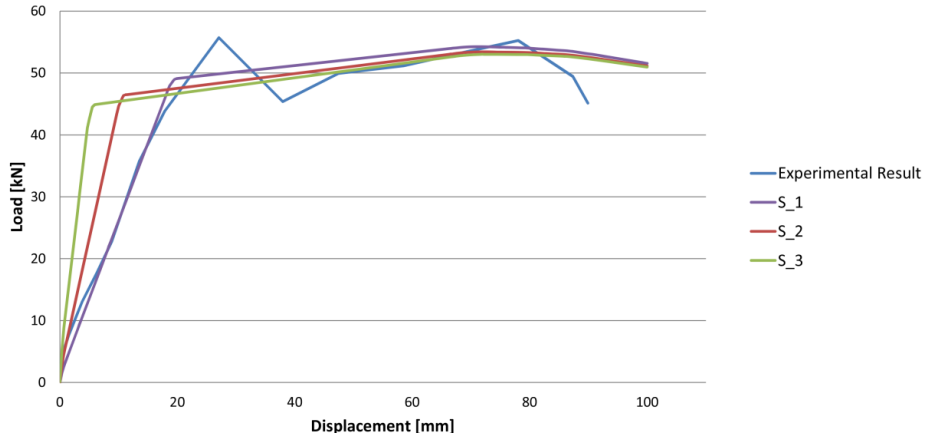

Figure 15. Parametric analysis on the stiffness of the connection between the diagonals and the main frame.

Differently from the results obtained using linear elastic analysis, the shear stiffness has influence on the nonlinear structural behaviour. While the compressive strength value perpendicular to the grain and the axial stiffness influence mainly the initial behaviour, the shear stiffness seems to affect mostly the nonlinear response of the timber frame wall, as shown in **Table 9** and **Figure 16.** It should be noted that the curves obtained from MOD SS_1 and MOD SS_2 are very similar, while a marked softening is experienced by SS_3 – that corresponds to having only axial forces in the diagonal elements of the timber frame wall. The influence of the positive and negative shear stiffness is studied independently in SS_4 and SS_5.

Table 9. Influence of shear stiffness in nonlinear analysis.

			SS_1	SS_2	SS_3	SS_4	SS_5	SS_6	SS_7	SS_8
LINK 1	u1	k_{1+}[KN/m]	0	0	0	0	0	0	0	0
		k_{1-}[KN/m]	10000	10000	10000	10000	10000	10000	10000	10000
		F_y [KN]	30.8	30.8	30.8	30.8	30.8	30.8	30.8	30.8
	u2	k_{2+} [kN/m]	10000	∞	0	0	10000	10000	5000	5000
		F_y [kN]	30.8	∞	0	0	30.8	15.4	30.8	15.4
		k_{2-} [kN/m]	10000	∞	0	10000	0	10000	5000	5000
		F_y [kN]	30.8	∞	0	30.8	0	15.4	30.8	15.4
	r3	k_{3+} =k_{3-} [kNm/rad]	0	0	0	0	0	0	0	0
LINK 2	u1	k_{1+}= k_{1-}[KN/m]	∞	∞	∞	∞	∞	∞	∞	∞
	u2	k_{2+} =k_{2-} [kN/m]	∞	∞	∞	∞	∞	∞	∞	∞
	r3	k_{in3+} = k_{in3-} [kNm/rad]	171	171	171	171	171	171	171	171
		k_{fin3+} = k_{fin3-} [kNm/rad]	47	47	47	47	47	47	47	47

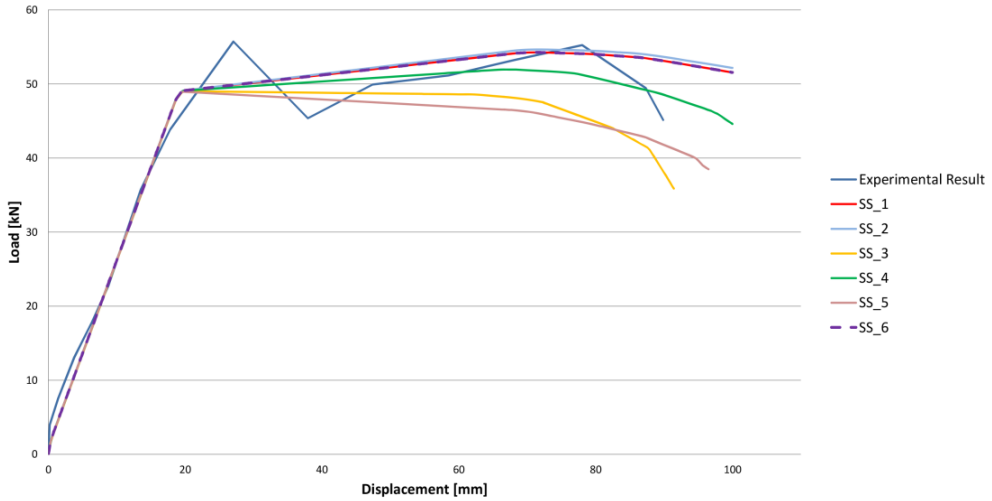

Figure 16. Influence of shear stiffness in nonlinear analysis.

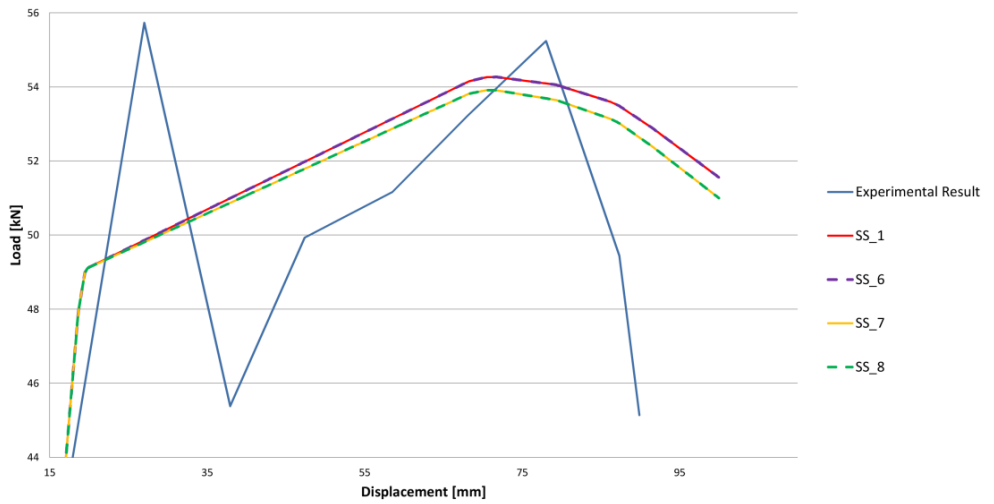

Figure 17. Influence of the shear stiffness.

2.6 Conclusion

In order to simulate the mechanical behaviour that was observed during the quasi–static in–plane cyclic tests carried out by Poletti (2013), analytical and numerical modelling of the timber wall were carried out.

Firstly, the analytical model of the timber joints was constructed by applying the component method. In particular, the axial and shear stiffness were computed for the connection between the diagonal elements and the main frame, while the rotational stiffness was evaluated for the half–lap connections of the main frame. Two main contributions to the stiffness were evaluated to obtain the axial and shear stiffness: the stiffness due to the contact areas between the wooden elements and the one provided by the nail. It should be noted that the evaluation of the axial stiffness in tension was a difficult task. While the shape of deformed nails confirmed the plane shear contribution – even though it was not so significant – not much information was available regarding their elongation. Hence, the evaluation of stiffness based on the elastic strain was performed and a very high value was obtained. Regarding the rotational stiffness of the half–lap joint, only the stiffness due to the contact areas between the corresponding wooden elements were considered. A summary of the obtained values is shown in **Table 10**.

Table 10. Stiffness values obtained from the analytical model.

AXIAL STIFFNESS			SHEAR STIFFNESS			ROTATIONAL STIFFNESS
$\mathbf{k_{c1.x}=k_{c2.x}}$ [kN/m]	$\mathbf{k_{e.x}}$ [kN/m]	$\mathbf{k_{sp.x}}$ [kN/m]	$\mathbf{k_{c1.y}=k_{c2.y}}$ [kN/m]	$\mathbf{k_{e.y}}$ [kN/m]	$\mathbf{k_{sp.y}}$ [kN/m]	$\mathbf{k_{rot}}$ [kN/m]
$2.85 \cdot 10^4$	$6 \cdot 10^4$	944	$2.85 \cdot 10^4$	$6 \cdot 10^4$	944	477

Subsequently, the timber frame wall was modelled numerically and the calibration of the model was performed by comparing the numerical and the experimental capacity curves. Four different models were considered according to the assumptions made to simulate the structural behaviour of the timber connections. MOD 0, MOD 1 and MOD_1 BIS – i.e. the models with rigid and hinged connections between the diagonal elements and the main frame – pointed out that (1) the contribution of the axial stiffness in tension is negligible, (2) the rotational stiffness between the diagonals and the main frame is not relevant and (3) all diagonals work similarly, independently of the connection being in tension or compression. A summary of the obtained results is shown in **Table 11.**

Table 11. Comparison between the models with rigid and hinged connection.

	MOD_0	MOD_1	MOD_1_BIS
Global stiffness K [kN/m]	$39.94 \cdot 10^3$	$39.87 \cdot 10^3$	$22.17 \cdot 10^3$

In order to study the semi–rigid behaviour of the connection between diagonals, posts and beams two link elements were considered: *Link 1* and *Link 2*. The former was located at each connection between the main frame and the diagonal elements in MOD 2 and MOD 3, the latter at each beam–post connection in MOD 3. Axial u_1, shear u_2 and pure bending r_3 stiffness were considered for the element deformational DOFs: while the axial and the shear stiffness were specified for *Link 1*, the rotational one was defined for *Link 2*. Linear elastic force–deformation relationships were initially used for *Link 1* in MOD 2 and in MOD 3. The tri–linear moment–rotation diagram was derived from experimental tests (Poletti, 2013) and used to define the rotational deformational DOF of *Link 2*. The obtained results confirmed the negligibility of the axial stiffness in tension of *Link 1*. A summary of the final stiffness values is presented in **Table 12**. Nonlinear elastic force–deformation relationships were introduced by considering the capacity of the two timber connections. The calibration of the capacity and stiffness of *Link 1* was obtained by carrying out parametric analyses. The obtained results have pointed out the influence of the shear stiffness on the nonlinear structural behaviour.

It has to be noted that assuring that all the numerical models were equivalent when changing the *Links* properties was crucial. Due to this, simple checks were performed to control that (1) both the models MOD 2 and MOD 3 degenerated to MOD 0 when all the stiffness of *Link 1* and *Link 2* had a value that tended to infinity and (2) MOD 3 degenerated to MOD 2 considering the same values of the stiffness for *Link 1* in both the models MOD 2 and MOD 3 and a value that tends to infinite for the rotational stiffness of *Link 2*.

Table 12. Calibration of the axial stiffness in MOD 2 and MOD 3.

			MOD 2_C	MOD 3_C
LINK 1	u_1	k_{1+} [KN/m]	0	0
		k_{1-} [KN/m]	$8.50 \cdot 10^3$	$10 \cdot 10^3$
	u_2	k_{2+} [KN/m]	$8.50 \cdot 10^3$	$10 \cdot 10^3$
		k_{2-} [KN/m]	$8.50 \cdot 10^3$	$10 \cdot 10^3$
	r_3	$k_{3+} = k_{3-}$ [KNm/rad]	0 0	0
LINK 2	u_1	$k_{1+} = k_{1-}$ [KN/m]	∞	∞
	u_2	$k_{2+} = k_{2-}$ [KN/m]	∞	∞
	r_3	$k_{in3+} = k_{in3-}$ [kNm/rad]	∞	171
		$k_{fin3+} = k_{fin3-}$ [kNm/rad]	∞	47
Global Stiffness K [kN/m]			$2.58 \cdot 10^3$	$2.56 \cdot 10^3$

The comparison between the analytical and numerical models showed a significant difference in terms of axial stiffness in tension. The experimental behaviour seems to be not perfectly captured by the assumptions for the mechanical behaviour of the nail. The numerical analysis suggested that no elongation of the nail occurred during the experimental tests. In order to evaluate a more reliable value for the extraction stiffness of the nail, the adherence between the steel of the nail and the wood should be considered. However, it has to be said that codes do not cover this case and the adherence provided by the smooth nail and the wood is usually neglected.

On the other hand, the compressive stiffness represented the key point to capture the behaviour of the timber connections and the component method was a powerful technique to evaluate it. Linear elastic analyses were performed using the stiffness values obtained by applying the component method considering only one contact area. The value of $5.75 \cdot 10^3$ kN/m was obtained for the stiffness of the timber frame wall: although it is higher than the experimental one, this is in agreement with previous studies that showed an overestimation of the component method (Descamps & Guerlement, 2009). The numerical stiffness value is reached by applying a reduction factor (RF) of around 2.5 to the values obtained from the component method.

In conclusion, it should be underlined that these results were carried out considering a pre–compression load of 25 kN. When the pre–compression load is higher, the stiffness of the timber frame wall is higher as the gaps close and the contact increases. A summary of the capacity curves obtained for the timber frame wall is presented in **Figure 18.**

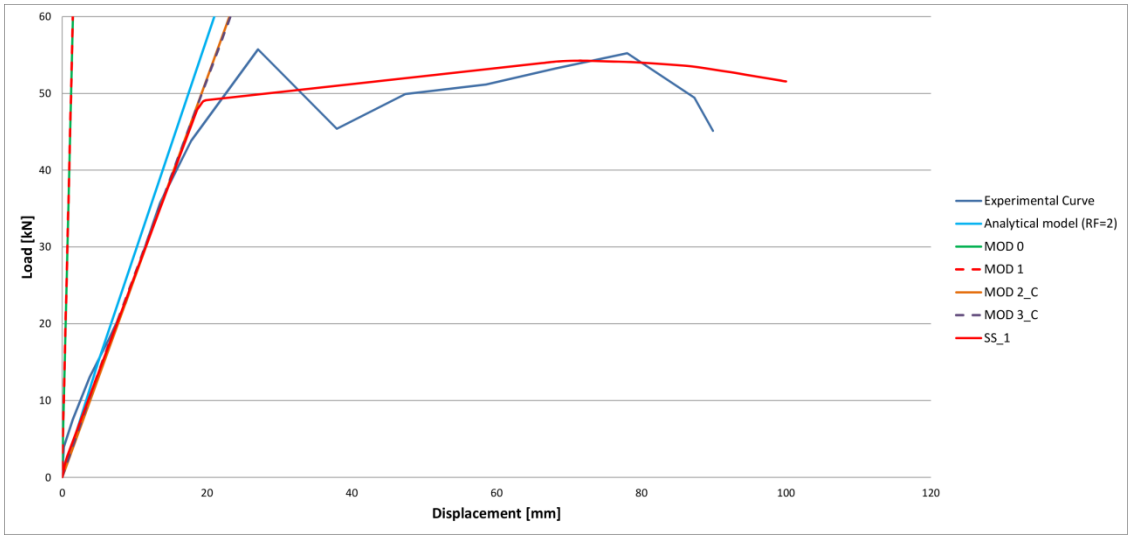

Figure 18. Summary of the capacity curves obtained from the modelling of the timber frame wall.

Chapter 3

Ica Cathedral

Considered as national monument since 1982, the Cathedral of Ica is one of the most representative churches built in coastal cities during the Viceroyalty of Peru. As most of the structures constructed with the *quincha* technique, the 2007 Pisco earthquake affected significantly Ica Cathedral. Today, the structure is heavily damaged with the collapse of several parts of the vaulted roofing frame system.

3.1 Introduction

3.1.1 Historical background

The Cathedral of Ica was originally constructed for the College of San Luis Gonzaga of the Society of Jesus. Work on the college began in 1746 and the cathedral was completed in 1759 according to the date inscribed on the central dome. However, it would seem that the construction continued for several years (Harth-Terré, 1948. [2003]).

Its ownership was transferred to the Mercedarian order in 1780 after the expulsion of the Jesuits from the Viceroyalty of Peru for political reasons and the church was devoted to Our Lady of the Mercy. The Mercedarians were responsible for the repair of the façade after the 1813 earthquake

that damaged the church as well as several buildings in Ica. Moreover, the choir loft that covers the main entrance of the cathedral may have been added by them at this time as the Jesuits did not require it for prayer (Cancino, et al., 2012).

When the Mercedarians left Ica after the independence of Peru (1821–1824), the church took the name of Iglesia Matriz de San Jerónimo. Several alterations and repairs to the church were carried out in the nineteenth century, also due to the damage provoked by the 1868 earthquake. The presence of the two bell towers – as well several altarpieces – was reported in an inventory carried out in 1878. The northeast bell tower was under repair in 1919 but was destroyed by the 1942 earthquake. Since 1946, the church served as a place of worship of the Roman Catholic Diocese of Ica until it was damaged during the 2007 Pisco Earthquake (**Figure 19**).

Figure 19. The front façade (left) (Cancino, et al., 2012) and the current condition of the internal space of Ica Cathedral (Image: https://www.flickr.com/people/thegetty/).

3.1.2 Historical damage

As mentioned in the previous section, Ica Cathedral has been occupied, renamed, repaired and altered by different religious orders since its construction. However, the main sources of historical damage are related to the seismic events that have occurred during its existence.

The western coast of South America is one of the most active seismic areas of the world. A peak ground acceleration (PGA) of 0.2g to 0.4g with 10% chance of exceedance in 50 years is associated with a substantial part of Peru (http://www.seismo.ethz.ch/static/GSHAP). Ica Cathedral is located in the level 3 seismic risk zone that is the highest seismic level classified by the Peruvian Building Code.

A summary of past earthquakes is presented chronologically in **Table 13**:

Table 13. Seismic events that have affected Ica Cathedral.

Date	Seismic Events
1813	The earthquake led to several repairs carried out by the Mercedarian Order, such as the reconstruction of the main façade in the Neoclassical style and the probable addition of the choir loft over the main entrance of the cathedral.
1868	Arica Earthquake (MW = 9.0) provoked significant damages that were repaired in 1874.
1942	Earthquake off the coast of central Peru (M_W = 8.2) caused the collapse of the northeast bell tower.
2007	Pisco Earthquake (M_W = 8.0) provoked the partial collapse of the several parts of the vaulted roof framing system and the loss of plaster at the pillars' and pilasters' bases.
2009	Earthquake off the coast of the central Peru (M_W = 5.8) aggravated heavily the damage of the previous earthquake including the total collapse of the main dome.

3.2 General description

3.2.1 Urban context

The cathedral is located at the southwest corner of Ica's main square corresponding to the intersection of two main streets, namely *La Liberdad* and *Bolivar*, as shown in **Figure 20**. The cathedral is oriented along the typical east-west axis and is adjacent to a three-story modern concrete structure and a fired brick structure to the west. A concrete portico and a square cloister are located towards its southern side.

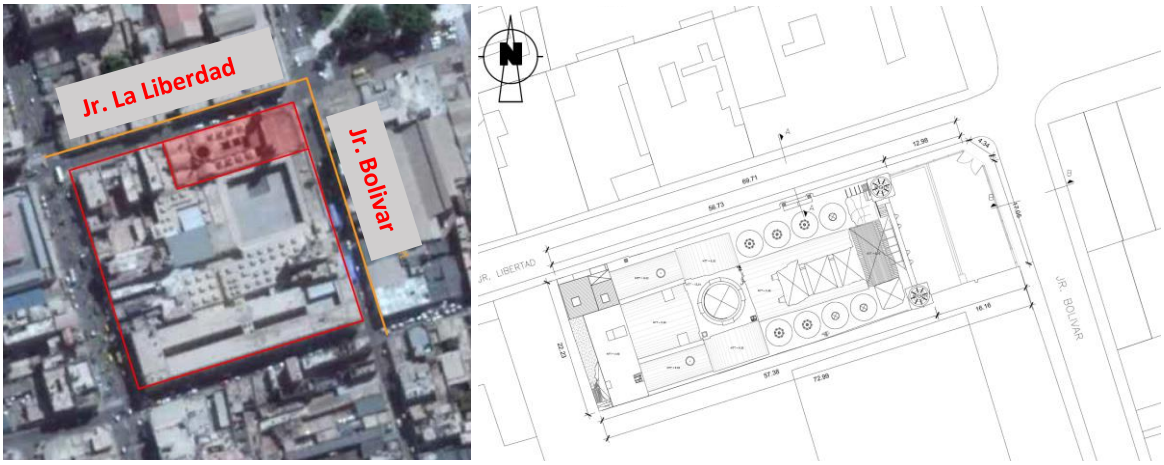

Figure 20. Satellite image (left) (2015 Google. Image 2015 Digital Globe) and the location of Ica Cathedral (right) (Garcia Bryce & Soto Medina, 2014).

The cathedral is located over compacted silty sand in a moderate flood zone without liquefaction problems. The foundation varies significantly for the configuration and dimension throughout the cathedral. In general, it is composed of rubble stone masonry with sand and lime mortar. Above it, a base course that goes all around the cathedral was constructed using fired brick masonry, rubble stone masonry or a combination of both. Moreover, remains of vaulted fired brick catacombs were found in the southern part of the cathedral (Cancino, et al., 2012).

3.2.2 Architecture

As most Jesuit churches in the New World, the layout of Ica Cathedral is based on the Church of the Gesù in Rome that was considered the model for the churches of the Society of Jesus. Although with some differences (Cancino, et al., 2012), similarities between the layout of the two churches are evident, as shown in **Figure 21** and **Figure 22.**

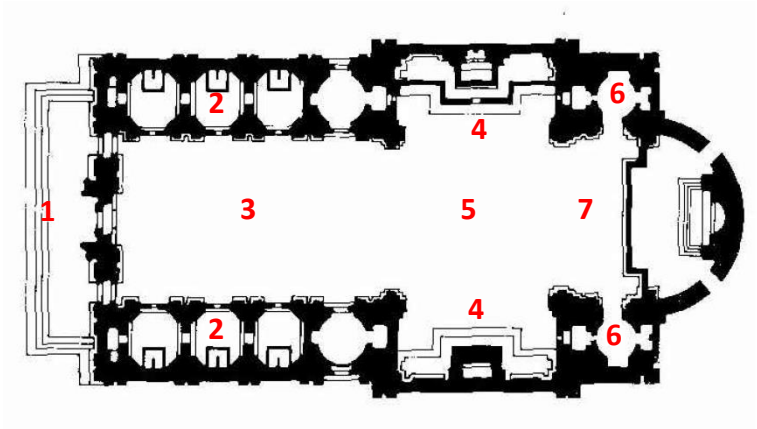

Figure 21. Schematic plan of the Church of Gesù in Rome: atrium (1), side aisles (2), main nave (3), arms of the transept (4), crossing of the transept (5), chapels (6) and altar (7).

The main entrance of Ica Cathedral is preceded by a walled *atrium* having a plan area of 20.5x13.25 m^2. The Neoclassical façade defines mostly the exterior appearance of the cathedral with rich decorations and two massive bell towers flanking on both its sides. Access to the cathedral is served by two entrances located at the front façade and at the northern wall, respectively. Moreover, a spiral staircase that is located in the base of the southern bell tower provides access to the choir loft. Another access leading to the sacristy is provided at the northern wall to the sacristy that is located at the western end of the cathedral.

The plan of Ica Cathedral is rectangular with a 1:2 proportion and an overall plan area of 22.5x48.5 m^2. It is characterized by changes in floor level and interior pillars, plasters and piers that separate the different spaces. The plan consists of the following parts (**Figure 22**):

- A **main entrance** – the so called *sotacoro* – that has a **choir loft** above and is flanked by two extensions at either lateral side;
- The **main nave** that is composed of four rectangular bays;
- **Two side aisles** each of which is composed of five square bays;
- The transversal **transept** that is essentially the continuation of the side aisles and intersects the main nave in the crossing;
- The **altar** that is flanked by two **chapels** on its lateral sides.

Around the altar and the chapels, a series of spaces is present: the sacristy, a reception, a deposit, offices and an internal court.

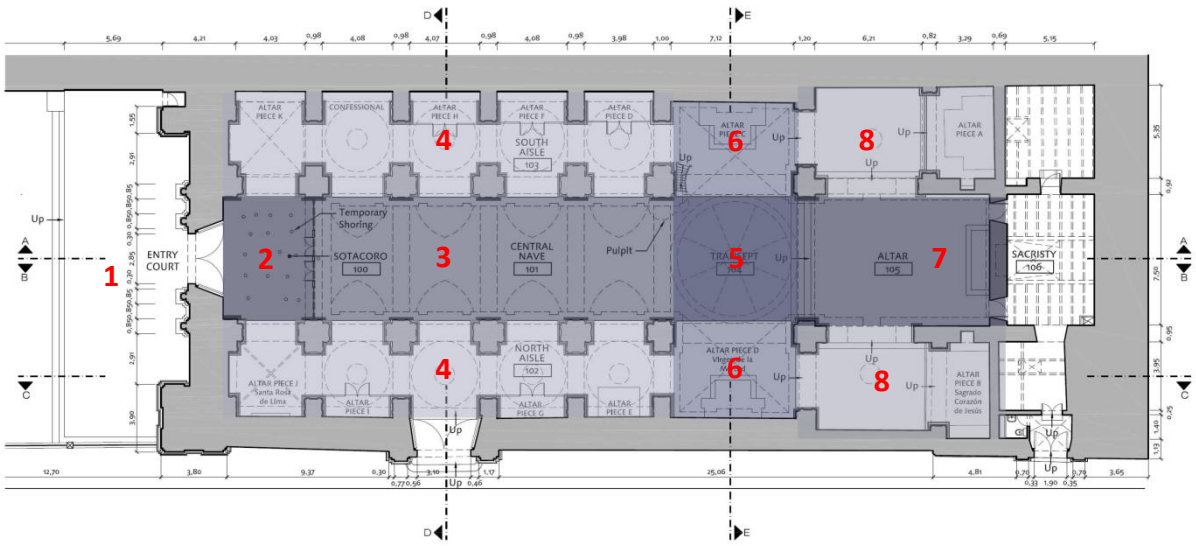

Figure 22. Schematic of the plan of Ica Cathedral: atrium (1), main entrance (2), main nave (3), side aisles (4), crossing of the transept (5), arms of the transept altar (6), altar (7) and chapels (8).

The vaulted roof framing system of Ica Cathedral consists of the following elements (**Figure 23**):

- A **large umbrella dome** that covers the crossing of the main nave and the transept;
- **Barrel vaults with lunettes** that cover the series of bays of the main nave and the *sotacoro*;
- **Barrel vaults** that cover the altar, the chapels and the lateral arms of the transept;
- **Small umbrella domes** that cover the bays of the side aisles;

- **Rib-vaulted ceilings with flat roofs** that are located at the first bay of the aisles flanking the *sotacoro.*

All the domes are topped by lanterns that are characterized by different geometries. The lighting of the cathedral is provided by these lanterns and by the windows in the upper part of the main nave.

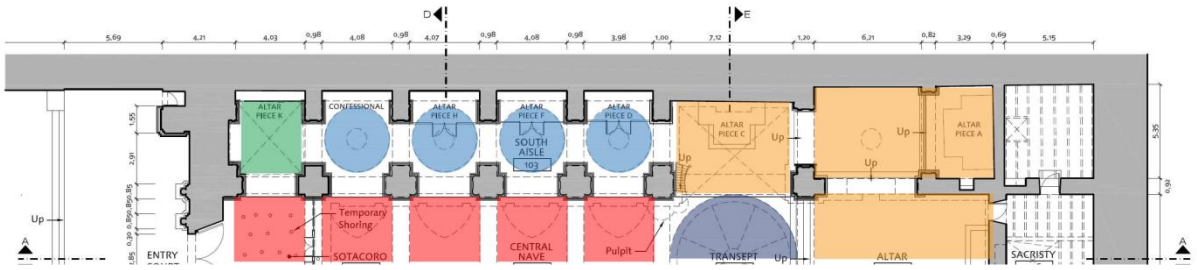

Figure 23. Vaulted roof framing system of the Ica Cathedral: barrel vaults with lunettes (red), barrel vault (orange), main dome (dark blue), aisles' domes (light blue), cross ribs vaults (green) and flat ceiling (white).

3.3 Structural systems

Ica Cathedral is composed of two structural systems: an external masonry envelope and an internal timber frame. An overview of the whole structure with a particular focus on the timber structure is provided in the following sections.

3.3.1 External masonry envelope

At the exterior, a massive and stable load–bearing masonry envelope surrounds the cathedral. It consists mainly of the front façade with two bell towers and the lateral longitudinal walls.

The façade is made of fired brick masonry with lime mortar. A thinner pediment is present at the top of the facade. On the internal face, the façade is connected to the choir loft floor by an embedment of the choir loft floor joists into the wall. The bell towers are composed of a timber structure that sits on a fired brick base. As previously mentioned, a staircase is present inside the base of the southern bell tower and similar cavities are assumed to be present also in the other one (Cancino, et al., 2012).

The longitudinal lateral walls are composed of three different layers of masonry: rubble stone, fired brick and mud brick, sequentially from the base upwards. These layers vary throughout the cathedral in terms of dimension and several irregularities are present, such as the transition zone between the northern bell tower and the lateral wall. According to Tolles et al. (2002), the lateral walls can be

considered having a low probability of lateral overturning as their slenderness ratios are less than five.

The external masonry envelope is typically finished with mud plaster and painted gypsum. However, cement plaster is used at the external base of the northern lateral wall and at the top of the bell towers.

3.3.2 Internal timber frame

The internal space of Ica Cathedral is divided by a series of pillars, pilasters and piers that support the complex vaulted roof framing system. In the following section, a general and qualitative description of the timber structure is provided. More details concerning the representative bay of the cathedral will be presented in **Section 3.5**.

The pillars and the pilasters are essentially hollow structures constructed by applying the *quincha* technique. In general, they are composed of numerous posts with a wood sill plate embedded in the fired brick base. Horizontal and vertical elements are used to connect the posts by means of nails and dowels, increasing the resistance against horizontal forces and buckling. The hollow structures are wrapped with flattened cane reeds or *caña chancada,* which are attached to the battens with nailed leather strips and finished with mud plaster and gypsum.

For a better understanding of the structure, the several pillars of Ica Cathedral can be classified as follows (**Figure 24** and **Figure 25**):

- **Four central pillars** that are located at the corner of the crossing of the main nave and the transept. Each of these pillars is composed of twelve vertical posts that are connected to each other by horizontal bracing. The four ones located in the inner core support the beams of the square frame that in turn carry the main dome (further detail in **Section 3.6.2**).
- **Eight nave pillars,** spaced at approximately 5m**,** that separate the main nave from the side aisles supporting (1) the barrel vaults with lunettes over the nave and (2) the beams at the base of the side aisle domes. Each pillar is composed of eight vertical posts and one tree trunk located in the central part, which are connected to each other by horizontal and diagonal elements (further detail in **Section 3.5.2**).

- **Pilasters**, i.e. engaged pillars, which are aligned with each nave pillar and are close to the lateral masonry walls. Each pilaster is composed of four vertical posts with horizontal and diagonal bracing.
- **Piers** that are made of mud brick with fired brick strengthening are located behind the pilasters of the side aisles – mainly on the cloister side.

The pillars have a fired brick foundation that extends from 0.50 m below the floor level to 0.80 m above creating a pillar base (Garcia Bryce & Soto Medina, 2014). The foundation of the pilasters is similar to those at the lateral masonry walls. However, it is important to notice that the bricks at the pilasters' base do not interlock with the brick course along the lateral walls (Cancino, et al., 2012).

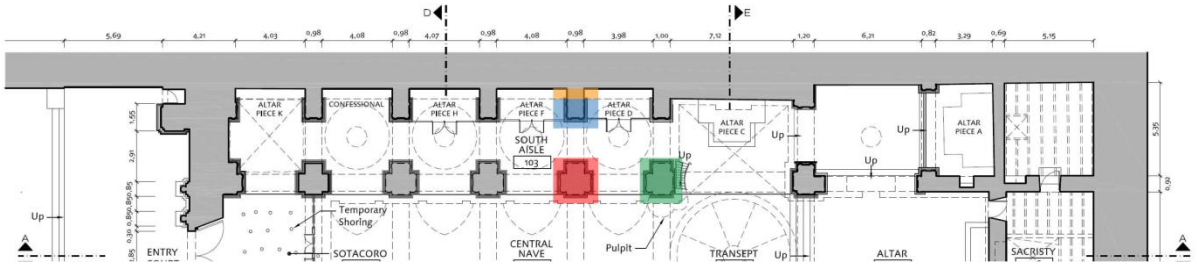

Figure 24. Pillars of Ica Cathedral: pillar of the crossing (green), nave pillar (red), pilaster (blue) and pier (orange) (Cancino, et al., 2012).

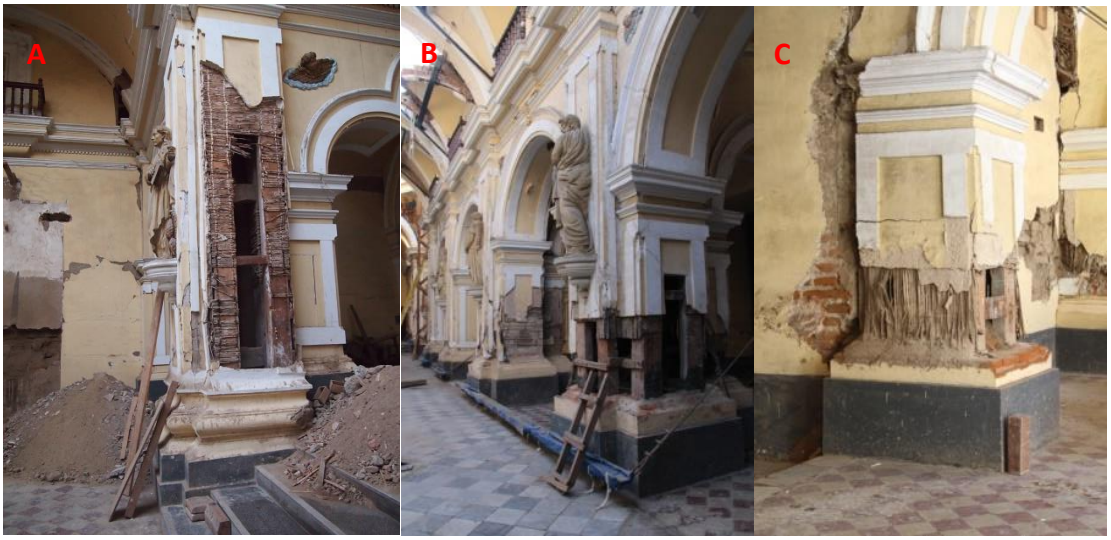

Figure 25. (A) Pillar of the crossing (Image: Emilio Roldán Zamarrón for GCI), (B) Nave pillar, (C) Pilaster with the pier behind.

A couple of **timber frameworks** joins (1) all the nave pillars in the east–west direction, (2) each nave pillar and pilaster in the south–north direction and (3) all the pillars of the transept in the south–north direction, as shown in **Figure 26**. Generally, each framework is composed of two main inclined

elements that are connected to the beams and the posts by means of diagonal elements. The connections between these elements are mortise and tenon with nails. Wooden arches that are likely to be non-structural are nailed on both sides of the timber framework.

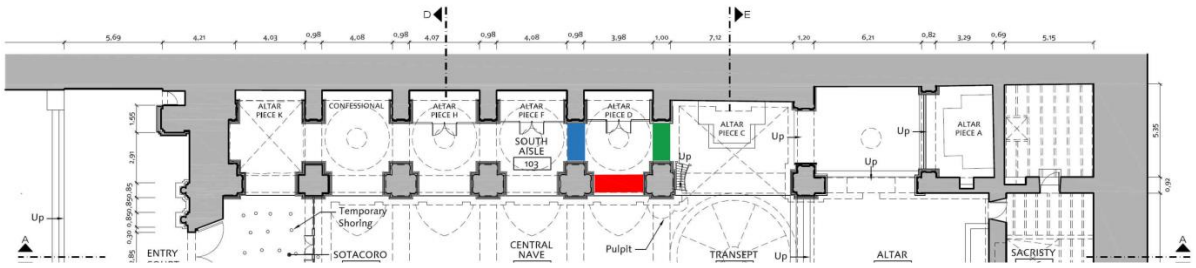

Figure 26. Couples of wooden frameworks between nave pillars (red), nave pillar and pilaster (blue) and pillar of the transept and pilaster (green).

A series of **longitudinal and transversal beams** rest on the posts with mortise and tenon connections. A connection between the timber and masonry structure is present at each transversal beam. However, the effectiveness of these joints has not been verified by any of the inspections that have been carried out in Ica Cathedral (**Figure 27**).

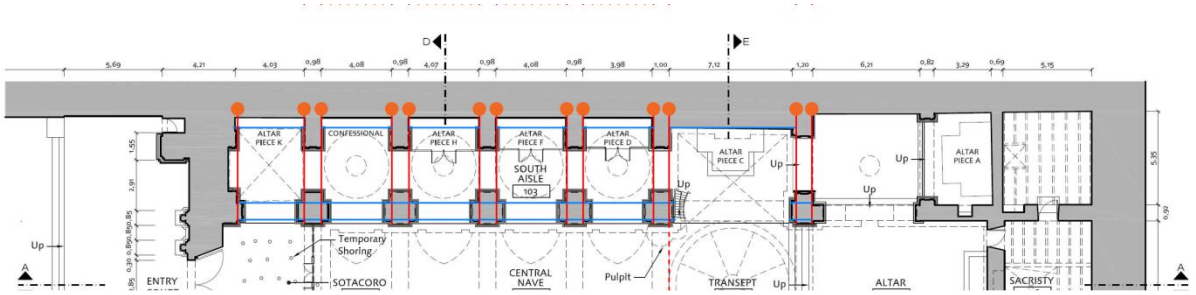

Figure 27. Schematic of the horizontal elements of Ica Cathedral: longitudinal beam (blue), transversal beam (red) and connection between timber and masonry structures (orange).

As mentioned in **Section 3.2.2,** a vaulted roof framing system is located on the top of this system. The main umbrella dome and the smaller ones that cover the side aisles seem to be similar in construction (Cancino, et al., 2012). In general, they are composed of several ribs and two ring beams. The latter are located at the top and at the bottom of each dome. Concerning the barrel vaults, they are constructed by a system of principal and secondary wood arches. At the central nave, the barrel vaults are characterized by lunettes corresponding to the location of the windows in the upper nave walls. Because of large spans, each curved timber element consists of several segments made of planks connected together by plain lap joints with four wrought iron handmade nails in a triangular pattern (Ferreira & D'Ayala, 2012).

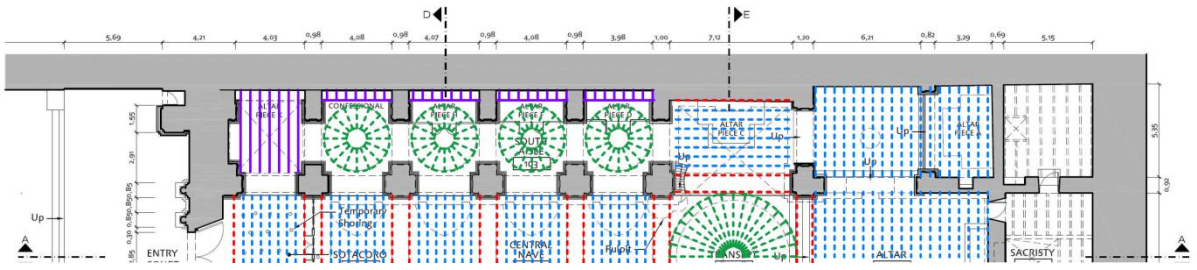

Figure 28. Schematic of the vaulted roof framing system of Ica Cathedral: principal arch (red), secondary arch (blue), vertical and horizontal ribs of the main dome and ribs of the aisle's dome (green) and flat ceiling (purple).

The intrados of the vaulted roof framing system is covered by plaster and *caña chancada* (flattened cane reeds) attached to the wooden arches with nailed leather strips, while its extrados is covered by *caña brava* (cane reeds) attached with nails and finished with layers of mud plaster. A flat wooden ceiling is used to cover the area surrounding the aisles' domes and the space between the timber and the masonry structures. Layers of fired brick masonry and sand, lime and cement mortar are located at the top of this flat roofed areas.

Three wood species are present in Ica Cathedral: cedar (*Cedrelaodorata*), sapele (*Entandrophagmasp*) and huarango (*Prosopissp*). While the former is a softwood species, the latter are hardwood ones. Each of these species is used for different purposes throughout the structure according to their characteristics. Cedar is used for the curved elements of the vaulted roof framing system. The timber species with the highest modulus of elasticity, i.e. huarango, is used for the central posts of the nave pillars supporting the arcade plates, hence the whole vaulted roof framing system. All the other wooden elements of the structure are made of sapele.

3.4 Recent damage

The 2007 Pisco earthquake affected significantly the Cathedral of Ica. The resulting condition of the cathedral, as well as damage, can be found in Cancino et al. (2009). The 2009 earthquake off the coast of the central Peru aggravated the damage with the total collapse of the main dome, already much damaged from the previous earthquake.

The current damage and decay of Ica Cathedral is presented in this section taking into account the situation after the 2007 Pisco earthquake (Cancino, et al., 2012) and the observations in the recent survey campaign (Greco, et al., 2015).

3.4.1 Side aisles

The damage and decay that are present in the southern side aisle are shown in **Figure 29.** Plaster detachment and disintegration of the masonry can be observed in the wall and in the base course due to humidity. Vertical cracks are present between the pilasters and the lateral wall due to the lack of connection between the bricks that compose the pier bases and the brick base of the masonry envelope. Moreover, horizontal cracking is present along the southern mud brick wall. The arches attached to the southern mud brick wall are partially collapsed. Out-of plane displacement is observed at the arches between the side aisle and the main nave.

Concerning the northern side aisle, horizontal cracking is present at the upper and lower levels. Minor inward out–of–plane displacement can be observed for the pillar wall. Vertical cracks affect some piers and one of the arches that is adjacent to the wall is partially collapsed.

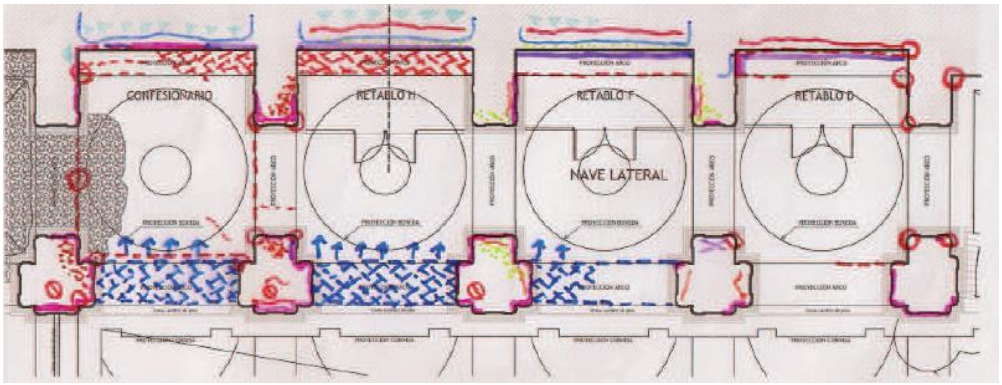

Figure 29. Graphic condition survey of the south side aisle: humidity (light blue arrows), vertical cracks (red circles), horizontal crack (red line), partial collapse (red hatch pattern), out-of plane displacement (dark blue hatch pattern and dark blue arrows) (Cancino, et al., 2012).

3.4.2 Main nave

The main nave is one of the most damaged parts of Ica Cathedral, as shown in **Figure 30**. Termite damage is located in correspondence to the primary arches of the barrel vaults, the lunettes' ribs and the nave pillars. The central portion of barrel vaults that are in the eastern end of the nave are partially collapsed. Several cracks can be observed on the vaulted roof framing system. Structural deterioration affects the nave pillars because of heavy termite damage, rot due to rising damp in the brick bases below and detachment of the plaster. Moreover, diagonal cracks can be observed as the result of the earthquakes experienced. Where the plaster has been lost, the wooden elements are exposed to further deterioration. The huarango tree trunk is still in good condition because of its

central position in the nave pillar and higher strength. It should be noted that the central portion of the eastern–most nave vault collapsed several months after the 2007 Pisco earthquake: the vault was intact until November 2007 with cracking in the area that would collapse later, as shown in **Figure 32**. This was likely due to the heavy termite damage of the wood element and the corrosion of the nailed connections (Cancino, et al., 2012), but also possibly creep effects.

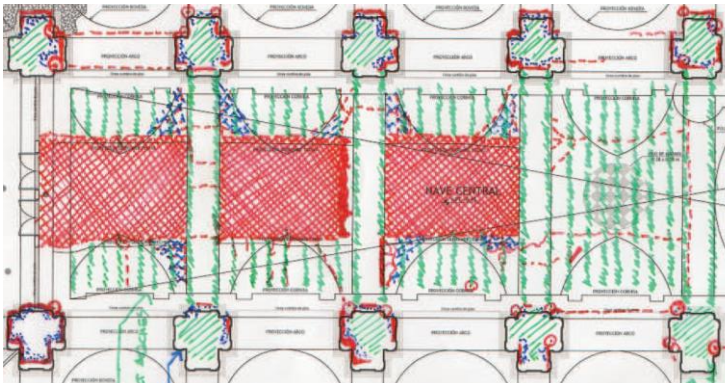

Figure 30. Graphic condition survey of the main nave: termite damage (green line), partial collapse (red hatch pattern), cracking (red line) (Cancino, et al., 2012).

A rocking mechanism of the pillars was observed during the 2007 Pisco earthquake with a structural disconnection between the pillars and their base and the pillars and the arches above. Moreover, the rocking of the pillars increased the demand to the already deteriorated wood vault arches breaking them into pieces and leading to failure of the mortise and tenon joints. The timber vaults of the cathedral collapsed due to the shear failure of the beams at the top of the lunettes as their shear strength and tensile strength perpendicular to the grain had been significantly compromised by termite damage (Ferreira & D'Ayala, 2012). At the same time, the beams of the lunettes may have prevented the total collapse of the barrel vault in these bays as shown in **Figure 31** (Cancino, et al., 2012).

3.4.3 Transept

Cracking and disconnection are present between the arms of the transept and the side aisles and the arms of the transept and the chapels. Moreover, out–of–plane displacement in correspondence to the southern lateral wall can be observed. A partial collapse of the southern section of the main dome was observed after the 2007 Pisco earthquake. Today, the main umbrella is totally collapsed, as shown in **Figure 32.**

Figure 31. (A) Partial collapse of the barrel vaults (Image: Emilio Roldán Zamarrón for GCI), (B) Mortise and tenon connections at the top of the lunette (Image: Emilio Roldán Zamarrón for GCI) (C) Corrosion of the nailed connection of the arches of the barrel vaults (Cancino, et al., 2012) (D) Detail of the lunette's beam (Cancino, et al., 2012).

Figure 32. (A) and (B) Partial collapse of the main dome after the 2007 Pisco earthquake (Cancino, et al., 2012), (C) and (D) Total collapse of the main dome actually.

3.5 Representative bay

3.5.1 Structure

A detailed description of the representative bay of Ica Cathedral is presented in terms of dimensions and types of connection of the wooden elements in the following section. In order to better understand its complex geometry, it is possible to divide the representative bay into the following parts (**Figure 33**):

- **A barrel vault with lunettes** that is composed of two principal arches and a series of secondary arches;
- **Two aisles' domes** that are composed of sixteen vertical ribs and two ring beams at the bottom and at the top;
- **Aisles' joists** that are used for the flat roofed area;
- **A system of longitudinal and transversal beams** that support the barrel vault and the aisles' roof system;
- **Two nave pillars and two pilasters** that support the upper system of longitudinal and horizontal beams (further details in **Section 3.5.2**);
- **Timber frameworks** that support the upper system of beams and connect the nave pillars and the pilasters.

The members in each part of the timber framing are connected to the adjacent members by means of different types of timber joints (Ferreira & D'Ayala, 2012). A brief summary of the connections of the representative bay is presented in **Figure 33** and in **Table 14**. In particular, the lunette structure that is located at each side of the barrel vault is composed of (1) an horizontal beam, (2) eight lateral ribs, (3) a central rib and (4) two diagonal elements. Mortise and tenon joints are used to connect the lunette's ribs and diagonals with the secondary arches of the barrel vault. The horizontal beam at the top of the lunette is perforated with multiple mortise holes to receive both the tenons of the secondary arches and lunettes' ribs. The diagonals and the ribs of the lunette are connected by means of one or two nails. The beam of the lunette is connected to the principal arches by means of mortise and tenon joints. It should be noted that the dimension and the layout of these mortise and tenon joints are different for each connection (Ferreira & D'Ayala, 2014). However, no quantitative information seems to be available about the lunette structure.

As previously mentioned, cedar, sapele, and huarango are the species of wood that are present in Ica Cathedral. Their distribution throughout the representative bay is described in **Table 15**.

Figure 33. The main parts of the representative bay: (A) Barrel vault with lunettes, (B) Aisles' domes, (C) Aisles' joists and (D) Timber framework.

Table 14. Connections of the representative bay in Ica Cathedral.
Note that the letters in the brackets refer to Figure 33.

Wood species	Structural elements
Nailed	Planks of the principal and secondary arches of the barrel vault (triangular pattern) – Vertical ribs of the domes (triangular pattern) – Diagonal elements of the pilasters and of nave pillars – Diagonal and horizontal elements of the timber frameworks with the posts of nave pillars and pilasters (A).
Mortise and tenon	Principal arches with the longitudinal beams – Posts of the pilasters and of the nave pillars with the longitudinal and transversal beams (B) – Horizontal elements with the posts of the nave pillars and of the pilasters (with dowels) – Lunettes' ribs/ Lunettes' diagonals with the beam at the top of lunettes – Lunettes' diagonals/ Lunettes' arches with longitudinal beams.
Half–lap	Transversal with longitudinal beams (C).
Not specified	Aisle's joists with transversal beam – Ring beams with the beams and the vertical ribs.

Table 15. Distribution of the wood species throughout the representative bay.

Wood species	Structural elements
Cedar	Planks of the principal and secondary arches of the barrel vault – Ribs of the domes – Lunettes' structure (with the exception of the beam on the top).
Sapele	Longitudinal and transversal beams – Horizontal bracing – Diagonal bracing – Beam on the top of lunettes – Aisle's joists – Posts of pilasters – Posts of the nave pillars (with the exception of the central one).
Huarango	Central post of the nave pillars.

3.5.2 Visual inspection and geometrical survey

An additional (and very limited in time) campaign has been recently undertaken in order to verify the current condition of Ica Cathedral (Greco, et al., 2015). The in–situ observations and the geometrical survey have allowed to complement the existing documentation concerning the structural configuration, as well as the dimensions and the types of connection of the wooden elements. In particular, the survey of a nave pillar and the visual inspection of the southern side aisle have provided new information regarding the representative bay.

The visual inspection of the nave pillar has confirmed that (1) the posts have different cross sections that vary significantly, (2) horizontal and diagonal elements connect the posts and (3) a huarango tree trunk is located in the inner part of the nave pillar. Moreover, it should be noted that the posts are laid directly on the fire brick base below and no evidence of the presence of the sill plate has been found (**Figure 34**). A geometrical survey of the main wooden elements that compose the nave pillar and the pilaster has been carried out. The characterization of the cross section for each post that compose the surveyed nave pillar is presented in **Table 16**. The number and the spacing of the wooden elements have been measured in order to characterize the horizontal and diagonal bracing that are present in the pillars. A detailed description can be found in **Figure 36**.

Figure 34. Survey of the nave pillar: (A) View of the nave pillar, (B) Connection between the posts and the fire brick base and (C) Detail of the huarango trunk tree.

Table 16. Approximate cross section dimensions of the posts of the nave pillar (Greco, et al., 2015).

Wooden post	Dimension [mm]
1, 2, 5, 7, 8, 9	220 x 120
3, 4	220 x 220
6	300 x 300

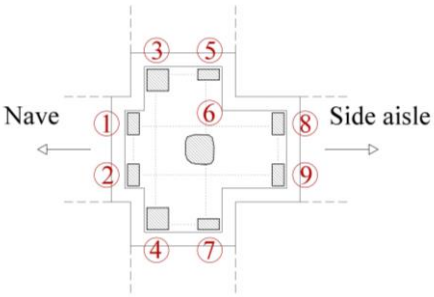

Inspection was possible in the damaged area of the southern side aisle and has confirmed the roof framing system described in the previous section. Geometrical information have been obtained concerning the transversal and longitudinal beams. In particular, it has been observed that the longitudinal beam that is adjacent to the masonry wall is composed of one wooden element with a cross section of 250x120 mm^2. On the other hand, the transversal beam consists of two of the same elements connected by leather strips. It should be mentioned that the ring beam at the bottom of the aisle's dome seems to be at the same level of these transversal and longitudinal beams.

3.5.3 3–D architectural model

The 3–D architectural model in AutoCAD of the representative bay has been constructed on the basis of the information available in literature (Cancino, et al., 2012), complemented by the recent survey described (Greco, et al., 2015). However, doubts still persist over the complex geometry of the representative bay and clarification of these doubts would require additional site visits. All the information used for constructing this model can be classified depending on the level of confidence (LC) associated with each of them. Four levels of confidence are considered here (**Figure 35**):

- LC3: Wooden elements that are characterized by visual inspection and geometrical survey;
- LC2: Wooden elements that are characterized by visual inspection;
- LC1: Wooden elements that are characterized by information available in literature;
- LC0: Wooden elements that are characterized by little or no information.

It should be mentioned that a standardization of the cross sections of the wood elements composing the pillars has been necessary due to the large variability present in the obtained data. Regarding the distribution of the horizontal and diagonal elements, no simplifications have been taken into account. The detailed layout of the nave pillar and the pilaster that has been used to create the

model is presented in **Figure 36**. Note here that the numbers in the vertical view (e.g. 1/3 and 2/4, indicate that this is the framework connecting posts 1-2 and 3-4).

The geometrical information is summarized in the following architectural drawings (**Figure 37** and **Figure 38**). The resulting 3–D architectural model is shown in **Figure 39** and has been used in the development of the 3-D finite element (FE) model shown in the following sections.

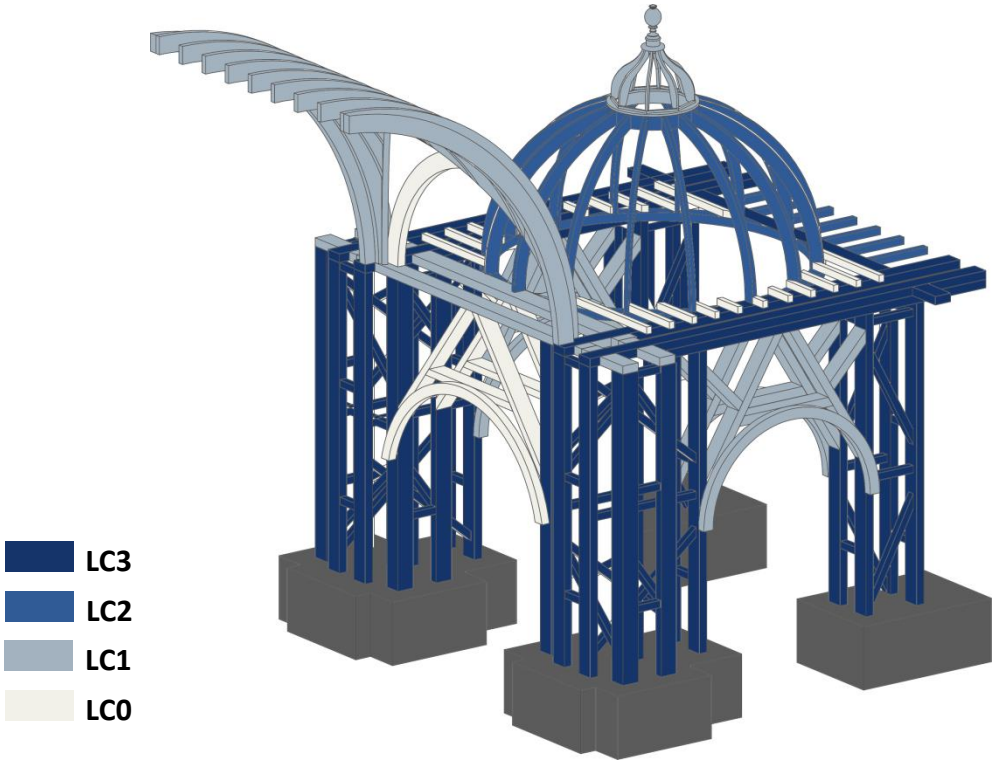

Figure 35. Mapping of the levels of confidence for the representative bay.

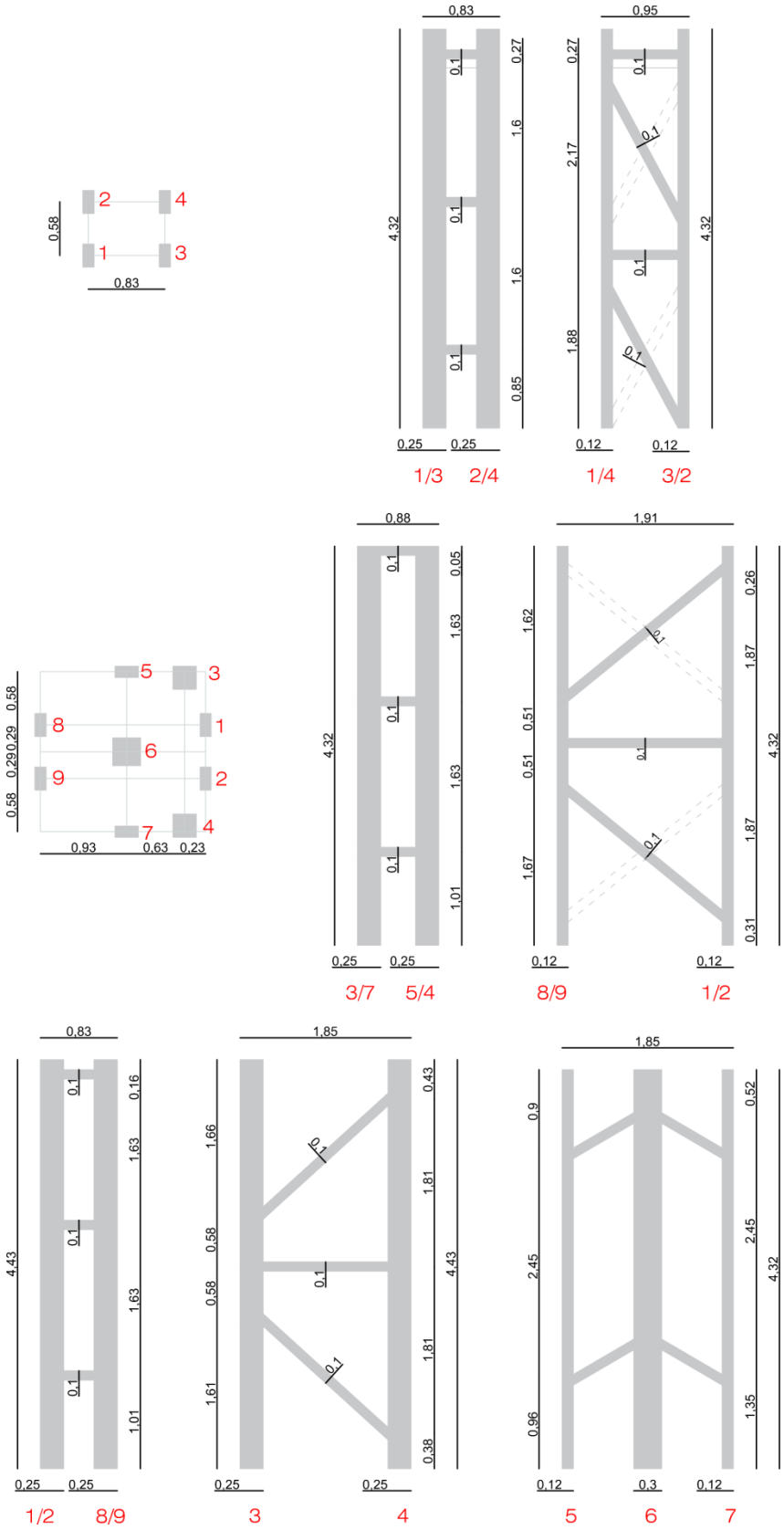

Figure 36. Characterization of the pilaster (top) and the nave pillar (bottom).

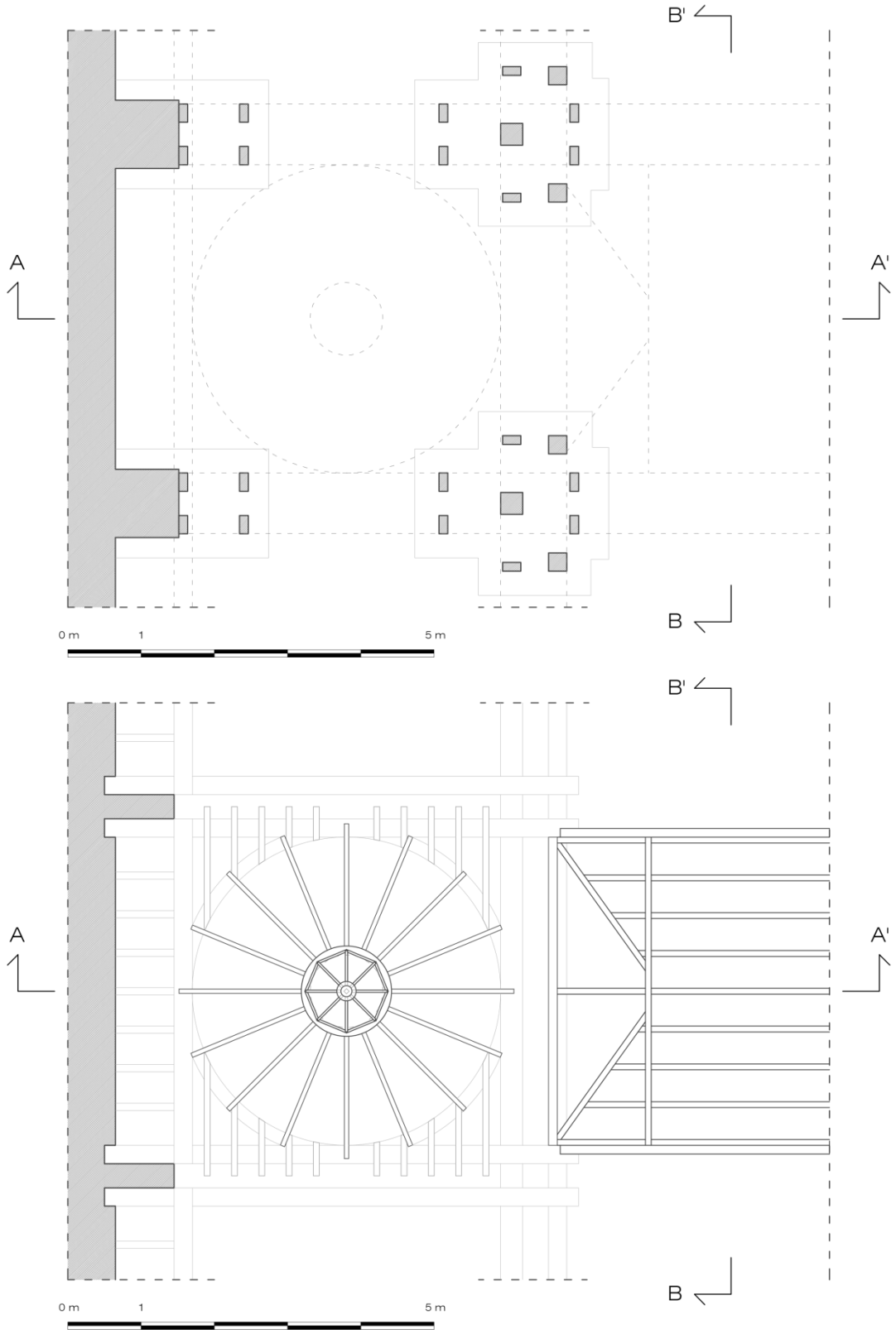

Figure 37. Ground plan (top) and roof plan (bottom) of the representative bay of the Ica Cathedral.

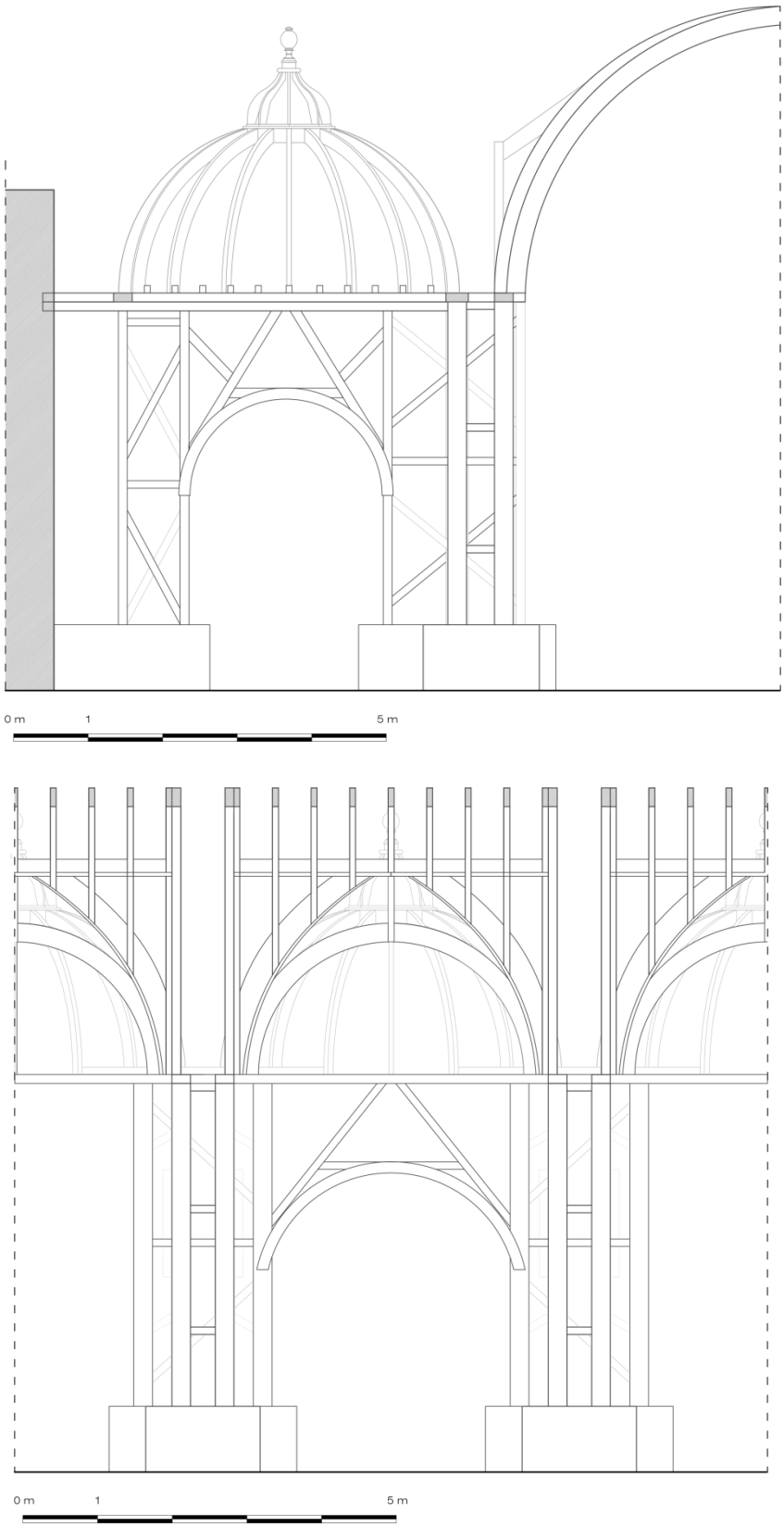

Figure 38. Section A–A' (top) and section B–B' (bottom) of the representative bay of the Ica Cathedral.

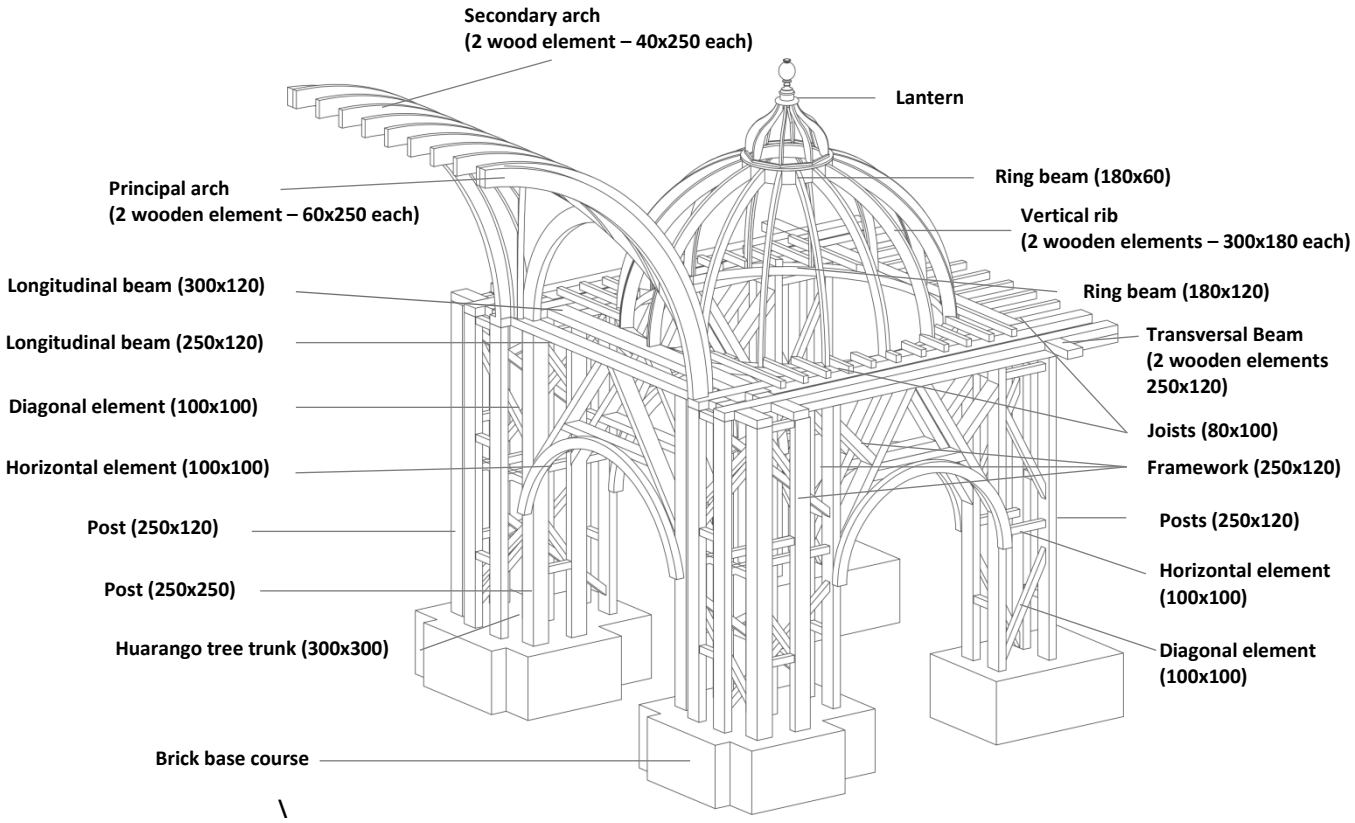

Figure 39. Main elements of the representative bay of the Ica Cathedral.
Note that the dimensions are in mm.

3.6 Transept

3.6.1 Structure

A qualitative description of the bay of the central dome is presented in the following section. Although the available information about this sector of Ica Cathedral is limited, an overview of the main parts which probably compose the transept is provided. In order to better understand the whole structure of the transept, the following parts can be identified:

- **The main dome** that is composed of thirty-two vertical ribs connected by a series of elements parallel to the ring beams that are located at the bottom and at the top;
- **A square frame** that is made of two wooden beams for each side which are connected at the corners;
- **Diagonal elements** that reinforce the square frame at the corners;
- **Crossing arches** that are composed of principal arches and are located at the lower part of each side of the square frame;

- **Two barrel vaults** that are composed of two principal arches, a series of secondary arches and vertical elements bracing the arches close to the longitudinal walls;
- **A system of longitudinal and transversal beams** that supports the barrel vaults and the aisles' roof system;
- **Four central pillars and four pilasters** that support the main dome and the system of the transversal and longitudinal beams (further details in **Section 3.6.2**).

Compared to the representative bay, it should be noticed that no evidence of the presence of timber framework is found in the transept. Collecting the information available in literature (Cancino, et al., 2012) and assuming some similarities to the representative bay, a brief summary of the possible connections and distribution of material of the transept is presented in **Table 17.**

Table 17. Possible connections of the transept in Ica Cathedral.

Type of joints	Structural linked elements
Nailed	Planks of the principal and secondary arches of the barrel vault (triangular pattern) – Vertical ribs of the main domes (triangular pattern) – Diagonal elements of the pilasters and of the pillars.
Mortise and tenon	Principal arches with the transversal beams – Posts of the pillar with the beams of the square frame (with leather straps) – Posts of the pilasters and of the pillars with the longitudinal and transversal beams – Horizontal elements of the pillars and of the pilasters (with dowels) – Ring beam at the bottom with the vertical ribs.
Half–lap	Beams of the square frame (with leather straps and nails)
Not specified	Ring at the top with the vertical ribs – Diagonal elements with the beams of the square frame – Vertical ribs with the parallel rings of the main dome – Vertical elements with the arches of the barrel vaults and the beams.

Table 18. Possible distribution of the wood species throughout the transept

Wood species	Structural elements
Cedar	Planks of the principal and secondary arches of the barrel vaults – Vertical ribs and parallel elements of the main dome – Ring beams at the bottom and at the top of the main dome – Vertical elements of the barrel vaults.
Sapele	Longitudinal and transversal beams – Horizontal bracing of the central pillars and of the pilasters – Diagonal bracing of the pilasters – Beams of the square frame –– Posts of the pilasters – External posts of the central pillars – Diagonal elements.
Huarango	Central posts of the central pillars.

3.6.2 Visual inspection and geometrical survey

During the recent campaign presented in **Section 3.5.2,** the visual inspection and the geometrical survey of the south–western central pillar of the transept have been carried out (Greco, et al., 2015). Inspection pits and partial collapses allowed access to one of the central pillars and the detailed configuration of the posts, and of the bracings has been assessed. As previously described in **Section 3.3.2**, typically the central pillar of the transept is composed of several wooden elements that differ in height, cross section, bracing and connections. The visual inspection has confirmed the hollow structure of the central pillar which consists of four main posts surrounded by eight posts with smaller dimensions. In particular, the former which has a higher height supports the beams of the square frame that in turns carries the main dome. Moreover, the survey performed on the lower part of the pillar suggests that these posts are made of huarango. The configuration and the indicative values of the measured cross sections are shown in **Table 19.** It should be noticed that only horizontal bracing has been observed and no evidence of diagonal elements has been found in the surveyed pillar, as shown in **Figure 40.** The characterization of the horizontal bracing can be found in **Table 20.**

Table 19. Configuration and cross section dimensions of the posts of the central pillar (Greco, et al., 2015).

Wooden post	Dimension [mm]
4, 5, 8, 9	240 x 240
3, 7	220 x 220
1, 2, 6, 10	220 x 100
11, 12	140 x 300

Figure 40. Posts and horizontal elements of the central pillar (Image: Emilio Roldán Zamarrón for GCI).

Table 20. Characterization of the horizontal connections of the central pillar (Greco, et al., 2015).

Connection	Number of connections	First connection level [m]	Dimension [mm]	Spacing [m]
1, 2 - 6, 10	3	1.35	70 x 100	1.40
5, 9 - 4, 8	3	0.40	110 x 220	1.60
8, 9 - 4, 5	3	1.00	110 x 220	1.45
3, 7	2	1.15	110 x 220	-
9, 12	3	0.50	100 x 100	1.50-2.00
8, 11	3	1.80	100 x 100	1.50-2.00

3.6.3 3–D architectural model

On the basis of the information available in literature (Cancino, et al., 2012), the data collected in the recent survey (Greco, et al., 2015) and some similarities to the representative bay, the 3–D architectural model in AutoCAD of the transept has been constructed. The resulting 3–D architectural model is shown in **Figure 41** and has been used in the development of the subsequent 3-D finite element (FE) model.

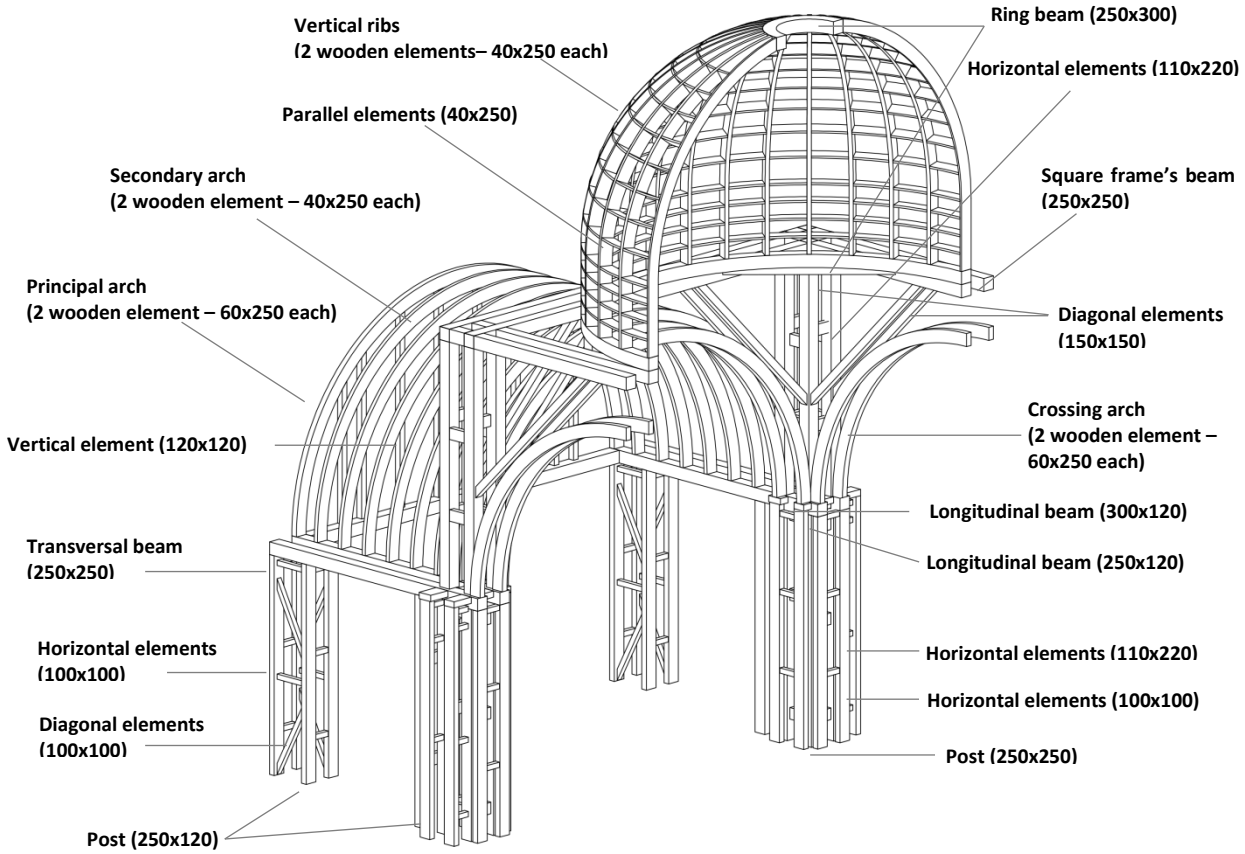

Figure 41. Main elements of the representative bay of the Ica Cathedral.
Note that the dimensions are in mm.

Chapter 4

The representative bay

The following chapter deals with the structural analysis performed on the representative bay of Ica Cathedral under vertical and lateral loads. Moreover, the influence of the timber connections is investigated and the most critical joints are identified using a representative bay. Considering self–weight and live load, the compliance with the various criteria specified by Eurocode 5 (2004) is evaluated by performing global and local verifications on the timber members and connections. Finally, in order to discuss the actual failure, a seismic assessment of the connections of the barrel vault is presented.

4.1 Definition of the model

4.1.1 Geometry

The 3D finite element model of the representative bay is constructed in SAP 2000 structural and earthquake engineering software. The numerical model includes all the parts of the representative bay described in the 3D architectural AutoCAD model with the exception of (1) the brick base course at the base of the pillars and of the pilasters, (2) the flat roofing system close to the masonry walls and (3) the “arches” below the system of beams, which are assumed as non-structural.

According to the generated 3D architectural AutoCAD model described in **Section 3.5**, the model of the representative bay is initially constructed in AutoCAD to deal with the complex curved geometry, as shown in **Figure 42**. In particular, it should be noted that the model has to be discretized in accordance to the desired mesh in SAP2000 as the meshing is performed automatically while importing the model from AutoCAD to SAP2000. This discretization is constructed by using *Line* and *Arch* for straight and curved elements, respectively. It should be mentioned that it is not possible to use *Spline* to better represent the irregular curvature present in the timber structure as it cannot be meshed in SAP2000. Hence, a regular curvature is assumed for all the curved elements of the barrel vault and the aisles' domes so that they can be constructed as *Arch* in AutoCAD. Sequentially, they can be imported as *Frame* element in SAP2000. It should be mentioned that the number of *Frame* elements that discretizes each *Arch* is assigned automatically by the software. Besides, IGES format is used as it is the only format that allows the import of curved elements from AutoCAD to SAP 2000. The resulting FE mesh in SAP2000 is composed of 1136 nodes and 1344 *Frame* elements, as shown in **Figure 43.** By assuming the few simplifications described in **Section 3.5**, the cross sections are assigned to each *Frame* element. A summary of all the cross sections can be found in **Figure 2.**

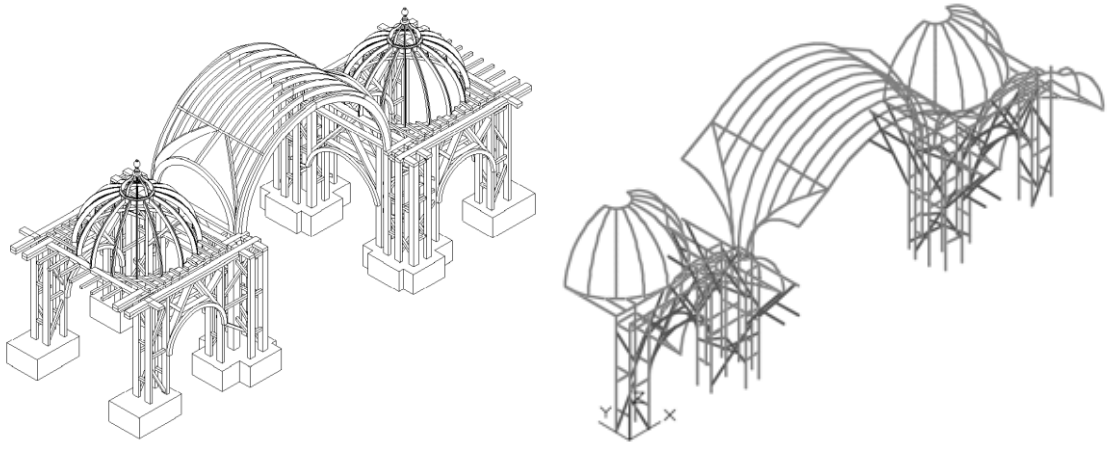

Figure 42. 3D architectural AutoCAD mode (left) and the discretized model in AutoCAD (right).

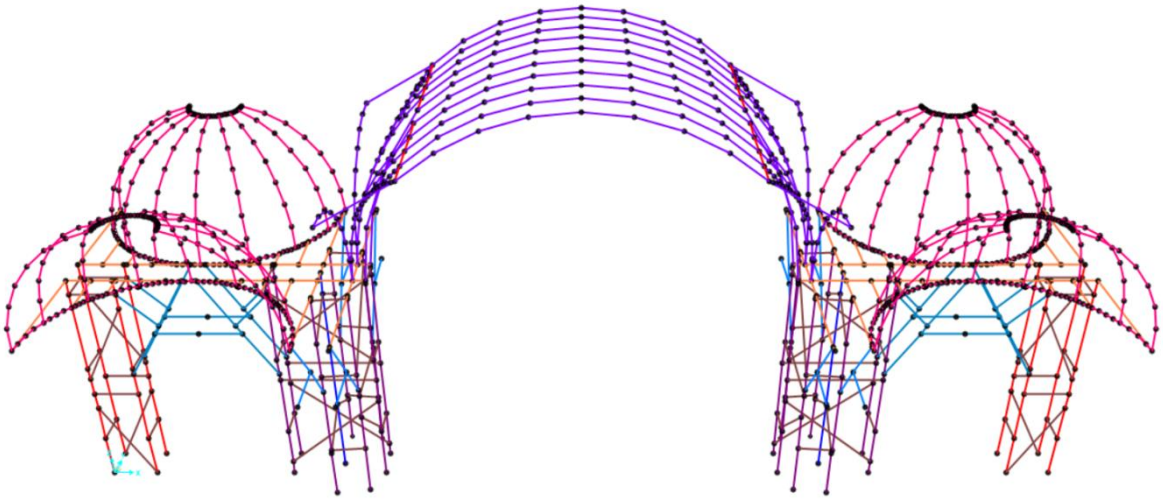

Figure 43. FE mesh in SAP 2000.

4.1.2 Material properties

The mechanical properties of timber depend on several parameters, such as density, shape and size, moisture content and presence of defects (such as knots, grain deviations, fissures and shakes). The material properties used in the numerical model of the representative bay are assumed on the basis of the results obtained from the experimental campaign carried out by the Pontificia Universidad Católica del Perú (PUCP) for the *Seismic Retrofitting Project* of the Getty Conservation Institute (GCI) (GCI & PUCP, 2014).

As described in **Section 3.5**, the wood species that are present in the representative bay are cedar, sapele and huarango. Testing of mechanical properties of cedar and huarango were carried out by PUCP on small clear specimens extracted from Ica Cathedral. On the contrary, no tests were performed on elements constructed in sapele, as they presented a higher level of deterioration. Hence, the characterization of sapele is derived from the testing on samples that were extracted by PUCP from Hotel El Comercio – which is also part of the Seismic Retrofitting Project (GCI & PUCP, 2014). It should be noted that the moisture content value of these sapele samples is higher than the reference one. Hence, adjustments are performed in order to correct some mechanical properties of sapele by applying EN 384 (2004) as follows:

- 3% change for every percentage point difference in moisture content for compressive parallel to grain strength;

- 2% change for every percentage point difference in moisture content for the modulus of elasticity;
- No adjustment for bending and tensile strength.

However, it is important to underline that a high level of uncertainties is still present on the properties for the mechanical characterization of the wood species present in Ica Cathedral as only a limited number of specimens were extracted. A summary of the material properties with the corresponding number of tests for each wood species is shown in **Table 21**. In particular, these material properties are used in the following to (1) evaluate an equivalent specific weight in **Section 4.1.3** and to (2) calculate the design load–carrying capacities in **Section 4.3.1.**

Table 21. Mean values of properties of the wood species by PUCP (GCI & PUCP, 2014).

	N° tests	Cedar	Huarango	Sapele*
Moisture content %	6	11.60	9.90	17.30
Density [g/cm3]	6	0.38	1.04	0.49
Modulus of elasticity in flexure [MPa]	4	$9.38 \cdot 10^3$	$16.88 \cdot 10^3$	$7.83 \cdot 10^3$ ($8.61 \cdot 10^3$)**
Bending strength [MPa]	4	75.77	152.96	61.47
Compressive strength parallel to grain [MPa]	4	27.26	92.18	33.39 (39.1)**
Compressive strength perpendicular to grain [MPa]	4	4.10	22.55	4.71
Shear strength[MPa]	4	8.67	20.79	6.29
Tensile strength parallel to grain [MPa]	3	21.19	61.86	47.87
Tensile strength perpendicular to grain [MPa]	7	0.88	1.91	1.64

* Values obtained from tests extracted from Hotel El Comercio

** Values corrected by applying EN 384 (2014)

4.1.3 Loading condition

As described in Chapter 3, Ica Cathedral is constructed with *quincha technique*: pillars, pilasters, beams, vaults and domes consist of timber elements with several covering layers. For the purpose of this thesis, the weight of these covering layers is assumed to be distributed throughout the various timber members of the structure. In particular, the weight of these layers is taken into account by an increase in the specific weight of the timber elements that carry them. In other words, the specific weight assigned to these elements in the numerical model is not equal to the value corresponding to the wood species in which the timber element is constructed. However, it should be noted that not all timber elements have an increase in the specific weight. The value of the specific weight corresponding to the wood species is assigned to the diagonal and horizontal elements composing the bracing of pillars as well as the huarango post as they are assumed to be not directly in contact

with these layers. This assumption is an attempt to simulate the hollow interior structure that is a characteristics of *quincha* pillars.

The equivalent specific weight γ_{eq} of the timber elements with covering layers with cane and mud, and plaster with mud and gypsum is calculated by applying the following equation:

$$\gamma_{eq} = \frac{\gamma_t \cdot V_t + \gamma_c \cdot V_c}{V_t} \quad \textbf{(11)}$$

where:

- γ_t is the specific weight of the timber element that is assumed according to **Table 21**;
- γ_c is the specific weight of the layer covering the timber element that is assumed with a value of 18 kN/m^3;
- V_t is the volume of the timber element;
- V_c is the volume of the covering layer assuming a thickness of 8.5 cm, as shown in **Figure 44.**

According to Garcia Bryce & Soto Medina (2014), a thicker layer of brick masonry is located in correspondence of the longitudinal and transversal system of beams. For these beams, the equivalent specific weight γ_{eq} is calculated as follows:

$$\gamma_{eq} = \frac{\gamma_t \cdot V_t + \gamma_m \cdot V_m}{V_t} \quad \textbf{(12)}$$

where:

- γ_t and V_t as defined above;
- γ_m is the specific weight of the masonry covering the corresponding timber element of the longitudinal and transversal system of beams;
- V_m is the volume of the covering masonry layer assuming a thickness of 30 cm, as shown in **Figure 44.**

In order to accurately calculate the volumes of the timber elements and of the covering layers, the construction of the 3D architectural model described in **Section 3.5** is crucial. It should be mentioned that the covering layers confine the wood elements and an increase in the stiffness of the structural system should be considered. As it is very difficult to evaluate this contribution, the confinement and stiffness effects are not taken into account in this thesis. Hence, the values of the modulus of elasticity assigned to the various elements in the numerical model is assumed to be equal to the

value corresponding to the wood species in which the timber member is constructed. A summary of the material properties assigned to each element of the model of the representative bay is presented in **Table 22**.

In order to assess the compliance with Eurocode 5 (2004) in **Section 4.3**, a live load is applied on the roofing system of the representative bay. In particular a value of 0.50 kN/m^2 is assumed considering that access to the barrel vault, the aisles' domes and the flat roofing system is only for maintenance and inspections. The obtained values applied to the numerical model for these elements are presented in **Table 23**. It should be noted that half of the value of the live load is applied on the elements located in the planes with symmetry, such as the main ribs of the barrel vaults. In terms of self-weight – that takes into account the contribution of the permanent and non-permanent load – this is not necessary as only half of the actual cross section is assigned for these elements.

4.1.4 Restraints

Regarding the boundary conditions, the base of the posts composing the nave pillars and of the pilasters is pinned. Suitable restraints are applied in terms of horizontal displacement and rotation as prescribed by the symmetrical condition of the structure. It should be noted that no restraint is assumed in correspondence to the connection between the transversal beams and the masonry walls as the timber structure of the representative bay is assumed to be self–supporting – some observations regarding the influence of these restrains on the structural behaviour can be found in **Section 4.2.2**. Concerning the timber joints, they are modelled as hinges or rigid connections depending on the mechanical behaviour of the timber joints present in the representative bay. However, a few adjustments are necessary in order to simulate a realistic distribution of internal forces throughout the structure. For instance, moment release at the ends of each element composing the deck and torsion release of connections between the transversal and longitudinal beams are assumed in order to avoid excessive torsional moment in the system of beams. A summary of the constraints that are assumed for the timber connections is presented in **Table 24.**

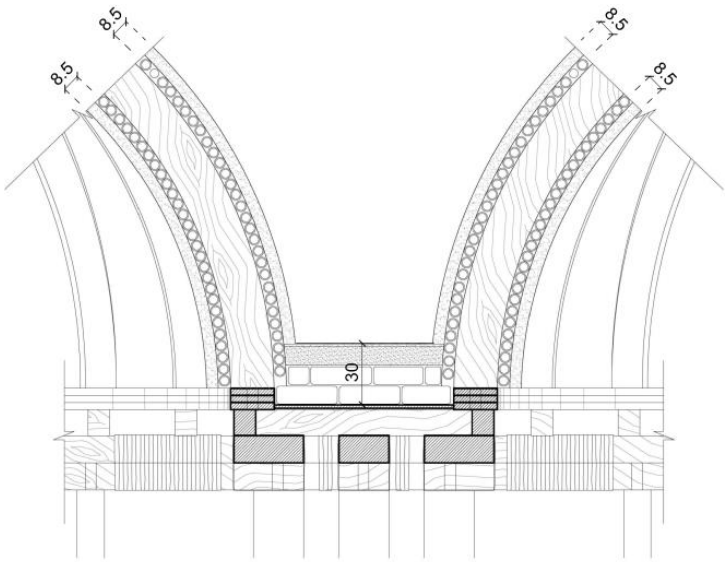

Figure 44. Assumptions on the covering layers on the timber structure (Garcia Bryce & Soto Medina, 2014).

Table 22. A summary of the geometrical and material properties for the model of the representative bay.

Structural Part	Element	Wooden Species	Equivalent Specific Weight [kN/m^3]	MOE [kN/m^2]	Base [m]	Height [m]
Barrel Vault with Lunettes	Principal Arch	Cedar	54.45	9.38E+06	0.12	0.25
	Secondary Arch	Cedar	54.45	9.38E+06	0.08	0.25
	Beam of the lunette	Sapele	54.45	8.61+06	0.06	0.25
	Diagonal of the lunette	Cedar	54.45	9.38E+06	0.08	0.25
	Arch of the lunette	Cedar	54.45	9.38E+06	0.12	025
Aisles' Domes	Vertical rib	Cedar	132.73	9.38E+06	0.18	0.12
	Ring beam at the top	Cedar	132.73	9.38E+06	0.06	0.18
	Ring beam at the bottom	Cedar	132.73	9.38E+06	0.06	0.18
Horizontal Elements	Longitudinal beam (I)	Sapele	70.83	8.61+06	0.25	0.12
	Longitudinal beam (II)	Sapele	70.83	8.61+06	0.30	0.12
	Transversal beam (III)	Sapele	70.83	8.61+06	0.25	0.25
	Longitudinal beam (IV)	Sapele	32.35	8.61+06	0.25	0.25
	Deck	Sapele	32.35	8.61+06	0.08	0.12
Framework	Longitudinal frame	Sapele	25.06	8.61+06	0.25	0.12
	Transversal frame	Sapele	39.69	8.61+06	0.25	0.12
Pilaster	Post	Sapele	33.25	8.61+06	0.25	0.12
Nave Pillar	Post (I)	Sapele	27.76	8.61+06	0.25	0.12
	Post (II)	Sapele	27.76	8.61+06	0.25	0.25
	Central post	Huarango	10.20	1.69+07	0.30	0.30
Bracing	Horizontal element	Sapele	4.81	8.61+06	0.10	0.10
	Diagonal element	Sapele	4.81	8.61+06	0.10	0.10

Table 23. A summary of the values of the live load applied to the numerical model.

Structural Part	Live load [kN/m]
Barrel Vault with Lunettes	0.28
Aisles' Domes	0.35
Horizontal Elements	0.20

Table 24. A summary of the constraints assumed for the timber connections of the representative bay.

Model of connection	Structural elements
Hinged	Posts of the pilasters and of the nave pillars with the longitudinal and transversal beams – Lunettes' ribs/ Lunettes' diagonals with the beam at the top of the lunettes – Lunettes' diagonals/ Lunettes' arches with longitudinal beams – Diagonal and horizontal elements of the pilasters and of nave pillars – Diagonal and horizontal elements of the timber frameworks with the posts of nave pillars and pilasters – Principal arches with the longitudinal beams – Vertical ribs of the aisles' dome with the ring beams – Joists of the deck with the transversal and ring beams.
Rigid	Transversal with longitudinal beams (with torsion release, when needed).

4.2 Structural Analysis

For the purpose of this thesis, it is assumed that the principal source of nonlinearity and permanent deformation comes from the timber joints. For this reason, the material behaviour of timber is assumed linear elastic isotropic and the classical beam theory, also known as the first order beam theory, is applied to perform structural analysis of the representative bay. The well–known assumptions on which the classical beam theory rest can be summarized as follows: (1) the cross section is planar and does not deform in its own plane, (2) small displacements with the exception of possible rigid body motion and small strain are assumed, and (3) the equilibrium equations are imposed on the initial undeformed configuration.

4.2.1 Analysis under vertical loading

A linear elastic analysis is performed on the model of the representative bay in order to investigate the capacity of sustaining vertical actions. A qualitative description of the distribution of internal forces and of displacements throughout the structure is presented in this section considering the following load scenarios: self-weight (G), live load (Q) and the load combination for ULS (1.35 G +1.50 Q). On the basis of the results obtained from this analysis, the evaluation of compliance according to

the various criteria specified by Eurocode 5 (2004) is carried out for serviceability limit states (SLS) and ultimate limit states (ULS) in **Section 4.3**.

The obtained results show that most of the elements of the structure are subjected to compressive axial forces. As expected, the highest and lowest values of axial forces occur in the posts and in the beams, respectively. Given the structural configuration, which resorts only to a small extent to triangular trusses, significant bending moments (and related shear forces) are observed in all elements with the exception of the horizontal and diagonal elements that work as struts or ties connecting the posts. In particular, high values of bending moments and shear occur in the beam at the top of the lunettes and in the longitudinal beams close to the masonry walls. In terms of displacement, the aisles' domes, the barrel vault and the longitudinal beam close to the masonry deform significantly compared to the rest of the structure. The deformed shape and the distribution of the axial forces obtained from the structure under the load combination for ultimate limit states are shown in **Figure 45** and **Figure 46.**

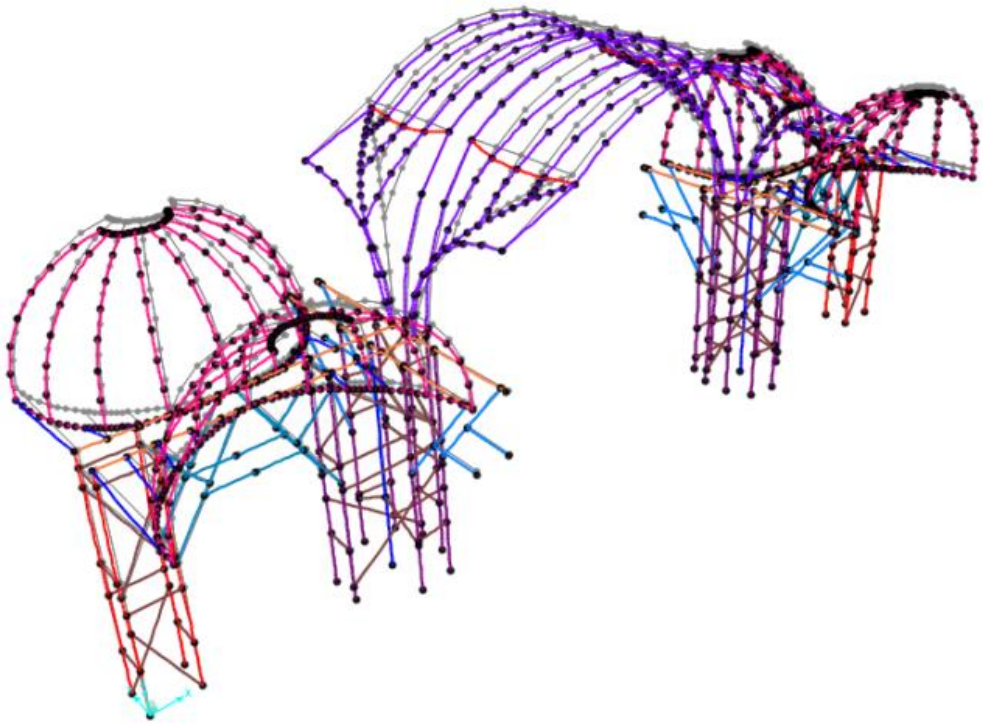

Figure 45. Deformed shape of the structure under the load combination for ULS.

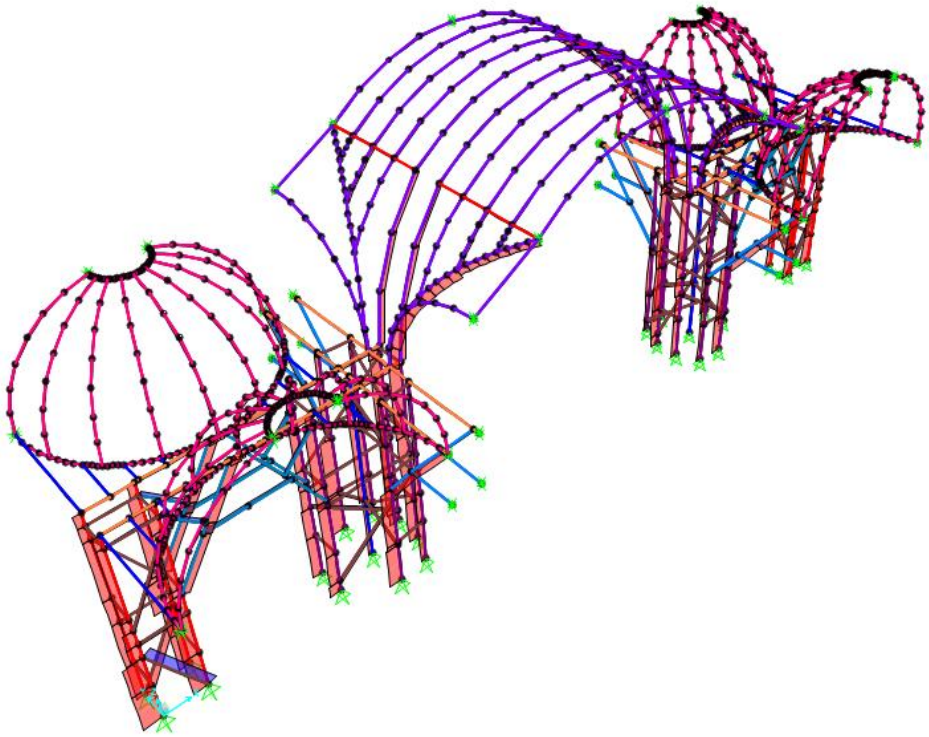

Figure 46. Distribution of axial forces in the structure under the load combination for ULS.

A comparison of the absolute maximum values of internal forces and displacements obtained considering the different load scenarios is presented in **Table 25**. It has to be noted that the values shown in **Table 25** for the load combination of ULS are not necessarily obtained by a linear combination of the values obtained under self – weight and live load individually. This is due to the fact that the maximum value of structural response does not always occur at the same location for different loading scenarios. Here, the subscripts 1, 2 and 3 indicate the local axes of the beam element, being 1 the longitudinal direction and 2,3 the directions along the cross section beam and height, respectively.

Table 25. Absolute maximum values of internal forces and displacements for different loading scenarios.
Note that (T) and (C) are the corresponding values axial forces in tension and in compression.

	P [kN]	$\mathbf{V_2}$ [kN]	$\mathbf{V_3}$ [kN]	**T** [kNm]	$\mathbf{M_2}$ [kNm]	$\mathbf{M_3}$ [kNm]	$\mathbf{u_1}$ [cm]	$\mathbf{u_2}$ [cm]	$\mathbf{u_3}$ [cm]
Self – weight (g_k)	20.8 (T) – 43.6 (C)	24.3	5.6	7.5	3.4	32	3.1	1.2	2.6
Live Load (q_k)	4.35 (T) – 7.1 (C)	4.4	19.5	1.1	0.7	4.5	0.4	0.3	0.6
(1.35 g_k +1.50 q_k)	34.7 (T) – 69.3 (C)	39.4	86	11.8	5.1	50.0	5.4	2.1	4.4

4.2.2 Parametric analyses under mass proportional lateral loading

Parametric analyses are carried out to investigate the effect of the principal timber joints of the representative bay by applying a lateral loading using a mass proportional approach. In particular, the lateral load is applied after having applied the self–weight load and only in the XX (or transversal) direction. In particular, the reference model that is described in **Section 4.1** is compared to several models that differ only by the assumptions made for specific sets of the timber connections. In particular, the following four models are considered considering independent sets of timber connections that are shown by red circles and rectangles in **Figure 47**:

- **SB 0**: Rigid connection for each joint;
- **SB 1**: Hinged connection for each joint of the posts with beams, diagonal and horizontal elements;
- **SB 2**: Hinged connection for each joint between the vertical ribs of the aisles' domes with the ring beams at the top and the bottom;
- **SB 3**: Hinged connection for each joint between the barrel vault and the lunettes.

It should be noted that only the specified set of timber joints is modelled as hinges for the specified model. In other word the models are not additive. The structural response of the representative bay is investigated in terms of structural stiffness from capacity curves, even if linear elastic behaviour only is considered. In particular, the control point is assumed as the node where the maximum lateral displacement is observed.

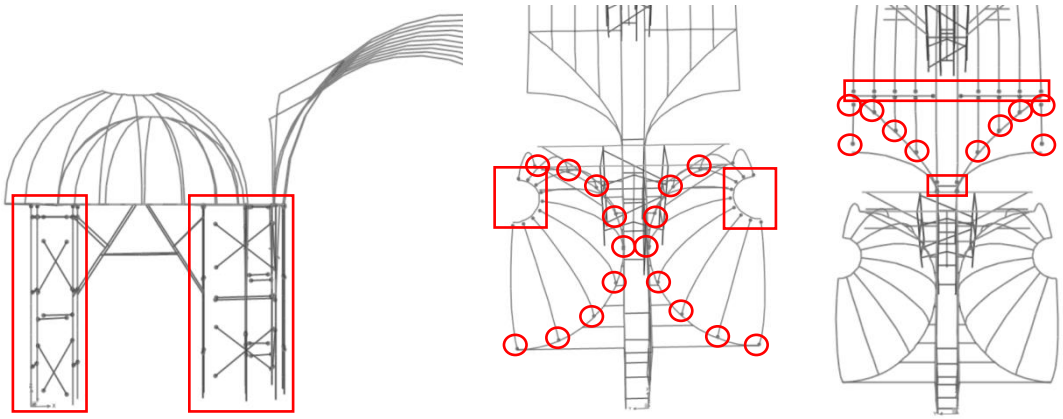

Figure 47. Sets of timber connections for parametric analyses performed on SB 1, SB 2 and SB 3.

As shown in **Table 26**, the value of linear elastic stiffness obtained in the model SB 0 with rigid connections is $7.7 \cdot 10^3$ kN/m. This value is the upper bound of the linear elastic stiffness provided by the structure when a lateral loading proportional to mass is applied. Releasing the timber connections of the posts with beams, diagonal and horizontal elements provides a value of global stiffness that is slightly lower than the previous one. On the contrary, a significant decrease in global stiffness is observed when the timber connections between the ribs and the ring beams of the aisles' domes are modelled as hinged in model SB 2. Finally, the linear elastic stiffness of the structure decreases drastically when bending moment is released for the nodes representing the set of the connections of the elements of the barrel vault with lunettes in model SB 3. The value reached in this model is almost the same of that obtained in the reference model of the previous section. The linear elastic stiffness of the structure obtained in the reference model, which is expected to be the best representation of the structure, had a value of $1.2 \cdot 10^3$ kN/m. The (linear elastic) capacity curves obtained for these models are shown in **Figure 48**.

Table 26. Values of global structural stiffness obtained using a parametric analysis on timber connections.

	REFERENCE MODEL	SB 0	SB 1	SB 2	SB 3
K [kN/m]	$1.2 \cdot 10^3$	$7.7 \cdot 10^3$	$6.4 \cdot 10^3$	$4.7 \cdot 10^3$	$1.3 \cdot 10^3$

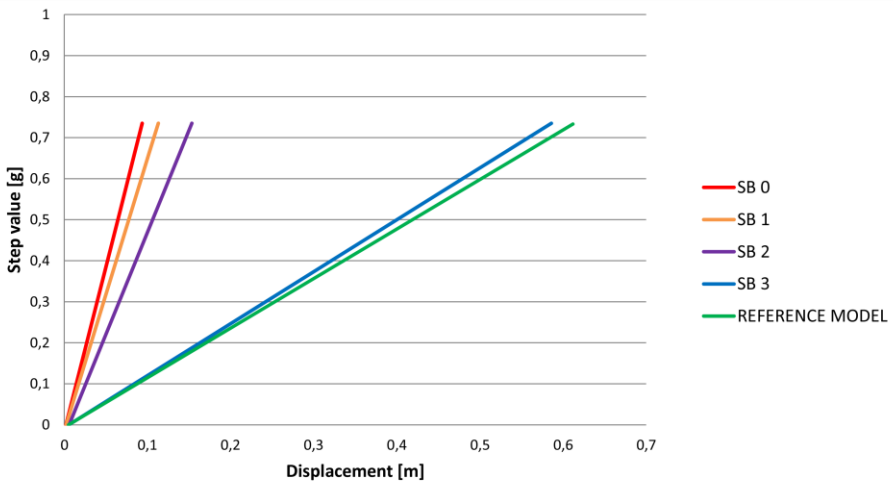

Figure 48. Capacity curves obtained from parametric analysis on the connections of the representative bay.

The obtained results show that the effect of the timber connections of the elements composing the barrel vault with lunettes is the most important to control the lateral stiffness. As a large number of connections is present in this part, the following three models are sequentially assumed considering subsets of the initial set of connections:

- **SB 3A**: Hinged connection for each joint of the principal arches, diagonals of lunettes and arch of lunettes with the system of beams below;
- **SB 3B**: Hinged connection for each joint at the ends of the main ribs of lunettes;
- **SB 3C**: Hinged connection for each joint between the ribs of lunettes and the beam at the top of them.

As shown in **Figure 49,** the timber joints between the principal arches, the diagonals of lunettes and the arches of lunettes and the system of beams below considered in model SB 3A are the most critical ones. The nodes representing the connections of the beams at the top of the lunettes that are released in model SB 3C have also a significant influence on the structural response. Finally, the structural behaviour of model SB 3B is very similar to that observed for model SB 0. A summary of the linear elastic values obtained by considering several subsets for the connections that are located in the barrel vault is presented in **Table 27**.

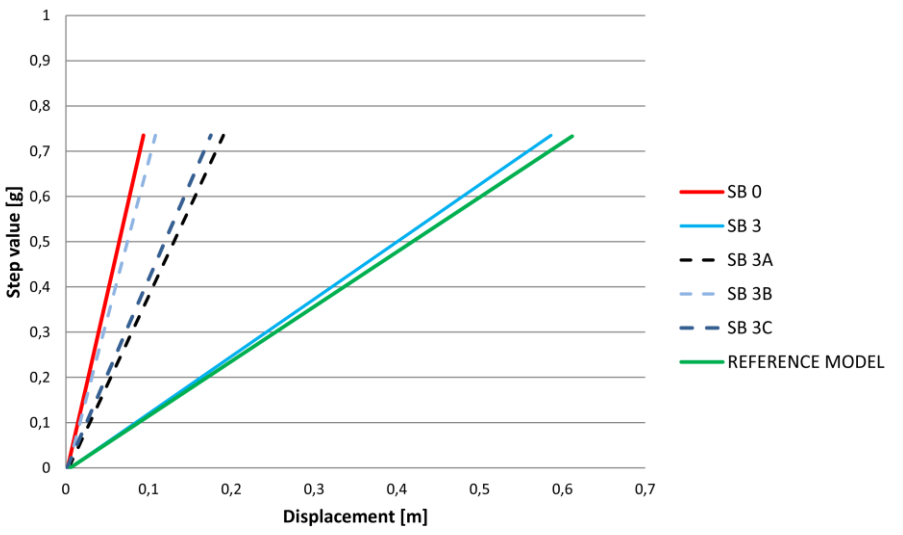

Figure 49. Capacity curves obtained from parametric analysis on the connections of the barrel vault.

Table 27. Values of stiffness obtained from parametric analysis on timber connections of the barrel vault.

	SB 3A	SB 3B	SB 3C
K [kN/m]	$3.8 \cdot 10^3$	$6.7 \cdot 10^3$	$4.1 \cdot 10^3$

The parametric analyses show that the timber joints of the barrel vault with lunettes have a significant influence on the structural behaviour of the representative bay. In particular, the timber

connections between the principal arches, the arches of lunettes and the diagonal elements of lunettes with the system of transversal and longitudinal beams are the most critical.

It is interesting to mention that the stiffness of the pillars is so much high that, adding horizontal restraints in correspondence of the connection between the transversal beams and the masonry walls, does not change significantly the value of the stiffness of the barrel vault. This is presented in **Table 28** where only a change from $1.3 \cdot 10^3$ kN/m to $1.5 \cdot 10^3$ kN/m is observed for the model SBB 3.

Table 28. Values of stiffness obtained from parametric analysis on timber connections.

	SBB 0	SBB 1	SBB 2	SBB 3	SBB 3A	SBB 3B	SBB 3C
K [kN/m]	$13.4 \cdot 10^3$	$13.2 \cdot 10^3$	$6.1 \cdot 10^3$	$1.5 \cdot 10^3$	$4.6 \cdot 10^3$	$10.8 \cdot 10^3$	$5.6 \cdot 10^3$

4.3 Compliance with Eurocode 5

This section deals with the calculations carried out for the timber elements of the representative bay in order to evaluate the compliance with the various criteria specified by Eurocode 5 (2004). Although incomplete geometrical information is available for the representative bay, as described in **Section 3.5**, the results of this analysis give an idea about the safety assessment of structures constructed with *quincha* technique and the Cathedral itself. The undamaged configuration of the representative bay, before the consequences of the recent earthquake, is considered to reach this aim.

According to Eurocode 5 (2004), requirements concerning structural reliability are linked to clearly defined limit states beyond which the structure no longer satisfies specified performance criteria. In particular, two types of limit states are considered: ultimate limit states (ULS) and serviceability limit states (SLS). The former are associated with collapse or with other forms of failure of the structure, such as loss of stability, and the latter includes the deformations resulting from the effects of loads, vibrations and moisture or other forms of performance in service conditions. The compliance of the representative bay is evaluated for both limit states on the basis of the results obtained in **Section 4.2.1**.

In order to reach this aim, it should be mentioned that some difficulties arise due to the complex geometry of the structure and the software package used. As the model is initially constructed by using AutoCAD to deal with the irregular curved geometry, haphazard labelling of elements and nodes of FE mesh takes place when the model is imported to SAP 2000. This creates difficulties in extracting results, especially considering that each structural part is composed of a large number of *Frame* elements. This is further complicated by the fact that the timber members have more than twenty cross sections in the representative bay. Finally, the combination of all the internal forces should be considered for each of these elements because of the three dimensional nature of the problem.

For the reasons mentioned above and the limited time available, the compliance of the bay is carried out by only considering the self– weight and live load in the load combinations prescribed by each limit state. It should be mentioned that both the permanent and the live loads are considered together and they are applied as self–weight in terms of equivalent specific weights, as described in **Section 4.1.3**. Besides, the complete verification is carried out only for all the straight timber

members in this thesis. The compliance of curved timber elements with the criteria specified by Eurocode 5 (2004) – especially in terms of stability – is complex and is left to future studies.

4.3.1 Stiffness properties and design values of load–carrying capacity

In order to carry out the verifications according to Eurocode 5 (2004), the following is assumed:

- For ultimate limit states, a uniform change of Young's modulus in the structure does not affect the distribution of internal forces, meaning that a discussion on using average of characteristic values is not relevant;
- For serviceability limit states, the creep behaviour is the same for the timber elements and connections and the relationship between the actions and the corresponding deformation is linear.

Under these assumptions, the mean values of the moduli of elasticity are adopted in the numerical model to perform the structural analysis. Considering that the representative bay is part of an existing structure dating back to the 18th century, the mean values of the moduli of elasticity for each wood species in **Table 21** are assumed without applying any coefficients.

The verification is carried out by comparing the results obtained from the structural analysis with the design value of each load–carrying capacity $\mathrm{R_d}$. The load–carrying capacity $\mathrm{R_d}$ is calculated for each wood species by applying the following expression:

$$\mathrm{R_d} = \mathrm{k_{mod}} \cdot \frac{\mathrm{R_k}}{\gamma_\mathrm{M}} \qquad \textbf{(13)}$$

where:

- $\mathrm{R_k}$ is the characteristic value of each load–carrying capacity;
- γ_M is the partial safety factor that is assumed as 1.3 for solid timber;
- $\mathrm{k_{mod}}$ is the modification factor that takes into account the duration of load and moisture content.

The modification factor $\mathrm{k_{mod}}$ is calculated depending on the load–duration class, the service class and the material. In particular, when a load combination consists of actions belonging to different load–duration classes, as in this case, the value of $\mathrm{k_{mod}}$ should be chosen for the action with the

shortest duration. Considering self–weight and live load for the load combinations, service class 2 and solid timber, the value of k_{mod} is assumed as 1.10.

It is not possible to calculate characteristic representative values for the mechanical properties of the wood species present in Ica Cathedral. No information is available about the value obtained from each test, so the calculation of the standard deviation σ cannot be performed. According to JCSS PROBABILISTIC APPROACH (2006), it is possible to calculate the expected values of the coefficient of variation (COV) of each property on the basis of the recommended ones of bending strength, bending moment and density. Besides, it is assumed that the relations provided can be assumed at any level, i.e. for components of any size and/or for climate and load conditions different from the reference conditions. Hence, the fifth percentile characteristic value R_k of each load–carrying capacity is calculated by applying the well–known formula:

$$R_k = -1.645 \cdot \sigma + R_m = -1.645\,(COV \cdot R_m) + R_m \quad (14)$$

where:

- R_m is the mean value of each load–carrying capacity;
- σ and COV are the standard deviation and coefficient of variation, respectively.

It should be mentioned that (1) the recommended coefficients of variation are calculated for European softwood and (2) the number of tests performed for evaluating the load–carrying capacity is very limited to have a reliable statistical characterization, as shown in **Table 22**. A summary of each load–carrying capacity R_d with the corresponding coefficient of variation adopted for each wood species is presented in **Table 29**.

Table 29. Design values adopted for the different wood species.

	COV	**Cedar**	**Huarango**	**Sapele***
Modulus of elasticity in flexure [MPa]	0.13*	$6.63 \cdot 10^3$	$11.95 \cdot 10^3$	$6.09 \cdot 10^3$
Bending strength [MPa]	0.25*	53.57	108.10	43.46
Compressive strength parallel to grain [MPa]	0.20	19.27	65.17	27.64
Compressive strength perpendicular to grain [MPa]	0.10	2.89	15.94	3.33
Shear strength [MPa]	013	6.13	14.70	4.44
Tensile strength parallel to grain [MPa]	0.30	14.98	43.73	33.84
5% value of modulus of elasticity $E_{0.05}$ [MPa]	0.13	$7.83 \cdot 10^3$	$14.12 \cdot 10^3$	$7.20 \cdot 10^3$
5% value of shear modulus $G_{0.05}$ [MPa]	0.13	$6.03 \cdot 10^3$	$10.86 \cdot 10^3$	$5.54 \cdot 10^3$

* Values of coefficient of variation recommended by JCSS PROBABILISTIC APPROACH (2006).

4.3.2 Brief introduction to verifications for ultimate limit states EC5.

A brief summary of the main verifications for ultimate limit states (ULS) that are used to assess the compliance of the representative bay with EC5 is presented in this section.

ULS – Tension and compression parallel to the grain

The following expression should be satisfied when axial forces are present in the timber elements:

$$\sigma_{t,0,d} \leq f_{t,0,d} \quad \textbf{(15)}$$

$$\sigma_{c,0,d} \leq f_{c,0,d} \quad \textbf{(16)}$$

where:

- $f_{t,0,d}$ and $f_{c,0,d}$ are the design tensile and compressive strength parallel to grain, respectively (**Table 29**);
- $\sigma_{t,0,d}$ and $\sigma_{c,0,d}$ are the design tensile and compressive strength parallel to grain, which are calculated as the ratio between the axial force and the cross section of the timber element.

It has to be mentioned that (1) tensile members have a uniform tension field throughout the length of the member and the entire cross section when it is associated with a low bending moment and (2) the compressive members can achieve compressive capacity not only for material crushing but also for buckling. Considering that the timber elements of the representative bay are generally subjected to combined internal forces, the verification under a combination of axial forces and bending moments is carried out, as explained in the following.

ULS – Shear

For shear with a stress component parallel to grain as well as for shear with both stress components perpendicular to the grain the following expression should be satisfied:

$$\tau_d \leq f_{v,d} \quad \textbf{(17)}$$

where:

- $f_{v,d}$ is the design shear strength (**Table 29**);

- τ_d is the design shear stress in the general case of biaxial shear $\tau_d = \sqrt{{\tau_{y,d}}^2 + {\tau_{z,d}}^2}$, where each shear contribution is calculated by applying the well–known Jourawsky's equation coming from the theory of elasticity.

ULS – Torsion

In order to verify the members that are subjected to torsion – hence, that are subjected to shear stress across the cross sections – the following expression should be satisfied:

$$\tau_{tor,d} \leq k_{shape} f_{v,d} \quad \textbf{(18)}$$

where:

- $f_{v,d}$ as above
- $\tau_{tor,d}$ is the design torsional tangential stress;
- k_{shape} is a factor depending on the shape of the cross–section.

In particular, the maximum value of torsional tangential stress of each element is calculated applying the following equation derived from the elastic theory for rectangular cross sections:

$$\tau_{tor,d} \leq \frac{T_d}{k_2\, h\, b^2} \quad \textbf{(19)}$$

where:

- T_d is the value of torsional moment on acting on the element;
- b and h are the smaller and larger cross sectional dimension, respectively;
- k_2 is calculated according to **Table 30.**

Table 30. Values of k_2 for rectangular cross sections (Garbin, 2015).

h/b	k	k_1	$k_2 = \frac{k_1}{k}$
1.0	0.675	0.1406	0.208
1.2	0.759	0.166	0.219
1.3	0.793	0.177	0.223
1.5	0.848	0.196	0.231
1.7	0.888	0.211	0.237
2.0	0.930	0.229	0.246
2.5	0.968	0.249	0.258
3.0	0.985	0.263	0.267
4.0	0.997	0.281	0.282
5.0	0.999	0.291	0.291
6.0	0.9999	0.298	0.298
8.0	1.000	0.307	0.307
10.0	1.000	0.312	0.312
∞	1.000	0.333	0.333

Finally, the factor k_{shape} is calculated for rectangular cross sections as the minimum value between 2 and $1 + 0.12\frac{h}{b}$, where b and h are defined as above.

ULS – Combined biaxial bending and axial force

As a combination of axial force and biaxial bending occurs generally in the elements, flexural bending and lateral torsional buckling are considered for columns and beams, respectively. However, verifications for both the stabilities are carried out for each element of the structure as the definition of column and beam is not strictly respected. It should be noted that the characteristic values of modulus of elasticity and shear modulus are used to carry these verifications.

Combined biaxial bending and axial force in compression for columns

In order to verify the stability of the columns subjected to combined axial force in compression and bending moment, the following equations are considered:

$$\left(\frac{\sigma_{c,0,d}}{k_{c,y}\ f_{c,0,d}}\right)^2 + \frac{\sigma_{m,y,d}}{f_{m,y,d}} + k_m \frac{\sigma_{m,z,d}}{f_{m,z,d}} \leq 1 \qquad \textbf{(20)}$$

$$\left(\frac{\sigma_{c,0,d}}{k_{c,z}\ f_{c,0,d}}\right)^2 + k_m \frac{\sigma_{m,y,d}}{f_{m,y,d}} + \frac{\sigma_{m,z,d}}{f_{m,z,d}} \leq 1 \qquad \textbf{(21)}$$

where:

- $\sigma_{c,0,d}$, $f_{c,0,d}$,
- $\sigma_{m,y,d}$ and $\sigma_{m,z,d}$ are the design bending stresses about the principal axes which are calculated by applying the well-known Navier's equations.
- $f_{m,y,d}$ and $f_{m,z,d}$ are the design bending strengths that are assumed with the same value in this study (**Table 29**);
- k_m is a modification factor the allows for an element redistribution of stress (yield behaviour) in the stress block and takes into account the effect of variation in material properties – it is assumed equal to 0.70.
- $k_{c,y}$ and $k_{c,z}$ are factors that depend on the values of slenderness of the timber elements.

In order to calculate the factors $k_{c,y}$ and $k_{c,z}$, the slenderness ratios λ_i and $\lambda_{rel,i}$ are calculated for $i = y, z$ as follows:

$$\lambda_i = \frac{l_{e,i}}{i_i} = l_{e,i}\sqrt{\frac{A}{I_i}} \quad (22)$$

$$\lambda_{rel,i} = \frac{\lambda_i}{\pi}\sqrt{\frac{f_{c,0,k}}{E_{0.05}}} \quad (23)$$

where:

- $l_{e,i}$ is the effective length calculated by applying the well-known factors derived from elastic theory shown in **Figure 50.**
- I_i is the moment of inertia corresponding to the considered axis i;
- $E_{0.05}$ is the fifth percentile characteristic value of the modulus of elasticity parallel to grain (**Table 29**).

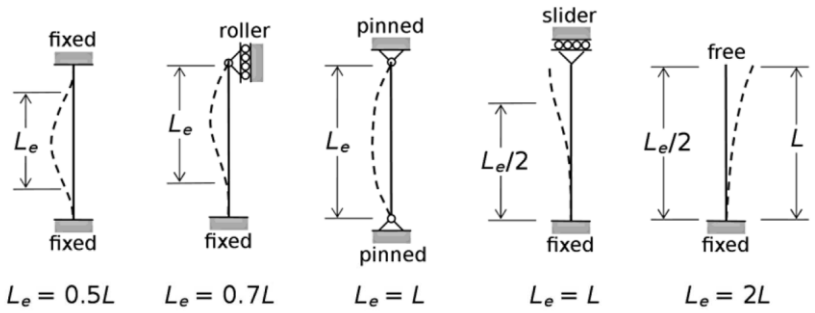

Figure 50. Factors used for the calculation of the effective lengths of column.

If $\lambda_{rel,y}$ and $\lambda_{rel,z}$ are smaller then 0.3, $k_{c,y}$ and $k_{c,z}$ are assumed 1; otherwise, they are calculated as follows:

$$k_{c,i} = 1 \Big/ k_i + \sqrt{k_i^2 - \lambda_{rel,i}^2} \quad (24)$$

where $k_i = 0.5\,(1 + \beta_c(\lambda_{rel,i} - 0.3) + \lambda_{rel,i}^2)$ with β_c is equal to 0.2 for solid timber.

Combined biaxial bending and axial force in compression for beams

In order to verify the lateral torsional stability of the beams that are subjected to combined axial force in compression and bending moments, as follows

$$\left(\frac{\sigma_{c,0,d}}{k_{c,i}\, f_{c,0,d}}\right) + \left(\frac{\sigma_{m,d,i}}{k_{crit}\, f_{m,d}}\right)^2 \leq 1 \quad (25)$$

where:

- $\sigma_{m,d,i}$ is the design bending stress considering the bending moment around axis i ;
- $\sigma_{c,0,d}$ is the design compressive stress parallel to grain;
- $f_{c,0d}$ and $f_{m,d}$ as above;
- $k_{c,i}$ is given by expression (24);
- k_{crit} is a factor that takes into account the reduced bending strength due to lateral buckling.

In order to calculate the factor k_{crit} the following expression is used,

$$k_{crit} = \begin{cases} 1 \ (\lambda_{rel,m} \leq 0.75) \\ 1.56 - 075\,\lambda_{rel,m} (0.75 < \lambda_{rel,m} \leq 1.4) \\ 1/{\lambda_{rel,m}}^2 \ (\lambda_{rel,m} > 1.4) \end{cases} \quad \textbf{(26)}$$

where $\lambda_{rel,m}$ is the relative slenderness for bending that is calculate in function of the critical bending stress $\sigma_{m,crit}$. In particular, this is calculated as

$$\lambda_{rel,m,i} = \sqrt{\frac{f_{m,k}}{\sigma_{m,crit,i}}} \quad \textbf{(27)}$$

$$\sigma_{m,crit,i} = \frac{\pi\sqrt{E_{0.05}\ I\ G_{0.05}\ I_{tor}}}{l_{ef}\ W_i} \quad \textbf{(28)}$$

where:

- $E_{0.05}$ and $G_{0.05}$ are the fifth percentile value of modulus of elasticity and shear modulus, respectively (**Table 29**);
- I_{tor} is the torsional moment of inertia of the cross section;
- W_i is the section modulus about the axis i;
- I is the moment of inertia about the other axis;
- l_{ef} is the effective length of the beam that is calculated depending on the support conditions and the load configuration.

In this study, the effective length is calculated by applying a factor equal to 0.9 and 0.78 considering beams with uniformly distributed load that are simply supported and fully fixed, respectively (Garbin, 2015).

Combined biaxial bending and axial force in tension

The following conditions should be both verified for the elements which are subjected to a combination of biaxial bending and axial force in tension:

$$\frac{\sigma_{t,0,d}}{f_{t,0,d}} + \frac{\sigma_{m,y,d}}{f_{m,y,d}} + k_m \frac{\sigma_{m,z,d}}{f_{m,z,d}} \leq 1 \quad \textbf{(29)}$$

$$\frac{\sigma_{t,0,d}}{f_{t,0,d}} + k_m \frac{\sigma_{m,y,d}}{f_{m,y,d}} + \frac{\sigma_{m,z,d}}{f_{m,z,d}} \leq 1 \quad \textbf{(30)}$$

where:

- $\sigma_{t,0,d}$, $f_{t,0,d}$, $\sigma_{m,y,d}$ and $\sigma_{m,z,d}$ as above;
- $f_{m,y,d}$ and $f_{m,z,d}$ are the design bending strengths that are assumed with the same value in this study (**Table 29**).

4.3.3 Brief introduction to verifications for serviceability limit states EC 5

The verification of the deformation - that generally varies considerably during the lifetime of the structure - is presented in this section. According to Eurocode 5 (2004), the instantaneous deformation u_{inst} and the final deformation u_{fin} should be evaluated. The former is calculated for the characteristic load combination, while the latter is calculated for the quasi-permanent one. In particular, under the assumption that components and connections have the same creep behaviour and the relationship between the actions and the corresponding deformations is linear, the final deformation u_{fin} is calculated as follows:

$$u_{fin} = u_{fin,G} + u_{fin,Q1} \quad \textbf{(31)}$$

where:

- $u_{fin,G} = u_{inst,G}(1 + k_{def})$ for permanent action (structural and not structural);
- $u_{fin,Q} = u_{inst,Q}\,(1 + \psi_2 k_{def})$ for live load;

In particular, $u_{inst,G}$ and $u_{inst,Q}$ are the instantaneous deformation for self-weight and live load, ψ_2 is the factor for the quasi-permanent value of variable actions assumed as 0.6 and k_{def} is the factor taking into account the service class. Since service class 2 and solid timber are considered in this study, the value of k_{def} is assumed as 0.8. However, it should be mentioned that ψ_2 could be chosen lower considering that an existing structure is under study.

The verification is carried out considering the recommended limit values for instantaneous and final deflections according to Eurocode 5 (2004). These are expressed in terms of the length of the timber element that has to be verified. It should be mentioned that for the symmetrical elements of the

structure, such as the beam close to the masonry and the beam at the top of the lunettes, the total span l is considered.

4.3.4 Global verifications

On the basis of the results obtained from linear elastic analysis, the verification of all the straight elements composing the representative bay is carried out. For the ultimate limit states, the verifications are satisfied for all the timber elements. In particular, the beam at the top of the lunettes (BEAM LUNETTE) results to be subjected to the highest amount of stresses, as shown in **Table 31**. **Table 32** and **Table 33** present examples of these verifications carried out for beams and posts. In particular, BEAM III and POST refer to the transversal beam between the aisles' domes and to the post of one of the pilasters. It should be mentioned that the verification regarding the torsional moment is not shown as torsion does not occur in these particular timber members.

Concerning the verification for SLS according Eurocode 5 (2004), the beams located at the top of the lunettes (BEAM LUNETTE) and those close to the masonry (BEAM IV) are not verified, as shown in **Table 34**. In particular, the first is verified for the instantaneous deflection but not for the total deflection with values of 1.3 cm and 2.7 cm, respectively. Both the verifications are not satisfied for the beam close to the masonry that show 2.0 cm and 4.1 cm as maximum instantaneous and final deflections, respectively.

However, it should be mentioned that (1) only incomplete information is available regarding the geometry, the material properties and the thickness of the covering layers used for the calculation of the specific weight in **Section 4.1.3,** (2) the influence of the masonry is completely not considered, (3) the most conservative model is considered in this analysis as most of the connections are modelled as hinges and (4) no increase in stiffness of the timber elements that are confined by the covering layers is taken into account. Finally, it should be said that existing historical structures can show high values of deformation without compromising their performance to an unacceptable level.

Geometry				
	Base [m]	Height [m]	Lenght [m]	Area BH [m2]	Area BL [m2]
BEAM LUNETTE	0,06	0,25	4,46	0,02	0,27

Internal Forces								
	P	V2	V3	T	M2	M3		
	KN	KN	KN	KN-m	KN-m	KN-m		
BEAM	0,39	12,09	3,83	0,22	3,52	4,63		
LUNETTE	-0,14	-8,74	-3,83	0,22	-0,12	-2,58		

Tension and Compression (// to grain)			
	Max P	σ.tod	
	kN	kN/m2	
T	0,39	26,20	OK
C	-0,14	-9,07	OK

Shear							OK
	l	Area	max V2	max V3	τ2max	τ3max	τmax
Element	m	m2	kN	kN	kN/m2	kN/m2	kN/m2
L1	0,45	0,02	12,07	3,78	1206,70	378,40	1264,64
L2	0,45	0,02	4,24	1,48	423,70	148,40	448,94
L3	0,45	0,02	0,61	0,83	61,40	83,40	103,56
L4	0,37243	0,02	8,824	3,639	882,40	363,90	954,49

Bending + Axial Force							Torsional Stability			Flexural Stability			Bi-axial Bending + Tension		OK	Bi-axial Bending + Compression + Flexural Stability		OK	Bi-axial Bending + Compression + Torsional Stability		OK
	P	M2	M3	σ	σ2	σ3	lef	0,90		le	1,00										
Element	kN	kNm	kNm	kN/m2	kN/m2	kN/m2	leff [m]	km		le [m]	4,46		Verify 1	Verify 2		Verify 1	Verify 2		Verify 1	Verify 2	
L1	0,38	1,99	3,94	25,40	3180,48	26240,67	leff [m]	0,70	4,01	I2 [m4]	0,0001	0,58	0,50	0,66		T	T		T	T	
L1	0,38	0,93	0,75	25,40	1492,64	4999,33	W2 [m3]	0,00063	I3 [m4]	0,0000	0,12	0,14				T	T		T	T	
L1	0,38	-0,12	-2,55	25,40	-195,04	-17030,67	W3 [m3]	0,00015	λ2	61,80	0,28	0,40				T	T	0,58	T	T	0,47
L2	-0,04	2,67	4,44	-2,40	4279,68	29628,00	I tor [m3]	0,00002	λ3	257,50	C	C				0,58	0,75	0,48	0,01	0,47	0,28
L2	-0,04	3,09	3,44	-2,40	4941,60	22938,00	σcrit2 [kN/m2]	6,55E+04	λ2rel	1,33	C	C				0,48	0,61	0,38	0,02	0,28	0,13
L2	-0,04	3,50	2,32	-2,40	5603,68	15458,67	σcrit3 [kN/m2]	1,14E+06	λ3rel	5,53	C	C				0,38	0,45	0,54	0,02	0,13	0,41
L3	-0,15	2,60	4,12	-9,93	4163,84	27492,67	λrel.m2	0,89	k2	1,48	C	C				0,54	0,70	0,55	0,01	0,41	0,41
L3	-0,15	2,84	4,13	-9,93	4536,00	27533,33	λrel.m3	0,21	k3	16,29	C	C				0,55	0,71	0,54	0,01	0,41	0,39
L3	-0,15	3,07	4,02	-9,93	4908,00	26786,00	kcrit2	0,90	kc2	0,47	C	C				0,54	0,70		0,02	0,39	
L4	0,00	0,00	0,00	0,01	0,00	0,00	kcrit3	1,00	kc3	0,03	0,00	0,00				T	T		T	T	
L4	0,00	1,01	2,40	0,01	1623,20	16004,00					0,30	0,39				T	T		T	T	
L4	0,00	2,03	4,68	0,01	3246,24	31218,67					0,58	0,77				T	T		T	T	

Table 31. Verification for ULS of the beam at the top of the lunette according EC 5 (2004).

Geometry				
	Base [m]	Height [m]	Lenght [m]	Area BH [m2]	Area BL [m2]
BEAM III	0,25	0,25	4,46	0,06	1,12

Internal Forces							
	P	V2	V3	T	M2	M3
	KN	KN	KN	KN-m	KN-m	KN-m
BEAM III	1,89	19,11	5,59	0,64	2,20	7,90
	-22,09	-38,04	-5,19	-0,62	-2,74	-4,92

Shear									OK
	l	Area	max V2	max V3	τ2max	τ3max	τmax		
Element	m	m2	kN	kN	kN/m2	kN/m2	kN/m2		
B8	0,45	0,06	4,47	5,59	107,33	134,14	171,79		
B9	0,45	0,06	1,52	1,82	36,41	43,70	56,88		
B10	0,04	0,06	1,61	0,06	38,69	1,37	38,71		
B11	0,41	0,06	19,114	4,232	458,74	101,57	469,85		
B12	0,446	0,06	16,535	2,916	396,84	69,98	402,96		
B13	0,37	0,06	13,728	4,863	329,47	116,71	349,53		
B14	0,07	0,06	13,669	5,186	328,06	124,46	350,87		
B15	0,18	0,06	38,04	3,802	912,96	91,25	917,51		
B16	0,27	0,06	11,653	3,492	279,67	83,81	291,96		
B17	0,446	0,06	14,46	1,731	347,04	41,54	349,52		
B18	0,446	0,06	17,158	3,548	411,79	85,15	420,50		
B19	0,06	0,06	17,64	2,097	423,36	50,33	426,34		
B20	0,38	0,06	6,486	0,182	155,66	4,37	155,73		
B21	0,446	0,06	3,936	2,581	94,46	61,94	112,96		

Tension and Compression (// to grain)			
	Max P	σ.tod	
	kN	kN/m2	
T	1,89	30,19	OK
C	22,09	353,41	OK

Bending + Axial Force							Torsional Stability			Flexural Stabilitity			Bi-axial Bending + Tension		OK	Bi-axial Bending + Compression + Flexural Stability		OK	Bi-axial Bending + Compression + Torsional Stability		OK
	p	M2	M3	σ	σ2	σ3	lef	0,78		le	0,50										
	kN	kNm	kNm	kN/m2	kN/m2	kN/m2	leff [m]	3,48	le [m]	2,23											
							km	0,70	I2 [m4]	0,0003											
B8	-13,38	1,39	-3,47	-214,05	533,53	-1330,75	W2 [m3]	0,00260	I3 [m4]	0,0003			0,03	0,04		0,03	0,04		0,01	0,01	
B8	-13,38	-1,10	-4,84	-214,05	-423,67	-1856,95	W3 [m3]	0,00260	λ2	30,90			0,04	0,05		0,04	0,05		0,01	0,01	
B9	-13,38	2,20	-3,44	-214,05	845,41	-1319,73	I tor [m3]	0,00055	λ3	30,90			0,04	0,04		0,04	0,04		0,01	0,01	
B9	-13,38	1,39	-3,49	-214,05	533,53	-1339,81	σcrit2 [kN/m2]	9,26E+05	λ2rel	0,66			0,03	0,04		0,03	0,04		0,01	0,01	
B10	-13,38	2,20	-4,04	-214,05	844,53	-1552,63	σcrit3 [kN/m2]	9,26E+05	λ3rel	0,66			0,04	0,05		0,04	0,05		0,01	0,01	
B10	-13,38	2,20	-3,98	-214,05	845,41	-1529,70	λrel,m2	0,24	k2	0,76			0,02	0,03		0,02	0,03		0,01	0,01	
B11	-20,19	0,37	3,20	-322,99	141,43	1227,34	λrel,m3	0,24	k3	0,76			0,04	0,05		0,04	0,05		0,01	0,01	
B11	-20,19	2,09	-4,04	-322,99	800,83	-1552,63	kcrit2	1,00	kc2	0,89			0,05	0,06		0,05	0,08		0,01	0,02	
B12	-20,19	-0,93	7,90	-322,99	-358,04	3033,52	kcrit3	1,00	kc3	0,89			0,01	0,01		0,01	0,01		0,01	0,01	
B12	-20,19	0,37	1,15	-322,99	141,43	441,45							0,05	0,05		0,05	0,05		0,01	0,01	
B13	-20,19	-2,74	3,70	-322,99	-1053,54	1421,34							0,01	0,01		0,01	0,01		0,01	0,01	
B13	-20,19	-0,93	-0,98	-322,99	-358,04	-374,75							0,05	0,05		0,04	0,04		0,01	0,01	
B14	-21,90	-2,08	4,69	-350,43	-798,53	1800,96							0,03	0,03		0,03	0,03		0,01	0,01	
B14	-21,90	-1,70	3,70	-350,43	-652,03	1421,34							0,05	0,05		0,05	0,05		0,01	0,01	
B15	-22,09	-1,39	-2,03	-353,41	-535,30	-779,25							0,04	0,04		0,04	0,04		0,01	0,01	
B15	-22,09	-2,07	4,65	-353,41	-795,53	1786,48							0,03	0,03		0,03	0,03		0,01	0,01	
B16	-4,98	-1,48	-4,92	-79,60	-566,63	-1890,85							0,05	0,05		0,05	0,05		0,01	0,01	
B16	-4,98	-2,41	-2,03	-79,60	-925,63	-779,25							0,04	0,05		0,05	0,05		0,00	0,00	
B17	-4,98	-0,70	1,01	-79,60	-270,22	386,57							0,03	0,03		0,03	0,03		0,00	0,00	
B17	-4,98	-1,48	6,83	-79,60	-566,63	2623,30							0,01	0,01		0,01	0,01		0,00	0,00	
B18	-4,98	0,88	-3,13	-79,60	337,50	-1201,69							0,06	0,07		0,07	0,07		0,00	0,01	
B18	-4,98	-0,70	3,93	-79,60	-270,22	1508,58							0,03	0,03		0,03	0,03		0,00	0,00	
B19	-4,98	1,01	-3,28	-79,60	389,41	-1257,98							0,03	0,04		0,04	0,04		0,00	0,00	
B19	-4,98	0,88	-2,15	-79,60	337,50	-826,18							0,02	0,02		0,02	0,02		0,00	0,00	
B20	1,89	1,17	-1,26	30,19	449,51	-483,15							T	T		T	T		T	T	
B20	1,89	1,10	-3,28	30,19	422,78	-1257,98							T	T		T	T		T	T	
B21	1,89	0,02	0,11	30,19	7,56	43,62							T	T		T	T		T	T	
B21	1,89	1,17	-1,02	30,19	449,51	-390,76							T	T		T	T		T	T	

Table 32. Verification for ULS of the transversal beam according EC 5 (2004).

Geometry					
	Base [m]	Height [m]	Lenght [m]	Area BH [m2]	Area BL [m2]
POST	0,25	0,12	4,32	0,03	1,08

Internal Forces							
	P	V2	V3	T	M2	M3	
	KN	KN	KN	KN-m	KN-m	KN-m	
POST	-	3,74	0,50	0,00	0,67	3,96	
	-63,59	-11,09	-2,50	-0,09	-0,18	-4,64	

Shear										OK
	I	Area	max V2	max V3	τ2max	τ3max	τmax			
Element	m	m2	kN	kN	kN/m2	kN/m2	kN/m2			
PP8	0,27	0,03	6,85	2,50	342,30	124,95	364,39			
PP9	1,60	0,03	3,74	0,50	186,75	25,20	188,44			
PP10	0,12	0,03	3,74	0,14	186,75	7,10	186,88			
PP11	0,11588	0,03	10,996	0,163	549,80	8,15	549,86			
PP12	0,33461	0,03	10,787	0,163	539,35	8,15	539,41			
PP13	0,33461	0,03	11,089	0,163	554,45	8,15	554,51			
PP14	0,69229	0,03	2,648	0,163	132,40	8,15	132,65			
PP15	0,85	0,03	2,648	0,071	132,40	3,55	132,45			

Tension and Compression (// to grain)			
	Max P	σ.tod	
	kN	kN/m2	
T	-	-	-
C	-63,59	-2119,67	OK

Bending + Axial Force							Torsional Stability			Flexural Stabilitity			Bi-axial Bending + Tension		OK	Bi-axial Bending + Compression + Flexural Stability		OK	Bi-axial Bending + Compression + Torsional Stability		OK
	p	M2	M3	σ	σ2	σ3	lef	1,00	le	1,00											
	kN	kNm	kNm	kN/m2	kN/m2	kN/m2	leff [m]	4,32	le [m]	4,32			Verify 1	Verify 2		Verify 1	Verify 2		Verify 1	Verify 2	
PP8	-24,24	-0,09	0,00	-807,87	-146,00	0,00	km	0,70	I2 [m4]	0,000036			C	C		0,04	0,00		0,18	0,05	
PP8	-24,42	-0,09	0,34	-813,93	-146,00	269,92	W2 [m3]	0,00060	I3 [m4]	0,000156			C	C		0,04	0,01		0,19	0,05	
PP8	-24,60	-0,09	0,67	-820,00	-146,00	539,76	W3 [m3]	0,00125	λ2	124,71			C	C		0,05	0,02		0,19	0,05	
PP9	-33,93	-0,07	0,67	-1131,10	-118,33	539,84	I tor [m3]	0,00109	λ3	59,86			C	C		0,08	0,02		0,26	0,07	
PP9	-35,01	-0,07	0,27	-1167,00	-118,33	217,04	σcrit2 [kN/m2]	3,16E+06	λ2rel	2,68			C	C		0,08	0,01		0,27	0,07	
PP9	-36,09	-0,07	-0,13	-1202,90	-118,33	-105,76	σcrit3 [kN/m2]	7,28E+05	λ3rel	1,28			C	C		0,08	0,01		0,27	0,07	
PP10	-36,10	-0,07	-0,13	-1203,47	-118,33	-105,76	λrel.m2	0,13	k2	4,32			C	C		0,08	0,01		0,27	0,07	
PP10	-36,19	-0,07	-0,14	-1206,20	-118,33	-112,72	λrel.m3	0,27	k3	1,42			C	C		0,08	0,01		0,27	0,07	
PP10	-36,27	-0,07	-0,15	-1208,97	-118,33	-119,60	kcrit2	1,00	kc2	0,13			C	C		0,08	0,01		0,28	0,07	
PP11	-62,07	-0,02	-0,18	-2069,00	-32,67	-144,88	kcrit3	1,00	kc3	0,49			C	C		0,23	0,02		0,47	0,12	
PP11	-62,15	-0,02	-0,17	-2071,60	-32,67	-137,36							C	C		0,23	0,02		0,47	0,12	
PP11	-62,23	-0,02	-0,16	-2074,20	-32,67	-129,76							C	C		0,23	0,02		0,47	0,12	
PP12	-62,67	-0,01	-0,16	-2088,83	-14,33	-125,04							C	C		0,23	0,02		0,48	0,13	
PP12	-62,89	-0,01	-0,13	-2096,37	-14,33	-103,28							C	C		0,23	0,02		0,48	0,13	
PP12	-63,12	-0,01	-0,10	-2103,87	-14,33	-81,52							C	C		0,23	0,02		0,48	0,13	
PP13	-63,14	-0,01	-0,10	-2104,67	-14,33	-81,36							C	C		0,23	0,02		0,48	0,13	
PP13	-63,37	-0,01	-0,07	-2112,17	-14,33	-59,60							C	C		0,23	0,02		0,48	0,13	
PP13	-63,59	-0,01	-0,05	-2119,67	-14,33	-37,84							C	C		0,23	0,02		0,48	0,13	
PP14	-38,04	0,00	-0,05	-1267,93	0,00	-41,52							C	C		0,08	0,01		0,29	0,08	
PP14	-38,50	0,00	0,00	-1283,47	0,00	3,44							C	C		0,09	0,01		0,29	0,08	
PP14	-38,97	0,00	0,06	-1299,00	0,00	48,48							C	C		0,09	0,01		0,30	0,08	
PP15	-38,99	0,00	0,06	-1299,57	0,00	48,48							C	C		0,09	0,01		0,30	0,08	
PP15	-39,56	0,00	0,03	-1318,63	0,00	24,24							C	C		0,09	0,01		0,30	0,08	
PP15	-40,13	0,00	0,00	-1337,73	0,00	0,00							C	C		0,09	0,01		0,30	0,08	

Table 33. Verification of a post of the pilaster with the criteria for ULS according EC 5(2004).

kdef	0,8	Istantaneous Deflection						OK	Total final deflection			NO
ψ2	0,6	Max u1	Max u2	Max u3	Max u1	Max u2	Max u3		Max u1	Max u2	Max u3	
L [mm]	4460,0	mm	mm	mm	mm	mm	mm		mm	mm	mm	
L/300 [mm]	14,9	3,5	0,0	12,6	0,9	0,0	3,3		7,9	0,0	28,6	
L/200 [mm]	22,3		SLE 1			SLE 2			Total final deflection			
		u1	u2	u3	u1	u2	u3		u1	u2	u3	
BEAM	Node	mm	mm	mm	mm	mm	mm		mm	mm	mm	
LUNETTE	LN1	3,5	0,0	11,5	0,9	0,0	3,0		7,9	0,0	25,9	
	LN2	2,3	0,0	12,6	0,6	0,0	3,3		5,1	0,0	28,5	
	LN3	0,8	0,0	12,6	0,1	0,0	3,3		1,7	0,0	28,6	
	LN4	0,8	0,0	9,5	0,1	0,0	2,4		1,5	0,0	21,4	
	LN5	3,6	0,0	1,8	0,8	0,0	0,4		7,9	0,0	3,9	

kdef	0,8	Istantaneous Deflection						NO	Total final deflection			NO
ψ2	0,6	Max u1	Max u2	Max u3	Max u1	Max u2	Max u3		Max u1	Max u2	Max u3	
L [mm]	4460,0	mm	mm	mm	mm	mm	mm		mm	mm	mm	
L/300 [mm]	14,9	4,0	0,0	19,8	0,9	0,0	2,7		8,9	0,0	40,6	
L/200 [mm]	22,3		SLE 1			SLE 2			Total final deflection			
		u1	u2	u3	u1	u2	u3		u1	u2	u3	
	Node	mm	mm	mm	mm	mm	mm		mm	mm	mm	
BEAM IV	BN24	4,0	0,0	19,8	0,9	0,0	2,7		8,9	0,0	40,6	

Table 34. Verification for SLS of deformations according EC5 (2004).

4.3.5 Local verifications

In addition to global verifications, verifications of the connections should be performed locally in order to evaluate the compliance of the structure with the criteria specified by Eurocode 5 (2004). For the purpose of this thesis, the connections of the beam at the top of the lunettes are considered. Firstly, the connections are verified under the combination ULS of vertical loads on the basis of the results obtained in **Section 4.2.1.** Afterwards, the seismic action is also taken into account applying the seismic action E**.** The evaluation of the seismic assessment of these connections is particularly important as they are thought to be the main reason of the collapse of the roofing system of Ica Cathedral after 2007 Pisco Earthquake (Ferreira & D'Ayala, 2014). The complete verification of all the timber elements under seismic load is left to further studies.

As described in **Section 1.5.1**, the beam that is located at the top of the lunettes is characterized by multiple mortise holes to receive both the tenons of the secondary arches of the barrel vault and the lunettes' ribs. Each of these curved timber elements is constructed with two elements and the tenon is constructed for the thickness of only one of these. In this way, the tenons of the secondary arches and of the lunette's rib are joined together in the hole of the lunette beam. Besides, this beam is connected to the principal arch of the batter vault by means of mortise and tenon joints. The dimension and the layout of these mortise and tenon joints are different for each connection (Ferreira & D'Ayala, 2014) but no quantitative information is available yet. To the purpose of this thesis, verifications are carried out for the connections shown in **Figure 51**.

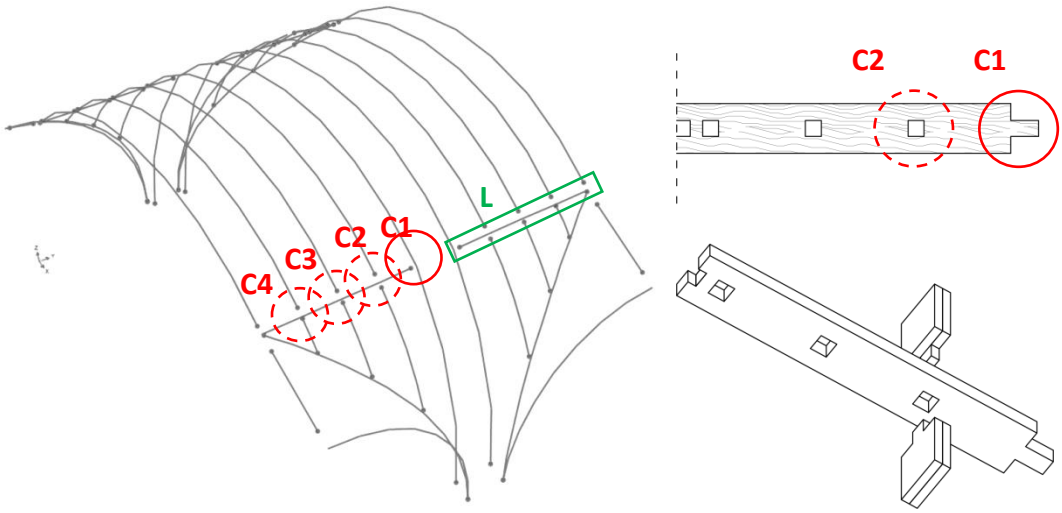

Figure 51. Beam at the top of the lunettes and its mortise and tenon connections.

The dimension of the mortise and tenon connection is evaluated on the base of the available photographic documentation and it is assumed the same for all the connections under study. In particular, the cross section of the tenons is assumed with a value of 40x80 mm^2. As assumed in **Section 4.1.1,** the cross section of the element of the beam as well as of the lunettes is 80x250 $mm^{2.}$

In order to evaluate the assessment of these connections, the following verifications are carried out:

- Local verification of the connection considering the internal forces that occur in the elements corresponding to the secondary arches and to the members of the lunettes;
- Local verification of the beam at the top of the lunettes considering the internal forces that occur in the elements corresponding to it.

In order to perform the first verification, the internal forces that are calculated in **Section 4.2.1** considering self-weight and live load are added under the assumption of linearity. The obtained results show that the elements corresponding to the secondary arches and to the members of the lunettes are mainly subjected to compressive axial forces and shear. The compressive stress σ is calculated as the ratio between the axial force P and the contact area between the elements, while the tangential stress τ is obtained as that between the shear V and the shear surface. It should be noted that the critical area corresponds to the cross section of the tenon for both cases. Hence, the obtained values of stresses that are presented in **Table 35** are compared to the corresponding design load–bearing capacities shown in **Table 29**. In particular, it should be noted that the highest values of stresses occur in connection C1 and connection C2. As shown in **Figure 51**, the first corresponds to the timber joint between the beam and the principal arch, while the second to that between the beam and the secondary arch. The verification results to be satisfied considering the strengths of sapele and cedar, respectively.

Table 35. Verification of the connections under the load combination for ULS.

	P [kN]	**V** [kN]	**σ** [kN/m^2]	**τ** [kN/m^2]	
C1	6.0	2.8	1871.9	874.4	OK
C2	3.9	2.2	1224.7	696.9	OK
C3	4.0	2.1	1257.6	411.6	OK
C4	5.1	1.3	2176.9	34.4	OK

Similarly, the internal forces are calculated for the beam at the top of the lunettes in order to carry the verification considering the cross section with the mortise. As shown in **Figure 52**, biaxial shear and bending moments occur in the beam.

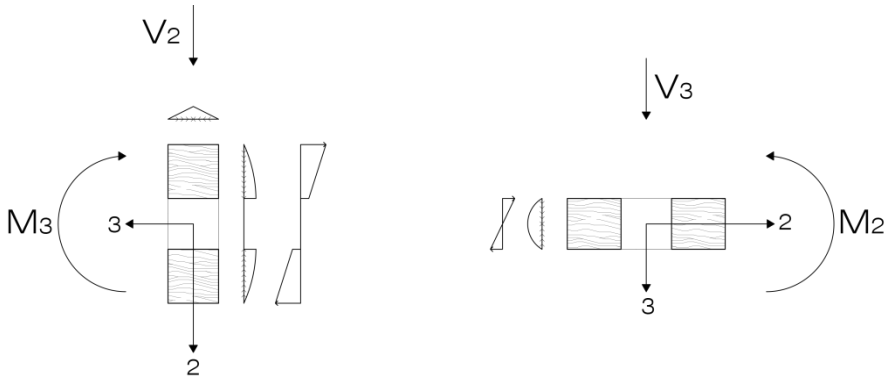

Figure 52. Distribution of the stresses in the beam at the top of the lunettes.

The maximum bending stress σ_{cmax} is calculated by applying Navier's equation and the verification is carried out as follows:

$$\sigma_{max} = \sigma_{max2} + \sigma_{max3} = \frac{M_2}{I_2}\frac{h}{2} + \frac{M_3}{I_3}\frac{b}{2} \leq f_{m,d} \qquad (32)$$

The maximum tangential stress τ_{max} is calculated applying Jourawsky's equation considering the bi–axial shear and the verification is carried out as follows:

$$\tau_{max} = \sqrt{\left(\tau_{21}(V_2) + \tau_{21}(V_3)\right)^2 + \left(\tau_{31}(V_2) + \tau_{31}(V_3)\right)^2} \leq f_{v,d} \qquad (33)$$

The obtained values of stresses that are presented in **Table 36** are compared to the corresponding design load–bearing capacities of sapele shown in **Table 29.** All the connections' safety is satisfied with the exception of the elements L1 and L4 – even though the stresses exceed only slightly the corresponding capacities. This seems to confirm some structural deficiency of the system.

Table 36. Verification of the beam at the top of the lunettes under the load combination for ULS.

	V2 [kN]	**V3** [kN]	**M2** [kNm]	**M3** [kNm]	**τ** [kN/m^2]	**σ** [kN/m^2]	
L1	8.7	2.7	0.1	1.8	4946.1	26699.5	NO
L2	3.1	1.1	2.5	1.7	1658.8	23977.1	OK
L3	0.4	0.6	2.2	2.9	26.0	41551.4	OK
L4	5.8	2.6	1.4	3.4	3311.8	48414.3	NO

In order to discuss the actual failure of the structure, the seismic assessment of the connections is carried out on the basis of the results obtained for linear elastic analysis. Under the assumption of linearity, each internal force of the element F_e is calculated as follows:

$$F_e = F_e\,(G) + 1.5\,F_e\,(E) \qquad (34)$$

where:

- F_e (G) is the internal force occurring in the element considering the self–weight G calculated in **Section 4.2.1**;
- F_e (E) is the internal force occurring in the element considering the seismic action E.

Following the same procedure applied previously, the verifications are carried out for the connections and the beam at the top of the lunettes. It should be said that the elements composing the beam are subjected also to a compressive axial force because of the horizontal loading. However, the obtained values are low compared to the other internal forces which provoke the collapse of the beam by themselves. According to the results presented in **Table 37** and **Table 38,** the failure is significantly due to the stresses that occur in the beams at the top of the lunette.

Table 37. Verification of the connections under the load combination G+1.5E.

	P [kN]	V [kN]	τ [kN/m^2]	σ [kN/m^2]	
C1	36.7	21.8	6809.2	11458.8	NO
C2	5.3	2.8	868.9	1650.3	OK
C3	5.1	2.9	905.8	1601.7	OK
C4	7.7	0.9	281.2	2416.4	OK

Table 38. Verification of the beam at the top of the lunettes under the load combination G+1.5E.

	V2 [kN]	V3 [kN]	M2 [kNm]	M3 [kNm]	τ [kN/m^2]	σ [kN/m^2]	
L1	16.6	1.8	0.5	10.1	9082.5	146061.3	NO
L2	14.5	5.3	2.7	5.1	7835.9	72991.4	NO
L3	10.0	9.6	4.9	3.3	5307.5	46940.0	NO
L4	10.0	10.9	6.2	5.6	5334.9	79865.7	NO

4.4 Conclusion

The 3D finite element model of the representative bay was constructed on the basis of (1) the generated 3D architectural AutoCAD model described **in Section 3.5** and (2) the characterization of the material properties obtained from the experimental campaign carried out by (GCI & PUCP, 2014). Structural analysis of the representative bay was performed assuming linear elastic isotropic material for timber and calculating equivalent specific weights to take into account the weight of the covering layers used in *quincha* technique.

The structural behaviour of the representative bay of Ica Cathedral was investigated considering different loading conditions. In order to evaluate the relative importance of the various timber members to the global behaviour of the representative bay, parametric analyses were carried out with different assumptions for the modelling of the timber connections and the boundary conditions. In particular, the results show that the timber connections of the elements composing the barrel vault with lunettes are the most important to control the lateral stiffness of the representative bay. The obtained results show that it is not possible to introduce directly the nonlinear behaviour of the timber joints present in the representative bay by following the approach used in **Chapter 2**. In fact, the characterization of these timber connections between the elements composing the barrel vault with lunettes – that was carried out by performing some experimental tests on full scale specimens – shows an almost linear relationship (GCI & PUCP, 2014).

Global and local verifications were carried out in order to evaluate the compliance of the representative bay under self–weight and live load with the various criteria specified by Eurocode 5 (2004). The results show that all the straight timber members are verified for ULS and only few are not verified for SLS. Concerning the latter, it should be mentioned that the values of displacement that are not verified are only slightly higher than those recommended, which seems less of an issue for historic buildings. Moreover, several conservative assumptions were considered in the definition of the numerical model. Finally, the seismic response of the representative bay was investigated with a particular focus on the beams at the top of the lunettes to discuss the actual failure of the Cathedral of Ica. According to the obtained results, the stresses that occur under seismic action in these beams are large enough to provoke the failure of the structure.

Chapter 5

The complete timber structure

Established the not direct possibility to introduce the nonlinear behaviour of the most critical timber connections in the representative bay, the numerical model of the whole timber structure is constructed by using MIDAS FX+ for DIANA software (TNO DIANA, 2014). The structural behaviour of the complex model is studied in terms of linear elastic analysis under self–weight, mass proportional lateral loading and eigenvalue analysis. The results obtained in this chapter and the thesis developed in parallel to this work (Sharma, 2015) represent the starting point for the research on the numerical model of the combined timber and masonry structures of Ica Cathedral.

5.1 Definition of the numerical model

The 3D finite element model of the whole timber structure of Ica Cathedral is constructed in DIANA software on the basis of the information available in literature (Cancino, et al., 2012) and the surveys performed by Garcia Bryce & Soto Medina (2014) and Greco et al. (2015).

For optimizing the construction procedure and for a better understanding of the numerical model, four sectors are defined on the basis of symmetries in the configuration of the complete timber structure of Ica Cathedral. As shown in **Figure 53**, the sectors that are considered are as follows:

- **Sector A** that is composed of the main entrance (the so–called *sotacoro*) and the two flanked extensions at either lateral side;
- **Sector B** that is composed of repeating units of the representative bay;
- **Sector C** that is composed of the crossing and the arms of the transept;
- **Sector D** that corresponds to the altar and the flanked chapels.

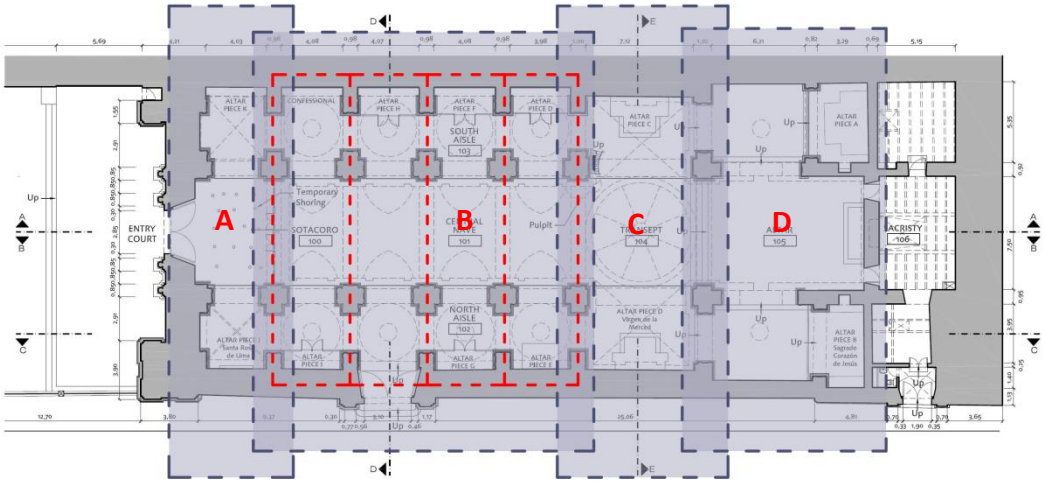

Figure 53. Configuration of sectors used of the numerical model.

All the sectors of the numerical models are constructed following the procedure applied in the previous chapter. Each model is initially created in AutoCAD to deal with the complexity of the geometry by using *Arch* and *Line*, and then imported and merged in DIANA. Differently from SAP 2000, it should be mentioned that the meshing is not performed automatically during the import of the model from AutoCAD. This opens up several possibilities of comparing the elements and mesh size to use in the FE mesh of the complete numerical model. Anticipating what is presented in detail in **Section 5.2.1.**, *Class–I beams* 2-noded elements that take into account the shear deformation are used for all the elements of this model. The FE mesh consist of 17209 elements and 15083 nodes.

Concerning the construction of the model corresponding to each sector, it should be mentioned that Sector B and C are constructed under the assumptions considered for the 3D–architectural models described in **Chapter 3** and **Chapter 4.** The properties assigned to each element belonging to Sectors B and C are presented in **Table 22** and **Table 39.** An even higher level of uncertainty is associated with Sectors A and D than the uncertainty discussed for Sectors B and C in **Chapter 3**. The geometrical configuration and the cross section of the elements belonging to the new sectors is assumed mainly on the basis of the available information in literature. In particular, It should be noted that Garcia Bryce & Soto Medina (2014) represents currently the only source for such

information for Sector D. Due to this, some simplifications are considered for the model of these sectors: (1) only one of the two levels covering the lateral extensions of Sector A is modelled and (2) arches similar to those used in the arms of the transept are assumed to compose the barrel vaults covering Sector D. In particular, it seems that posts are embedded in the masonry wall between the altar and the chapels to support these barrel vaults but no information seems to be available. For this reason, the barrel vaults are assumed to be carried by wooden beams connected with the posts of the central pillars and masonry walls. Moreover, diagonal elements are constructed below these beams to reduce the large span in correspondence to the trilobite openings connecting the altar with each chapels. Regarding the distribution of material throughout these sectors, very little information is available and similarities are assumed with the representative bay and the transept to complete the model. A summary of the properties that are assumed in these sector is shown in **Table 40.** Finally, elements made of cedar are added in the barrel vaults of the transept, of the altar as well as of the chapels in order to avoid multiple local modal modes in the FE model. If these elements are not present in the structure, the cane and rendering will provide the necessary restraint effect. The bracing elements are assumed made of cedar as the elements that they are connecting, and they have a cross section 0.15 x 0.15 m^2.

The same material characterization proposed by (GCI & PUCP, 2014) and presented in the previous chapter is assumed also in this model. Besides, similar calculations for the specific weight, as performed in **Section 4.1.3**, are made to take into account the weight of the covering layers of the structure for Sectors A, C and D.

Regarding the boundary conditions, the base of the posts composing the nave pillars and of the pilasters is gain pinned. Translational displacements are restrained in correspondence of the connections of the beams and the diagonals supporting the barrel vaults of the altar and chapel with the masonry walls. All the timber joints are modelled as rigid connections, as shown in **Figure 54**.

Table 39. A summary of the geometrical and material properties for Sector C.

Structural Part	Element	Wooden Species	Equivalent Specific Weight [kN/m^3]	MOE [kN/m^2]	Base [m]	Height [m]
Main Dome	Vertical rib	Cedar	60.78	9.38E+06	0.08	0.25
	Horizontal element	Cedar	60.78	9.38E+06	0.04	0.25
	Ring beam	Cedar	60.78	9.38E+06	0.30	0.25
Square frame	Beams	Sapele	40.60	8.61+06	0.25	0.25
	Horizontal element	Sapele	40.60	8.61+06	0.25	0.25
Framework	Arch	Sapele	39.16	8.61+06	0.15	0.15
	Penditive	Sapele	39.16	8.61+06	0.12	0.25
	Diagonal	Sapele	36.16	8.61+06	0.15	0.15
Central pillar (upper part)	Central post	Huarango	17.76	1.69+07	0.25	0.25
Central pillar (upper part)	Central post	Huarango	4.81	1.69+07	0.25	0.25
	Lateral posts (1–2)	Sapele	23.61	8.61+06	0.12	0.25
	Lateral post (3–7)	Sapele	23.61	8.61+06	0.25	0.25
	Lateral post (6–10)	Sapele	23.61	1.69+07	0.25	0.12
	Lateral post (11–12)	Sapele	23.61	8.61+06	0.12	0.25
Bracing	Horizontal element (3–7 / 4–5 / 8–9 / 4–8 / 5–9)	Sapele	4.81	8.61+06	0.11	0.22
	Horizontal element (1–2 / 6–10 / 8-9 / 11–12)	Sapele	4.81	8.61+06	0.10	0.10
Aisles	Principal arch	Cedar	78.39	9.38E+06	0.12	0.25
	Secondary arch	Cedar	78.39	9.38E+06	0.08	0.25
	Vertical element	Sapele	4.81	8.61+06	0.12	0.12
	Beam I	Sapele	4.81	8.61+06	0.25	0.25
	Beam II	Sapele	4.81	8.61+06	0.25	0.25
	Beam III	Sapele	4.81	8.61+06	0.25	0.25

Table 40. A summary of the geometrical and material properties for the model of sector A and D.

Structural Part	Element	Wooden Species	Equivalent Specific Weight [kN/m^3]	MOE [kN/m^2]	Base [m]	Height [m]
Horizontal element (Sector A)	Aisle deck	Sapele	69.83	8.61+06	0.10	0.15
	Main nave deck	Sapele	4.81	8.61+06	0.25	0.12
	Longitudinal beam I	Sapele	69.83	8.61+06	0.25	0.25
	Longitudinal beam II	Sapele	4.81	8.61+06	0.25	0.25
Barrel vault (Sector D)	Arch of the altar	Cedar	99.51	9.38E+06	0.08	0.25
	Arch of the chapels	Cedar	92.58	9.38E+06	0.08	0.25
	Beams	Sapele	70.83	8.61+06	0.25	0.25
	Diagonals	Sapele	4.81	8.61+06	0.15	0.15

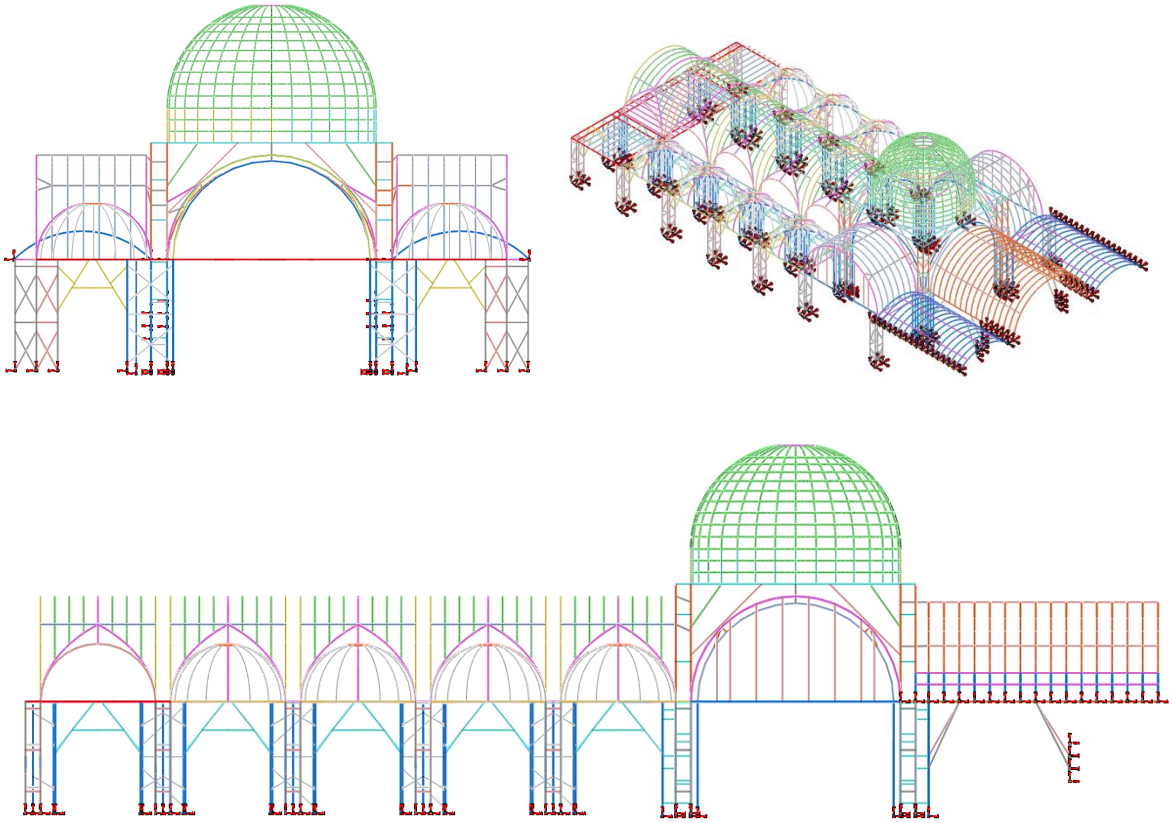

Figure 54. Numerical model of the complete timber structure of Ica Cathedral.

5.2 Structural analysis

5.2.1 Preliminary analysis

As previously anticipated, DIANA offers several classes of beam element – which can be meshed automatically or manually – and the possibility to divide each element specifying a factor. In order to choose the optimized FE mesh for the model of the complete timber structure, preliminary studies are carried out on the model of the representative bay by performing linear elastic analyses under self–weight.

The model of the representative bay is initially meshed by using *Class–I* and *Class–II beam* elements with the same mesh size used in the model presented in **Chapter 4**. It should be mentioned that both the elements are modelled as a classical beam, i.e. two–node straight element with a transverse displacement expressed by a cubic Hermite shape function. The difference between *Class–I* and *Class–II beam* elements concerns the numerical integration performed: while the former is

integrated only along the beam axis, the latter is integrated in the area of the cross section as well. Moreover, while *Class–II beam* element is modelled according the Bernoulli theory, the incorporation of shear deformation can be taken into account for *Class–I beam* (TNO DIANA, 2014). The results obtained by using SAP 2000 in **Chapter 4** are compared with those obtained by modelling the representative bay with these elements in DIANA. In particular, the relative error between the two solutions is calculated in terms of reactions and internal forces occurring in the main elements. The absolute maximum error occurs when the calculation is carried out for the reaction corresponding to the post in the inner part of the nave pillar. For each class of beam element, the obtained values of the absolute error in this case are shown in **Table 41.** In particular, the largest error is observed when it is calculated comparing *Frame* element in SAP 2000 and both the classes without shear deformation in DIANA. On the contrary, almost no error is obtained when the shear deformation is taken into account in *Class– I beam* element, hence when the cross–section remains plane but not perpendicular to the slope of the beam axis.

Table 41. Absolute maximum error considering different elements in DIANA.

	Absolute maximum error (%)
***Class – I beam* element**	10.1
***Class – I beam* element with shear deformation**	0.7
***Class – II beam* element**	11.8

Afterwards, different mesh sizes are considered in order to validate the FE mesh to be applied to the model of the complete timber structure. Hence, other two models are created dividing each element of the original FE mesh into two and four elements. The relative error calculated as previously for the reaction of the central post shows that considering smaller mesh size does not diminish significantly its value. In particular, the relative error calculated by comparing the value obtained considering *Frame* element in SAP 200 and *Class–II beam* element in DIANA is exactly the same for all the mesh sizes, meaning that the meshes are sufficiently refined.

On the basis of the obtained results, *Class–I beam* elements are used to model the complete timber structure taking into account the shear deformation according to the theory of Timoshenko – in particular, no shear stress correction factors are specified.

5.2.2 Analysis under self–weight

This section presents the linear elastic analysis performed on the model of the complete timber structure under self–weight. Concerning the representative bays, the results show the same qualitative distribution of displacements and internal forces observed in **Section 3.3.1**, as expected. The transept, and in particular the crossing, represents the most critical part of the complete timber structure under self–weight. Due to this, the following section focuses on this specific structural part.

Figure 55 presents the vertical displacements throughout the complete timber structure. Relatively high value of displacement is observed in some parts of the structure, such as the vertical displacement of 1.8 cm that occurs in the ring beam at the bottom of the main dome and in the central part of the barrel vault covering the altar. However, this high value of deformation can be attributed to the same considerations that are made regarding the representative bay in **Chapter 4**. It should be noted that the displacement that is observed in the longitudinal beams close to the masonry walls is 5.0 mm, approximately. Compared to the results obtained from the analysis of the representative bay in **Chapter 4**, this value is almost four times lower – as expected considering the assumption regarding the timber joints.

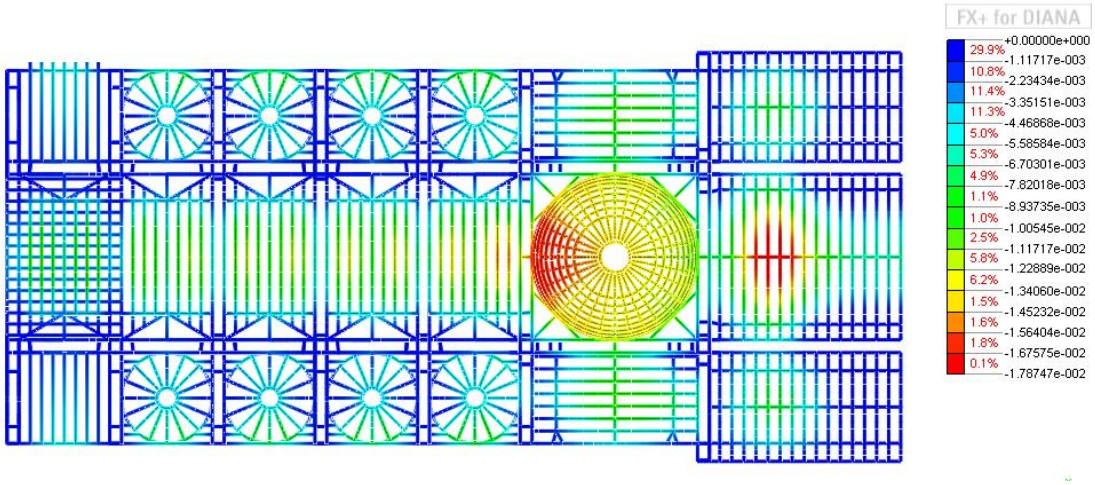

Figure 55. Vertical displacements of the timber structure of Ica Cathedral under self-weight.

In terms of internal forces, it should be mentioned that the crossing of the transept represents the most critical part. While elements that compose the main dome show relatively low values of compressive axial force, the ring beam at the bottom is subjected to significant combined internal forces. Besides, biaxial bending and torsional moments occur in the beam that compose the square wooden framework surrounding the ring beam. The diagonal elements that support the square

wooden frameworks are subjected to compressive axial force working as struts. Proceeding downward from the top to the bottom, significant compressive axial force with biaxial bending moments is observed in the posts of the central pillars supporting the structure above. It should be noted that the sum of the vertical reactions calculated at the bottom of each post constituting the four central posts is more than 40% of the weight of the total structure (5955 kN).

5.2.3 Mass proportional lateral loading

In order to investigate the behaviour of the structure under horizontal loads, mass proportional lateral loading is applied to the model in XX and YY directions – i.e. longitudinal and transversal directions, respectively. It should be noted that the structure is symmetrical, then only one analysis is performed for the direction YY. It is not possible to estimate a global stiffness for the structure, as it is carried out for the model of the frame wall in **Chapter 2**. Therefore, a comparison of the stiffness values of the main structural parts composing the timber structure is carried out in this section. This study is also performed in order to better understand the contribution of the timber structure to the future combined model with timber and masonry structures.

The structural response of the complete timber structure is studied by considering several control points of translational displacement in the principal structural parts. On the whole, the control points are chosen by taking into account the symmetry of the structure and the location where the maximum horizontal displacements are observed in each structural part. In particular, it should be mentioned that the control points AD1 and AD2 presented in **Figure 42** corresponds to nodes at the top of the aisles' domes close to the main dome and to the façade, respectively. Concerning the control point BV, this corresponds to a node located at the top of one of the primary arches of the barrel vault with lunettes close to the main dome. Chosen the control point for each structural part, the corresponding global stiffness is evaluated for each loading direction.

As shown in **Figure 42**, the obtained results point out that similar stiffness values are obtained considering the displacements of the control point MD when the load is applied in different directions, as expected. The values of stiffness obtained for the control points of the aisle's domes, AD1 and AD2, are higher than those obtained for of the main dome. Moreover, both the displacements of the control points AD1 and AD 2 are significantly different when the lateral loading is applied in XX and YY directions – in particular, smaller displacements are observed in XX direction. This significant difference in stiffness is shown also by the control point BV. On the contrary, larger

displacements in XX direction are observed for the control points corresponding to nodes of the barrel vault covering the arms of the transept and the altar, TR and AL respectively. Finally, this difference in the structural behaviour is even more accentuated in correspondence of the barrel vault covering the main entrance of the timber structure: the value of stiffness obtained in XX directions is less than half of that obtained in YY one.

The deformed shapes of the timber structure are shown in **Figure 56**, **Figure 57** and **Figure 58**. It should be noted that the values of the horizontal displacements are calculated for a lateral loading of 1.00g. The obtained results show clearly that it is difficult to evaluate a global stiffness value of the structure as the displacement of each point of the structure differs in value and direction. It is also noted that the most of the displacement concentrates in the upper part of the structure, which remains as the less stiff region.

Table 42. Values of stiffness considering different structural parts [g/m].

	Direction		
Main structural part	**+XX**	**–XX**	**±YY**
Main Dome (MD)	6.23	5.94	5.84
Barrel Vault (BV)	13.49	12.59	8.47
Aisle Dome 1(AD1)	13.98	13.94	9.81
Aisle Dome 2 (AD2)	16.40	15.94	14.35
Arm of the Transept (TR)	14.24	13.28	20.47
Altar (AL)	9.88	10.29	10.80
Main entrance (ME)	60.32	61.33	158.08

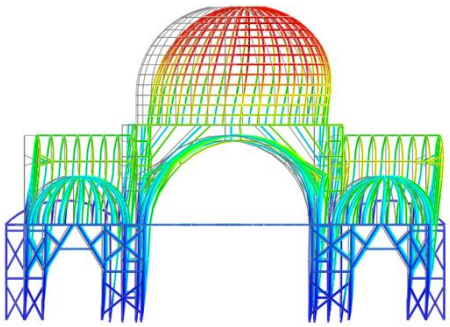

Figure 56. Deformation under lateral loading ±YY direction.

MIN VALUE (blue): $+3.45 \cdot 10^{-3}$m
MAX VALUE (red): $-1.95 \cdot 10^{-1}$m

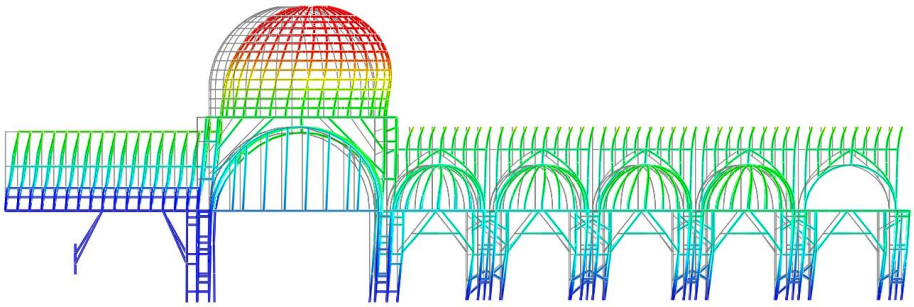

Figure 57. Deformation under lateral loading –XX direction

MIN VALUE (blue): $-5.17 \cdot 10^{-3}$m
MAX VALUE (red): $-1.73 \cdot 10^{-1}$m

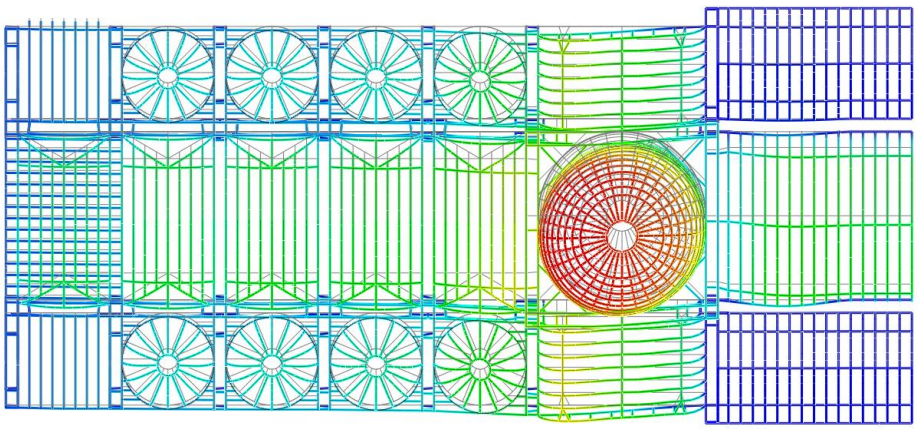

Figure 58. Deformation under lateral loading ±YY direction

MIN VALUE (blue): 3.45e–0.03 m
MAX VALUE (red): 1.95e–0.01 m

5.2.4 Eigenvalue analysis

Eigenvalue analysis is performed in order to provide an insight into the dynamic response of the complete timber structure of Ica Cathedral. As described in **Section 5.1**, elements are added to the numerical model of the complete timber structure with the attempt to eliminate some local modes with low values of participating masses – in particular, regarding the principal and the secondary arches of the arms of the transept as well as of the chapels and altar. On the basis of the results obtained from this analysis, improvements are carried out in the future combined model with timber and masonry structures.

Natural frequencies and natural mode shapes are calculated by performing eigenvalue analysis in DIANA (TNO DIANA, 2014). The percentage of the mass of the structure contributing to its dynamic behaviour is calculated for each natural mode of vibration. In particular, the modes with high values of participation masses are investigated as they generally correspond to the most relevant modes to characterize the dynamic response of the structure. In particular, **Table 43** shows the modes for which the modal participation mass percentage is higher than 2%. Selected mode shapes are shown in **Figure 59** illustrating the behaviour of the main structural parts composing the complete timber structure. As indicated before, the most flexible area is the cupola and then the main nave, which partly justifies the collapses found in the timber structure after the earthquake. Finally, it should be mentioned that the total cumulative percentage of mass participation reaches 90% for frequencies around 12.6 Hz.

Table 43. Modes with the modal participation mass percentage higher than 2%.

Mode	Frequency (Hz)	Modal Participation Mass		
		X-X (%)	**Y-Y** (%)	**Z-Z** (%)
1	1.41	0.00	23.74	0.00
2	1.51	22.96	0.00	0.01
3	1.75	0.01	4.27	0.00
4	1.96	0.00	8.37	0.00
5	2.08	42.80	0.01	0.04
6	2.11	0.00	20.87	0.00
52	2.57	7.71	0.00	0.14
72	2.96	0.00	9.22	0.00
98	4.10	0.12	0.01	2.44
100	4.20	0.08	4.06	0.00
105	4.55	0.00	2.06	0.01
255	5.19	0.10	0.02	3.12
308	6.57	0.72	0.00	2.25

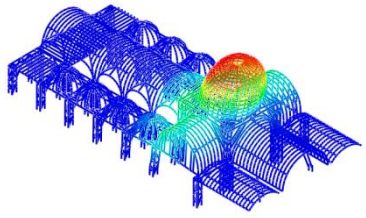

Mode 1 (1.41 Hz)

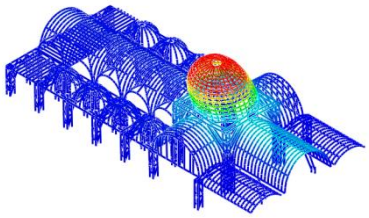

Mode 2 (1.51 Hz)

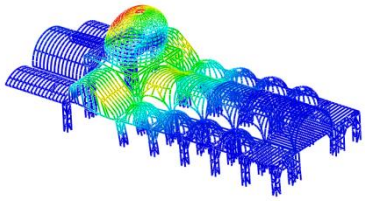

Mode 4 (1.96 Hz)

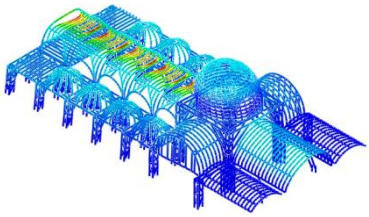

Mode 5 (2.08 Hz)

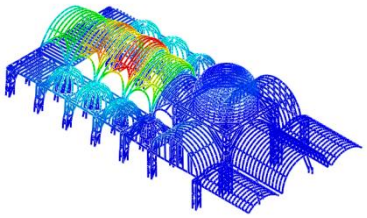

Mode 6 (2.11 Hz)

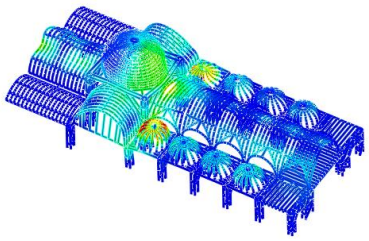

mode 98 (4.10 Hz)

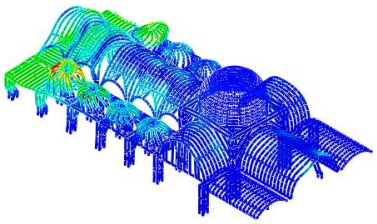

Mode 100 (4.20 Hz)

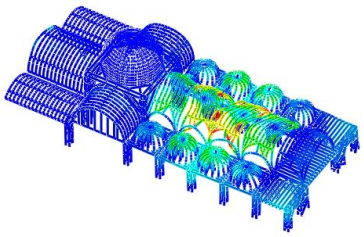

Mode 105 (4.55 Hz)

Figure 59. Selected mode shapes of the timber structure of Ica Cathedral.

Chapter 6

Conclusion

This thesis presents the study performed to assess the structural performance of the timber structure of Ica Cathedral. A multidiscipline approach emerged to be crucial in order to bring light to the several uncertainties – that still are present in the structure – and to formulate reasonable assumptions. Moreover, a combination of softwares was necessary to be used for the purpose of performing different studies. While SAP 2000 was chosen to model the *Link* element to simulate the semi–rigid behaviour of the timber connections, MIDAS FX+ for DIANA was used to explore different possibilities for the FE mesh of the model of the complete timber structure. Both the numerical models were constructed by creating different models in AutoCAD. The 3D–architectural models that were initially created in AutoCAD were used to better understand the configuration and the behaviour of the timber structure. Moreover, they were very important to evaluate the contribution of the covering layers used in *quincha* technique. On the basis of these 3D–architectural models, the model with *Line* and *Arch* was created for each structural part in AutoCAD to deal with the complex geometry and these were allow imported to SAP 2000 and to MIDAS F+ for DIANA.

Returning to the focus of this thesis, analytical and numerical modelling of the timber wall were constructed in order to simulate the mechanical behaviour that was observed during the quasi–static in–plane cyclic tests carried out by Poletti (2013). The former was constructed by applying the

component method, while the latter was calibrated by comparing with experimental results and applying the inverse fitting method. In order to study the semi–rigid behaviour of the timber connections, linear and nonlinear analyses were carried out. The comparison between the analytical and numerical models showed a significant difference in terms of axial stiffness in tension pointing out the need to consider more aspects that are not currently covered by codes. On the whole, the obtained results show that the experimental results were approximated well by the numerical model.

The deep insight into the main features that characterise Ica Cathedral allowed to compare the information available in literature (Cancino, et al., 2012) and (Garcia Bryce & Soto Medina, 2014) with the results of the recent survey (Greco, et al., 2015). The 3–D architectural models of the representative bay and of the transept represent the result of this process and they contribute to upgrade the documentation regarding Ica Cathedral.

Structural analysis was performed on one of the representative bays of Ica Cathedral under vertical and lateral loads. The most critical joints were identified performing parametric analyses allowing to select the most important timber connections to be surveyed, experimentally tested and numerically modelled in further studies. In fact, the obtained results show that it was not possible to introduce the nonlinear behaviour of the timber joints in the model of Ica Cathedral on the basis of the experimental results provided by (GCI & PUCP, 2014). Global and local verifications were carried out in order to evaluate the compliance of the representative bay under self–weight and live load with the various criteria specified by Eurocode 5 (2004). According to the results obtained from the global verifications, all the straight timber elements are verified for ULS, while few elements do not respect the recommended limit values of displacements. High values of deformation can be attributed to some uncertainties and to conservative assumptions that are considered. However, it should be said that high values of deformation are present in existing historical structures without compromising their performance to an unacceptable level. Finally, the actual failure was discussed with a seismic assessment of the connections present in the beams located at the top of the barrel vaults with lunettes. The obtained results show that the stresses that occur under seismic action in these beams are large enough to provoke the failure of the structure.

Established that it was not possible to introduce directly the nonlinear behaviour of the most critical joints in the representative bay, the numerical model of the complete timber structure of Ica Cathedral was constructed and studied by performing linear elastic analyses under self–weight, mass

proportional lateral loading and eigenvalue analysis. The obtained results show that (1) the crossing of the transept represents the most critical part when the complete structure is considered, (2) it is difficult to evaluate a global stiffness value of the structure, (3) the upper part of the complete structure is the less stiff region. The obtained results represent the starting point for further research on the numerical modelling of the combined timber and masonry structures present in Ica Cathedral.

According to the results of this research project and given the above conclusions, some interesting topics were identified for future works. In particular,

- Further research regarding the semi-rigid behaviour of the timber connections investigated in the timber frame wall considering the contribution of the nails and both the contact surfaces for each timber joint;
- Improvement of the knowledge available regarding the connections, the material and the configuration of the timber elements present in Ica Cathedral by mean of testing and geometrical surveys;
- Problem of stability – flexural and torsional – for the curved roof framing system of Ica Cathedral;
- Complete seismic assessment of the timber elements in order to discuss the performance of structures constructed with *quincha* technique;
- Investigation of the nonlinear behaviour of the timber structure modelling the timber joints with a similar approach to that used in Chapter 2 ;
- Structural analysis of the numerical model of the combined model with timber and masonry structures with particular attention to the modelling of their connection and to their difference in stiffness.

References

Branco, J., 2008. *PhD Thesis. Influence of the joints stiffness in the monotonic and cyclic behaviour of traditional timber trusses. Assessment of the efficacy of different strengthening techniques,* Guimaraes: University of Minho and University of Trento.

Branco, J., Descamps & T, 2015. Analysis and strengthening of carpentry joints. Available online 23 May 2015, available http://www.sciencedirect.com/science/article/pii/S0950061815006029.

Bulleit, M. W., Bogue Sandberg, L., Drewek, M. W. & O' Bryant, T., 1999. Behaviour and modelling of wood-pegged timber frames. *Structural Engineering, ASCE,* 125(1), pp. 3-9.

Cancino, C., Lardinois, S., D'Ayala, D. & Ferreira, C. F., 2012. *Seismic Retrofitting Project : Assessment of Prototype Buildings,* Los Angeles: The Getty Conservation Institute.

Carbajal, F., Ruiz, G., Schexnayder, C. J. & ASCE, F., 2005. Quincha Construction in Peru. *Practice periodical on structural design and construction*, February, pp. 10, 56-62.

Chang, W., Hsu, M. F. & K., K., 2006. Rotational performance of traditional Nuki joints with gap I: theory and verification. *Journal of Wood Sciences,* Issue 52, pp. 58-62.

Chopra, A. K., 2012. *Dynamics of Structures: Theory and Applications to Earthquake Engineering.* 4th Edition ed. Englewood Cliffs, New Jersey: Prentice Hall.

CSI, 2014. *Analysis Reference Manual for SAP 2000, ETABS, SAFE and CSiBrisge.* Berkeley, California, USA: Computers & Structures.

Descamps, T., 2013. *Old carpentry joints,* University of Mons, Belgium: Training school on assessment and reinforcement of timber elements.

Descamps, T. & Guerlement, G., 2009. Component method for the assessment of the axial, shear and rotational stiffness of connections in old timber frames. In: *Proceedings of the 9ème Congrès National de Mécanique.* Marrakech: FS Semlalia.

Drdácký, M., Wald, F. & Sokol, Z., 1999. Sensitivity of historic timber structures to their joint. In: *Proceedings of the 40th Anniversary Congress of the IASS.* Madrid.

Ercüment, E., 2002. Timber joint design: the geometric breakdown method. *Building Research & Information,* 30(6), pp. 446-469.

Eurocode 5, 2004. *EN 1995-1-1:2004: Design of timber structures - Part 1-1: general - common rules and rules for buildings.* Brussels: CEN, European Committee for Standardization.

Feio, A., 2005. *Inspection and diagnosis of historical timber structures: NDT correlations and structural behaviour. PhD thesis.,* Guimaraes, Portugal: University of Mihno.

Ferreira, C. F. & D'Ayala, D., 2012. Numerical modelling and structural analysis of historical ecclesiastical buildings in Peru for seismic retrofitting. In: *Proceedings of the 8th International Conference on Structural Analysis of Historical Constructions, 15-17 October 2012.* Wroclaw, Poland: Wroclaw, SAHC.

Ferreira, C. F. & D'Ayala, D., 2014. Structural analysis of timber vaulted structures with masonry walls. In: *Proceedings of the SAHC2014-9th International Conference on Structural Analysis of Historical Constructions, Mexico City, Mexico 14-17 October 2014.* Wroclaw, Poland: F. Peñan and M. Chavez.

Ferreira, C. F., D'Ayala, D., Fernandez Cabo, J. L. & Diez, R., 2013. Numerical Modelling of Historic Vaulted Timber Structures. *Advanced Materials Research,* Volume 778, pp. 517-525.

Garbin, E., 2015. *Presentaion SA5_Basic design of timber structures.* University of Padova, SAHC.

Garcia Bryce, J. & Soto Medina, M., 2014. *Proyecto de conservación y estabilización sismorresistente Catedral de Ica,* Ica: The Getty Conservation Institute - Pontificia Universidad Catolica del Peru.

GCI & PUCP, 2014. *SRP Testing Modelling Report Testing Chapter III_20140315_V5_review PUCP&GCI,* Los Angeles: The Getty Conservation Institute.

Greco, F., Karanikoloudis, G., Lourenço, P. B. & Mendes, N., 2015. *Experimental in situ testing campaign on adobe historic structures in Peru, within the Getty SRP,* Guimarães: The Getty Conservation Institute.

Harth-Terré, E., 1948. [2003]. Los artífices vascos en el Perú Virreina. In: *IIème Congrès d'Etudes Basques = Eusko Ikaskuntzaren VII. Kongresua = VII Congreso de Estudios Vascos.* Ikaskuntza, Donostia [San Sebastián]: Eusko, pp. 451-54.

Holzer, S. M. & Köck, B., 2009. Investigations into the structural behaviour of German baroque timber roofs. *International Journal of Architectural Heritage,* 3(4), pp. 316-338.

ISO 21581, 2010. *Timber structures — Static and cyclic lateral load test method for shear walls,* Swizerland: International Organization for Standardization.

Jurina, L. & Righetti, M., 2007. Traditional building in Peru. In: *XVI IIWC Internation Conference and Symposium.* Florence - Venice - Vicenza: 11th-16 Nov 2007.

Kock, B. & Holzer, S. M., 2010. The load–displacement behaviour of halved joints. In: *Proceedings of the 11th World Conference on Timber Engineering.* Riva del Garda, Italy.

Kock, H., Eisenhut, L. & Seim, W., 2013. Multi-mode failure of form-fitting timber connections – Experimental and numerical studies on the tapered tenon joint. *Engineering Structures,* Volume 48, pp. 727-738.

Lambe, T. W. & Whitman, R. V., 1969. *Soil Mechanics.* New York: John Wiley & Sons.

Miller, J. F. & Schmidt, R. J., 2004. *Capacity of pegged mortise and tenon joinery,* University of Wyoming, USA: Department of Civil and Architectural Engineering.

Palma, P. & Cruz, H., 2007. Mechanical Behaviour of Traditional Timber Carpentry Joints in Service Conditions - Results of Monotonic Tests. In: *Proceedings of "From material to Structure - Mechanical behaviour and failures of the timber structures.* XVI International Symposium: IWC, ICOMOS.

Palma, P., Garcia, H., Ferreira, J. A. & Cruza, H., 2012. Behaviour and repair of carpentry connections – Rotational behaviour of the. *Journal of Cultural Heritage,* Volume 13s, p. S64–S73.

Parisi, M. A. & Piazza, M., 2008. Seismic strengthening of traditional carpentry joints. In: *The 14th World Conference on Earthquake Engineering.* Beijing, China.

Piazza, M., Tomasi, R. & Modena, R., 2005. *Strutture in legno.* Milano: Hoepli.

Poletti, E., 2013. *PhD Thesis. Characterization of the seismic behaviour of traditional timber frame walls.* Portugal: University of Mihno.

Quinn, N., D'Ayala, D. & Moore, D., 2012. Experimental testing and numerical analysis of quincha under lateral loading. In: *Proceedings of SAHC, Structural Analysis of Historical Constructions.* Wrocław, Poland: Jerzy Jasieńko.

Rautenstrauch, K., Hädicke, W., Löffler, A. & Müller, J., 2010. Simulation and research of a rounded dovetail connection. In: *Proceedings of the 11th World Conference on Timber Engineering.* Riva del Garda, Italy.4

Rodriguez Camilloni, H., 2003. Quincha architecture: The development of an antiseismic structural system in seventeenth century Lima. In: *Proceedings of the First International Congress on Construction History.* Madrid, 20th-24th January 2003: S. Huerta, Madrid: I. Juan de Herrera, SEdHC, ETSAM, A. E. Benvenuto, COAM, F. Dragados.

Schmidt, G. R. & Daniels, C. E., 1999. *Design considerations for mortise and tenon.,* University of Wyoming, USA.

Sharma, S., 2015. *Structural analysis of the masonry envelope of Ica Cathedral, Peru,* Guimaraes, Portugal: SAHC Masters Thesis.

Tampone, G., 1996. *Il restauro delle strutture di legno.* Milano: Hoepli.

Tannert, T., Lam, F. & Vallée, T., 2011. Structural performance of rounded dovetail connections: experimental and numerical investigations.. *European Journal of Wood and Wood Products,* pp. 471-482.

TNO DIANA, 2014. [Online] Available at: http://tnodiana.com/DIANA-manuals

Tolles, E. L., Kimbro, E. E. & Ginell, W., 2002. *Planning and Engineering Guidelines for the Seismic Retrofitting of Historic Adobe Structures,* Los Angeles: The Getty Conservation Institute.

Tomasi, R., Piazza, M., Parisi, M. A. & Branco, J., 2007. Analisi sperimentale su collegamenti tradizionali e rinforzati nelle capriate. In: *Convegno Nazionale L'Ingegneria Sismica in Italia.* Pisa, Italy.

Tomaževic, M., 1999. *Earthquake-resistant design of masonry buildings.* London: Imperial College.

Vasconcelos, G. & Lourenço, P. B., 2009. In-Plane Experimental Behavior of Stone Masonry Walls under Cyclic Loading. *Journal of Structural Engineering,* 135(10), pp. 1269-1277.

Wald, F., Mares, Z., Sokol, M. & D. F., 2000. Component Method for Historical Timber. *The Paramount Role of Joints into the Reliable Response of Structures. NATO Science Series,* 4(129), pp. 417-424.

Further Development

The combined timber and masonry structures

This section presents additional integrated research carried out on the basis of the results obtained from the two thesis developed in parallel by Ciocci (2015) and Sharma (2015). The former is focused on the internal timber structure, while the latter on the external masonry envelope. The aim of this collaboration is to investigate how both the structural systems interact and influence the global behaviour of Ica Cathedral. The obtained results represent the foundation work for further developments.

1.1 Introduction

The results obtained from both the theses point out that the interaction between the timber and masonry structures is a critical factor that greatly influences the structural response of Ica Cathedral. A summary of these results which provide the motivation to proceed with this challenging endeavour are summarised below:

- Nonlinear seismic analysis on the masonry envelope shows much more extensive damage in the masonry than seen in the real structure (Sharma, 2015). Moreover, such damages are observed at lateral loads lower than or equal to the design peak ground acceleration

corresponding to the location of Ica Cathedral by the Peruvian Code. This is despite the fact that the performance of the Ica Cathedral globally can be considered acceptable during the 2007 Pisco earthquake (Cancino, et al., 2012).

- Eigenvalue analysis of the masonry envelope results in no mode of vibration in which both the longitudinal walls of the cathedral are activated simultaneously (Sharma, 2015). On the other hand, experimental results obtained from the ambient vibration tests report most modes to involve both the walls together (Greco, et al., 2015). This can be safely assumed to be due to the connection of both these walls by the timber structure.
- The transversal beams close to the longitudinal masonry walls do not comply with the criteria specified by Eurocode (2004) for the Serviceability Limit State, as mentioned in (Ciocci, 2015). Along all the possible causes, this is likely due to ignoring the influence of the masonry.
- Eigenvalue analysis of the complete timber structure performed in (Ciocci, 2015) shows a co-relation with the existing damage in Ica Cathedral due to the experienced earthquakes. Performing an eigenvalue analysis on the combined model with the timber and the masonry structure can provide a more in-depth co-relation.
- As mentioned in (Ciocci, 2015), the results obtained from the mass proportional lateral loading of the complete timber structure show clearly that it is difficult to evaluate a global stiffness value of the timber structure as the displacement of each point differs in value and direction. It is interesting to evaluate the stiffness of the combined model and compare the results with those obtained from the timber and masonry structures considered independently.

1.2 Definition of the numerical model

The finite element model of both timber and masonry structural systems is constructed in Midas FX+ for DIANA software, as shown in **Figure 1**. The numerical model is primarily based on the individual models initially prepared for them. All the details regarding the FE mesh, material properties, special features and considerations of these numerical models can be found in (Ciocci, 2015) and in (Sharma, 2015). In particular, *Class–I beam* elements are used to model the complete timber structure taking into account the shear deformation according to the theory of Timoshenko, while *3D isoparametric solid linear* elements are used to model the masonry structure. in addition, *one-noded translation*

spring dashpot elements are used to simulate the influence of the adjoining cloister (TNO DIANA, 2014).

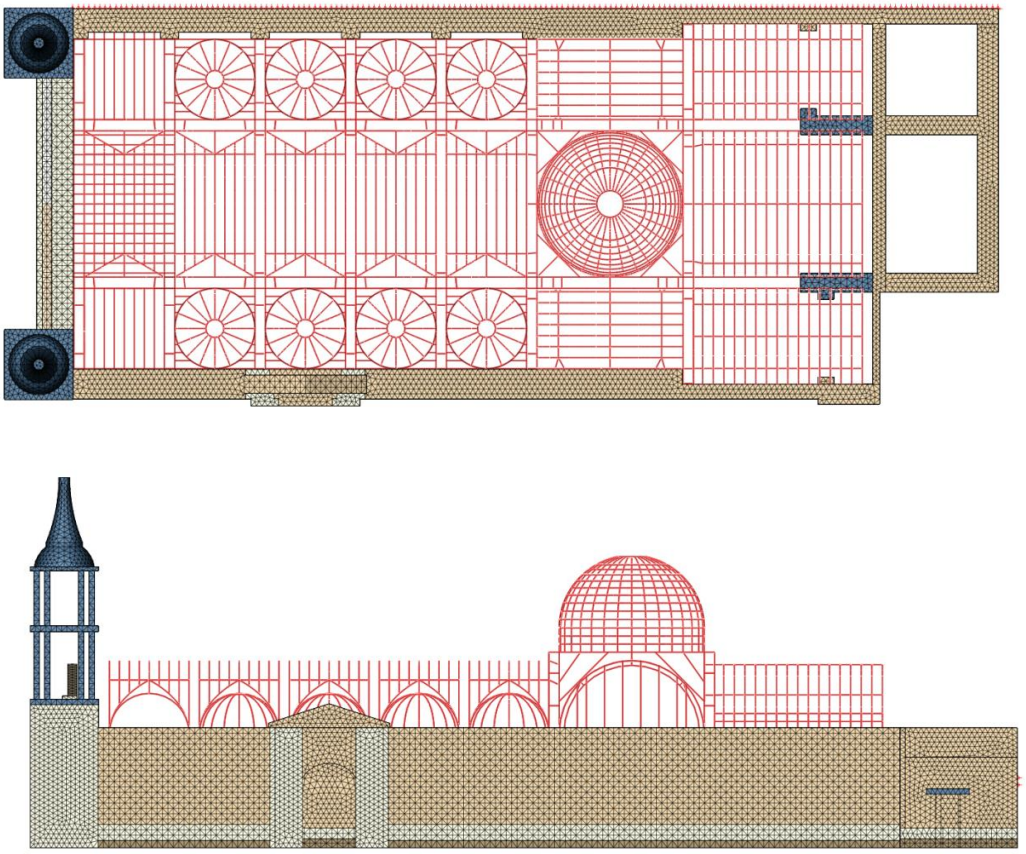

Figure 1. Numerical model of the combined model with both timber and masonry structures.

However, few geometrical adjustments are necessary in order to integrate both the models together. The crucial aspect that has to be considered with particular attention is the connection existing between the two structural systems. It should be mentioned that very little information is available in literature regarding the geometry of these connections (Cancino, et al., 2012). In order to perform this study, the connections are assumed to be between (1) the wooden beams in the upper part of the *sotacoro* and the fired brick façade and the longitudinal masonry walls, (2) the transversal wooden beams of the bays and the longitudinal masonry walls and (3) the wooden beams supporting the barrel vaults of the chapels and altar and the masonry walls (**Figure 2**). These connections are modelled in the numerical model by merging the nodes of the beam elements and the corresponding ones generated by imprinting them on the masonry. It should be mentioned that 0.3 m timber plates are assigned to the upper part of the masonry wall flanking the altar, as shown in **Figure 2**. This is

necessary to avoid the high concentration of stresses – that occurs even performing the analysis under self-weight – that was not observed during the experimental campaign (Greco, et al., 2015).

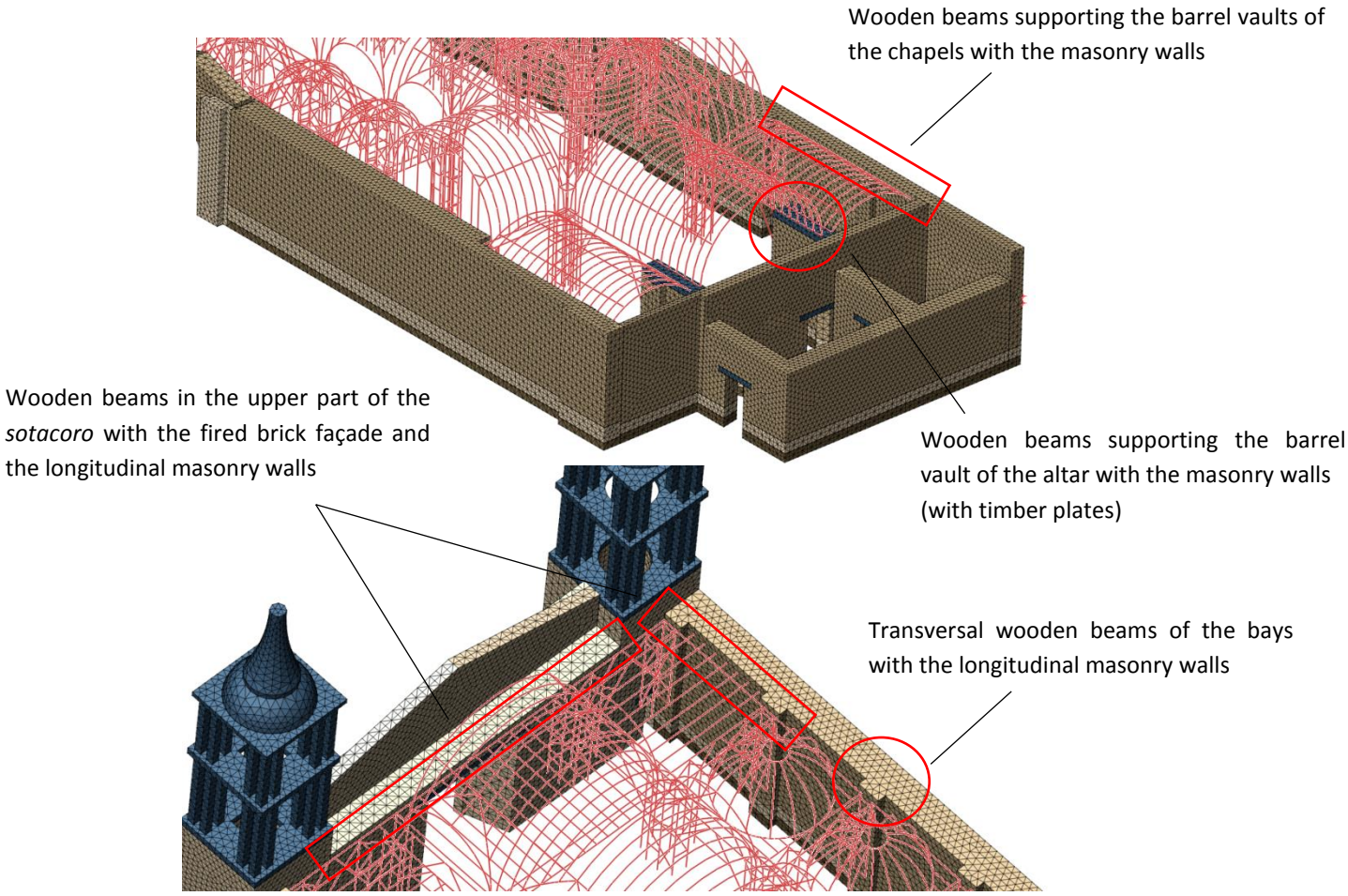

Figure 2. Details of the connections in the numerical model of the combined structures.

Finally, it should be mentioned that few elements are added when non-linear dynamic analysis is performed. These elements are added in the barrel vaults of the transept, of the altar as well as of the chapels in order to avoid multiple local modal modes in the model and to simulate the restraining effect provided by the cane and rendering in the real structure. The bracing elements are assumed made of cedar as the elements that they are connecting and they have a cross section 0.15 x 0.15 m2, as assumed in (Ciocci, 2015). Moreover, *Class–II beam* elements are used for this analysis as they can be used for nonlinear analysis (TNO DIANA, 2014).

The material properties assigned to the timber structure of the combined model are assumed to be the same as those considered in (Ciocci, 2015). Concerning the material characterization of the

masonry structure, the values obtained after calibrating the numerical model with dynamic identification tests in (Sharma, 2015) are assumed in this study.

Regarding the boundary conditions, the base of the posts composing the timber structure are pinned as well as the nodes at the bottom of the masonry walls. It should be mentioned that all the timber joints are modelled as rigid connections.

1.3 Structural analysis

In order to understand the behaviour of the combined structures of Ica Cathedral linear and nonlinear structural analyses are performed on this model. This section includes nonlinear analyses under self-weight, mass proportional lateral loading and nonlinear dynamic loading.

1.3.1 Eigenvalue analysis

An eigenvalue analysis is performed on the combined model of the timber and masonry structures. The modal participation masses of the first thirty modes in each direction are presented in **Table 1**. Additionally, **Table 2** shows the modes having modal mass participation percentage above 2%. It should be noted that some of the first modes are very similar to those obtained when only the complete timber structure is considered individually. However, it should be noted that the masonry is always activated. It can also be observed that both the longitudinal walls get activated simultaneously in the modes of vibration. Thus, the results of this analysis correspond better to the results obtained experimentally from the ambient vibration tests carried out on Ica Cathedral (Greco, et al., 2015). Selected mode shapes contributing significantly to the dynamic behaviour of the combined structure are shown in **Figure 3**.

The deformed mode shapes obtained from the eigenvalue analysis identify the main dome, the central part of the barrel vault with lunettes, the upper part of the barrel vault covering the chapels and the altar as the most likely vulnerable regions of the structure. It should be mentioned that these regions correspond to the mainly damaged ones present in the structure as a result of the experienced earthquakes (Cancino, et al., 2012). For instance, this can be clearly observed in the second mode of vibration – which corresponds to a frequency of 1.50 Hz and a modal mass participation of 3.6% in the XX direction (longitudinal) of the numerical model (**Figure 3**).

Finally, it should be noted that the combined model of the timber and masonry structures reaches a cumulative percentage of mass participation of 80% around 19.00 Hz. The same is reached for the timber structure and masonry envelope around 4.00 Hz and 17.00 Hz, respectively.

Table 1. Modal participation masses for the first thirty modes in each direction (left).
Table 2. Modes with the modal participation mass percentage higher than 2% (right).

Mode	Frequency (Hz)	Modal Participation Mass		
		X-X (%)	**Y-Y** (%)	**Z-Z** (%)
1	1.42	0.00	8.20	0.00
2	1.51	3.59	0.00	0.00
3	1.68	0.00	1.30	0.00
4	2.07	0.52	2.82	0.00
5	2.09	0.73	2.28	0.00
6	2.20	0.00	4.05	0.00
7	2.26	0.00	1.70	0.00
8	2.31	3.14	0.00	0.00
9	2.33	0.00	0.24	0.00
10	2.34	0.01	0.21	0.00
11	2.36	0.00	0.10	0.00
12	2.37	0.01	0.00	0.00
13	2.37	0.05	0.00	0.00
14	2.38	0.03	0.00	0.00
15	2.38	0.08	0.01	0.01
16	2.41	0.00	0.12	0.00
17	2.42	0.08	0.01	0.03
18	2.42	0.02	0.00	0.01
19	2.43	0.00	0.00	0.00
20	2.43	0.01	0.00	0.00
21	2.43	0.01	0.00	0.00
22	2.43	0.00	0.00	0.00
23	2.43	0.00	0.00	0.00
24	2.43	0.00	0.00	0.00
25	2.43	0.00	0.00	0.00
26	2.43	0.00	0.00	0.00
27	2.43	0.02	0.01	0.06
28	2.49	0.00	0.00	0.00
29	2.49	0.00	0.00	0.00
30	2.49	0.00	0.00	0.00
Total Cum. Percentage (%)		8.30	21.04	0.13

Mode	Frequency (Hz)	Modal Participation Mass		
		X-X (%)	**Y-Y** (%)	**Z-Z**
1	1.42	0.00	8.20	0.00
72	3.04	028	7.20	0.01
102	4.02	5.62	0.05	0.01
461	8.60	4.13	0.01	0.03
6	2.20	0.00	4.05	0.00
2	1.51	3.59	0.00	0.00
108	4.29	3.38	0.09	0.01
106	4.17	0.40	2.91	0.05
4	2.07	0.52	2.82	0.00
8	2.31	3.14	0.00	0.00
5	2.09	0.73	2.28	0.00
84	3.46	2.60	0.00	0.00
382	7.74	2.49	0.00	0.08
66	2.92	0.24	2.16	0.01
1172	17.11	0.00	0.00	2.29

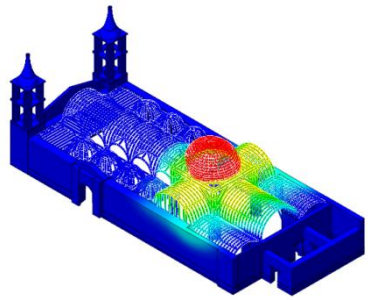

Mode 1 (1.42 Hz)

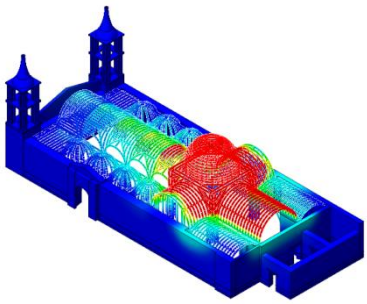

Mode 2 (1.51 Hz)

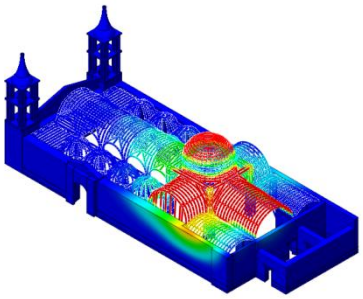

Mode 5 (2.09 Hz)

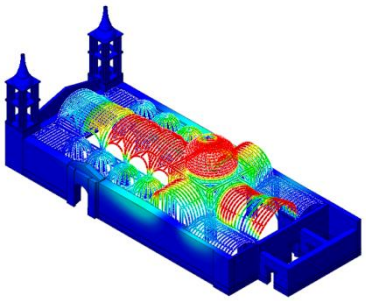

Mode 6 (2.20 Hz)

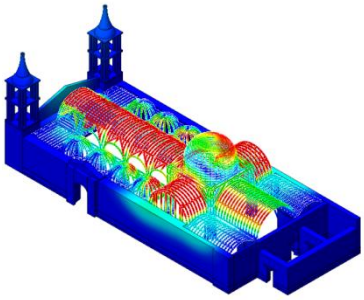

Mode 8 (2.31 Hz)

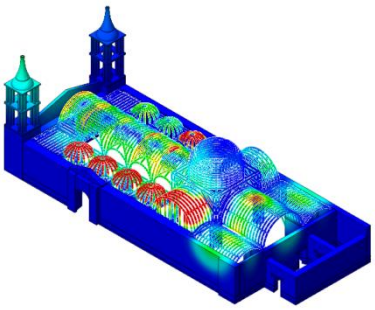

Mode 72 (3.04 Hz)

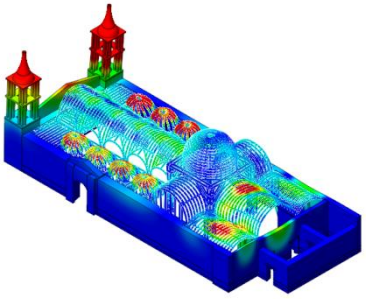

Mode 102 (4.02 Hz)

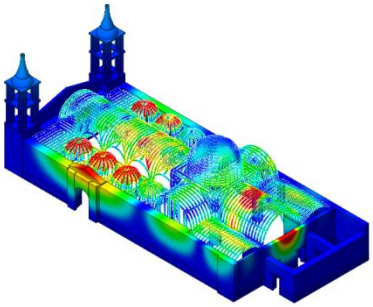

Mode 106 (4.17 Hz)

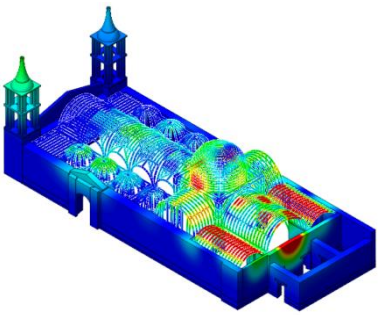

Mode 108 (4.17 Hz)

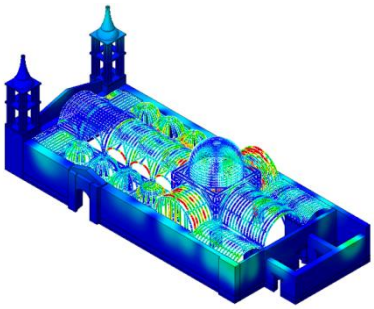

Mode 461 (8.60 Hz)

Figure 3. Selected mode shapes of the combined structures of Ica Cathedral.

1.3.2 Nonlinear analysis under self–weight

A nonlinear analysis is performed under self-weight applied in ten steps.

The deformed shape and distribution of vertical displacements in the combined model of the masonry and timber structure can be observed in **Figure 4**. It can be observed that the higher values of vertical displacement occur throughout the timber structure. In particular, the maximum vertical displacement is calculated in the upper part of the barrel vault covering the altar with a value of 2.0 cm, approximately. Significant values of displacement can also be observed in the transept including the main dome and the barrel vaults with lunettes. It should be noted that negligible change is observed in the vertical displacements occurring in the timber structure with and without the presence of the masonry envelope.

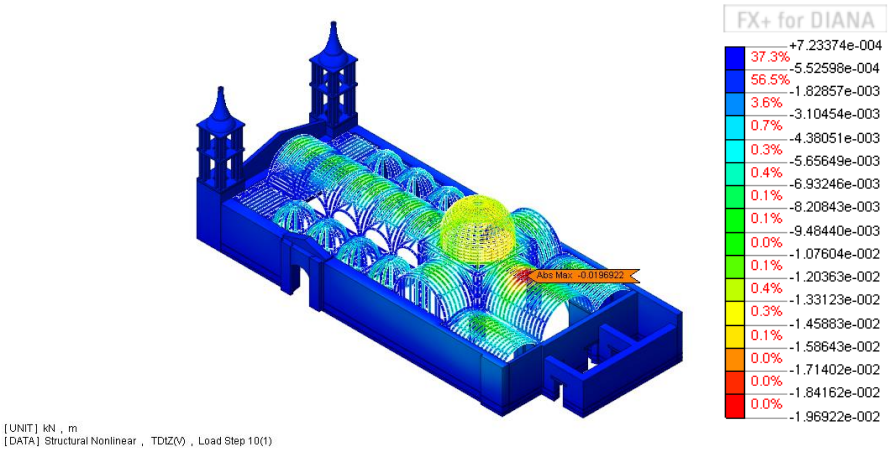

Figure 4. Distribution of vertical displacements and the location of maximum vertical displacement.

As shown in **Figure 5**, the distribution of the maximum principal stresses is studied in the masonry envelope in presence of the timber structure – the latter is hidden in **Figure 5** to simplify the reading of the results. It is observed that the highest value of tensile stresses occur near the openings and at the location of the connections between the timber structure with the masonry envelope.

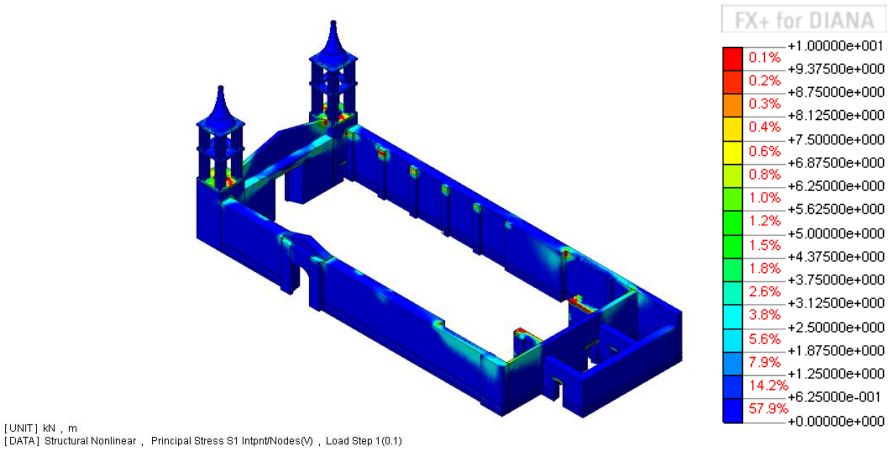

Figure 5. Distribution of the maximum principal stresses in the combined model.

Similarly, the distribution of the minimum principal stresses is investigated throughout the masonry envelope in presence of the timber structure (**Figure 6**). It should be noticed that the highest value of compressive stresses occur at the base of the walls, as expected. Local concentrations of high values of compressive stresses are observed in the regions of the masonry envelope on which the timber structure rests upon, i.e. the barrel vaults covering the altar and the chapels.

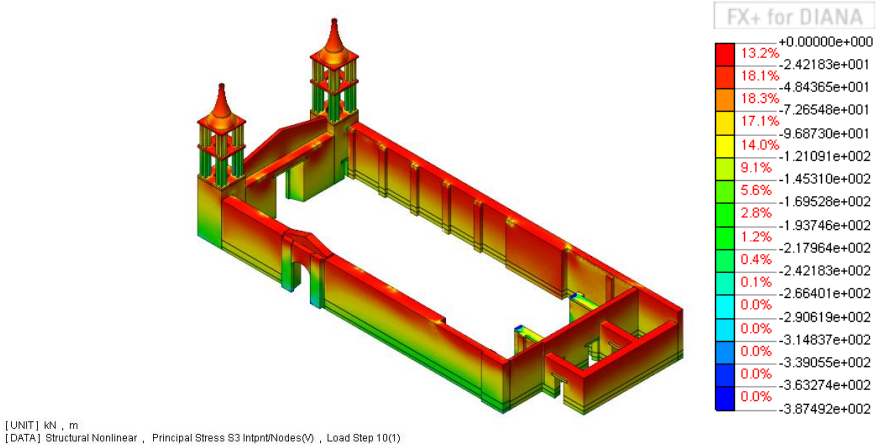

Figure 6. Distribution of minimum principal stresses in the combined model

1.3.3 Mass proportional lateral loading

In order to assess the seismic capacity of the structure, two mass proportional lateral loading analyses are performed. The lateral loads in these two analyses are applied in the XX- and YY-directions of the numerical model as the failure mechanisms of the masonry envelope identified in these two directions are the most interesting in (Sharma, 2015). The following section presents the

results of these analyses in terms of lateral load capacity and capacity curves, failure mechanism in the masonry and co–relation with cracks observed in-situ. The failure mechanism in the timber structure is not possible to be studied as timber is assumed to be a linear elastic and isotropic material. Comparison in terms of elastic stiffness is carried out with the results obtained from the timber structure and masonry envelope studied individually in (Ciocci, 2015)and in (Sharma, 2015). The load capacity of the combined model is also compared with respect to the load capacity of only the masonry envelope.

It should be mentioned that a number of problems are encountered in order to converge at a numerical solution to the combined model under mass proportional lateral loading analyses. For instance, a sudden change occurs in the value of stiffness matrices while applying lateral loading after vertical loading. These problems are resolved by trying out various iterative solution procedures and other techniques to improve convergence in nonlinear structural analysis provided by DIANA software (TNO DIANA, 2014).

XX- (longitudinal) direction

The maximum lateral load that can be applied to the numerical model of the combined timber and masonry structures in the XX- direction is 0.45g. The deformed mesh of the model when this load is applied is presented in **Figure 7**.

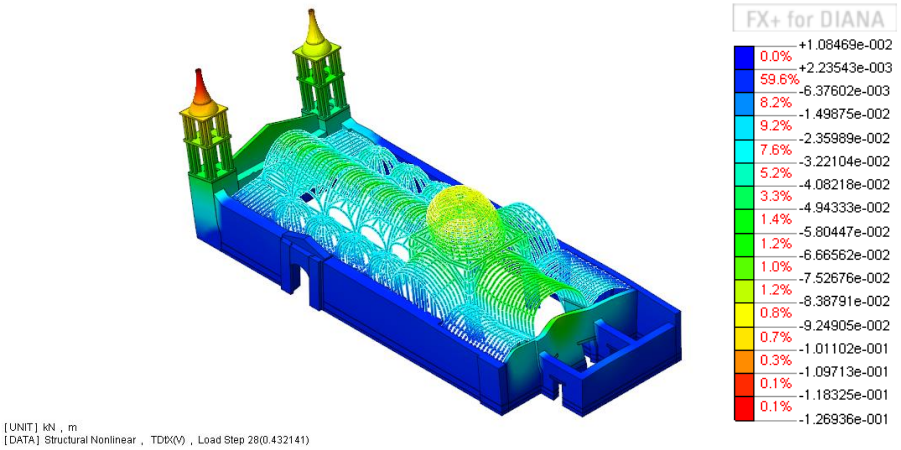

Figure 7. Deformed mesh of the numerical model under applied loading in XX– direction.

It can be observed that high values of displacements are recorded in the façade, in the adjoining bell towers and in the main dome. Also the transversal wall of the altar and chapels undergo large deformation. The failure mechanism in the masonry under this loading is identified as the out of

plane failure of the facade and the bell towers. This is studied in terms of high values of incremental displacements recorded at that part of the structure. The failure mechanism develops as tensile damages between the base of the bell towers and the adjoining longitudinal walls. It is to be noted that in the northern bell tower these damages progress from the connection between the two structural elements through the base of the bell tower. On the other hand, cracks leading to the failure of the southern bell tower progress from the connection between the bell tower and the wall to the adobe masonry of the longitudinal wall. Flexural damages also develop at the base of the facade. More damages can also be seen in the connection of the choir loft to the facade. Additionally, local failures can also be observed in the connection of the transversal walls of the altar with other adjoining walls (**Figure 8**)

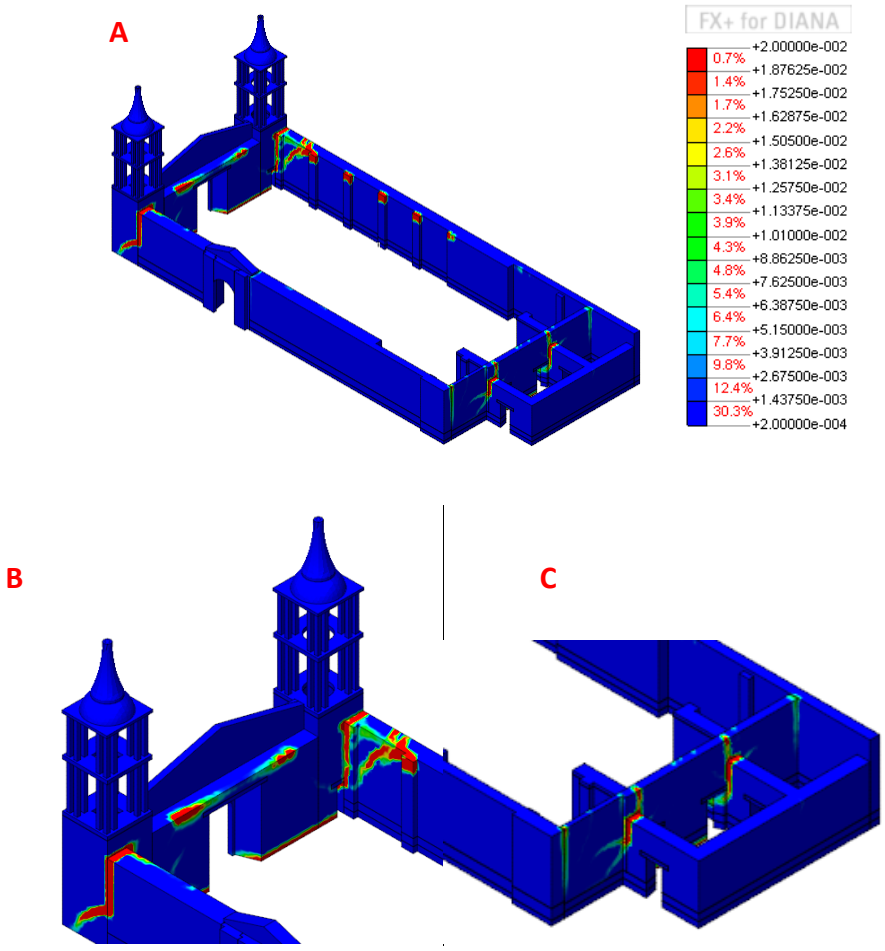

Figure 8. Crack pattern depicting the failure mechanism: A) global crack pattern and the close up view of the tensile strains in B) the connection between the bell towers and facade and C) in the proximity of the altar (XX– direction).

As the structure enters the post-peak part of the capacity curve, the façade and the bell towers behave independently from the rest of the structure. This is verified by high values of incremental

displacements observed in that part of the numerical model. Additionally, tensile strains and correspondingly damages progress extensively in the region. This is also confirmed by the high concentration of tensile strains observed in the region of the connection between the choir loft and the façade (**Figure 9**). The concentration of tensile strains in this region is very interesting as the separation of the pediment from the facade was also observed in-situ (Cancino, et al., 2012).

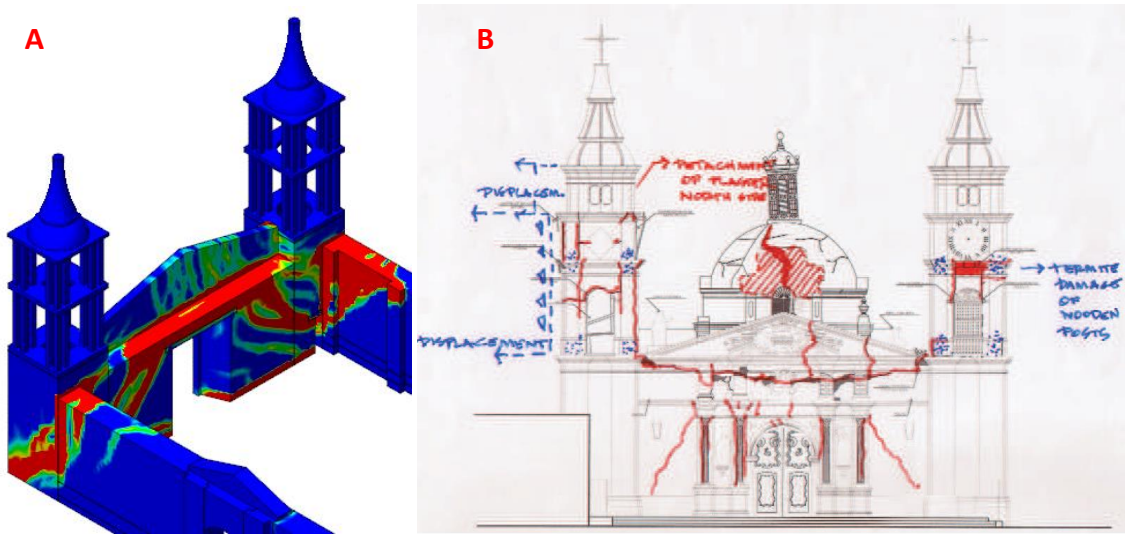

Figure 9. Cracking occurring in correspondence to the connection between the pediment and the facade observed in A) the numerical model and B) in-situ (Cancino, et al., 2012).

The capacity of the numerical model of the combined timber and masonry structures is presented in terms of a load displacement diagram in **Figure 10**. In particular, the curves MTS and MS refer to the numerical model of the combined structure and of the masonry envelope, respectively. The other legends refer to various structural parts of the model of the complete timber structure TS: in particular MD, BV, AD2 and TR refer to one node of the main dome, of the barrel vault with lunette close to the transept, of the small dome close to the cloister covering the bay adjacent to the façade and of the transept. More details can be found in (Ciocci, 2015).

Load displacement diagrams of only the masonry envelope and various components of the timber structure are also plotted along with it. It can be observed that the combined structure presents an increase in lateral load capacity to 0.45g in this direction compared to 0.36g observed when only the masonry envelope is considered. No appreciable difference can be observed in the stiffness presented by the masonry envelope and the combined structure under this direction of loading. It is also interesting to note the relationship between the stiffness of the various wooden structural components and that of the combined model. It should be noted that the stiffness value obtained for

TS_AD2 – i.e. for one node of the small dome close to the cloister covering the bay adjacent to the façade – is the most similar to that obtained from the combined model.

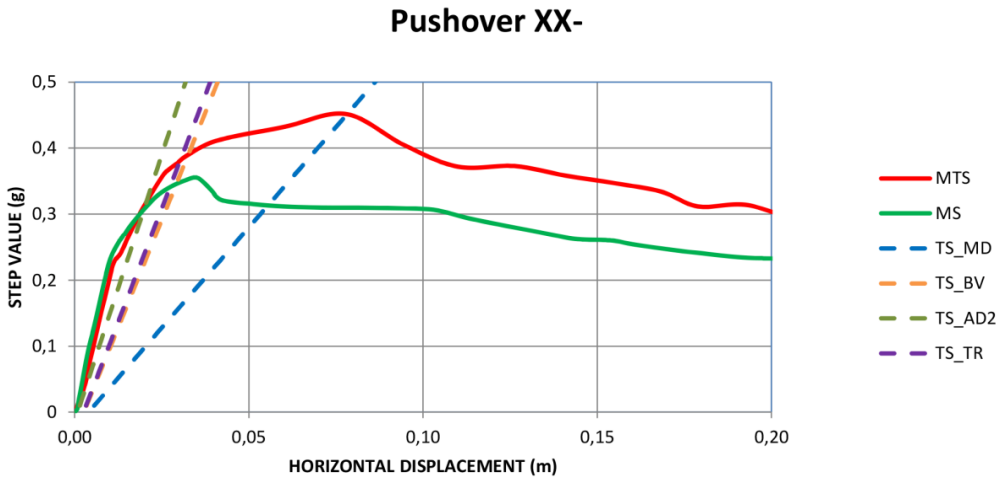

Figure 10. Comparison of the load displacement diagrams of the numerical models of the combined masonry and timber structures, the masonry envelope and various parts of the complete timber structure (XX– direction).

YY- (transversal) direction

The maximum lateral load that can be applied to the numerical model of the combined masonry and timber structure in the YY- direction is 0.28g. The deformed mesh of the model when this load is applied is presented in **Figure 11**.

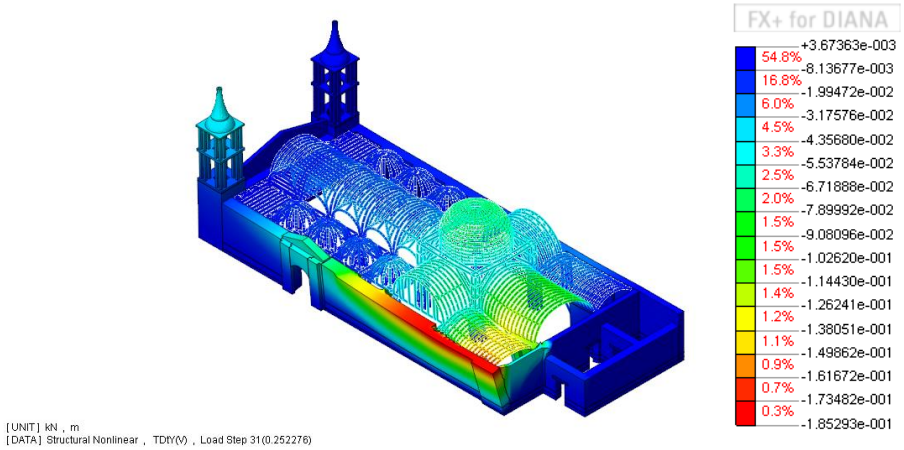

Figure 11. Deformed mesh of the numerical model under applied loading in YY– direction.

It can be observed that high values of displacements are recorded in the longitudinal wall adjacent to the street, in the transept and in the barrel vaults covering the altar and the chapel on the side of the

street. The failure mechanism in the masonry under this loading is identified as the out of plane failure of this entire longitudinal wall. This failure mode also includes out of plane failure and separation of the northern bell tower from the brick facade and a portion of the transversal wall of the altar. Flexural cracks also occur throughout the length of the longitudinal wall: while these cracks are present at the rubble stone base in correspondence to the north–western corner of the cathedral, they are observed at the interface between adobe masonry and the fired brick base course in the part close to the northern bell tower. As previously analysed, the failure mode is studied in terms of high values of principal tensile strains and correspondingly cracking occurring in these regions (**Figure 12**).

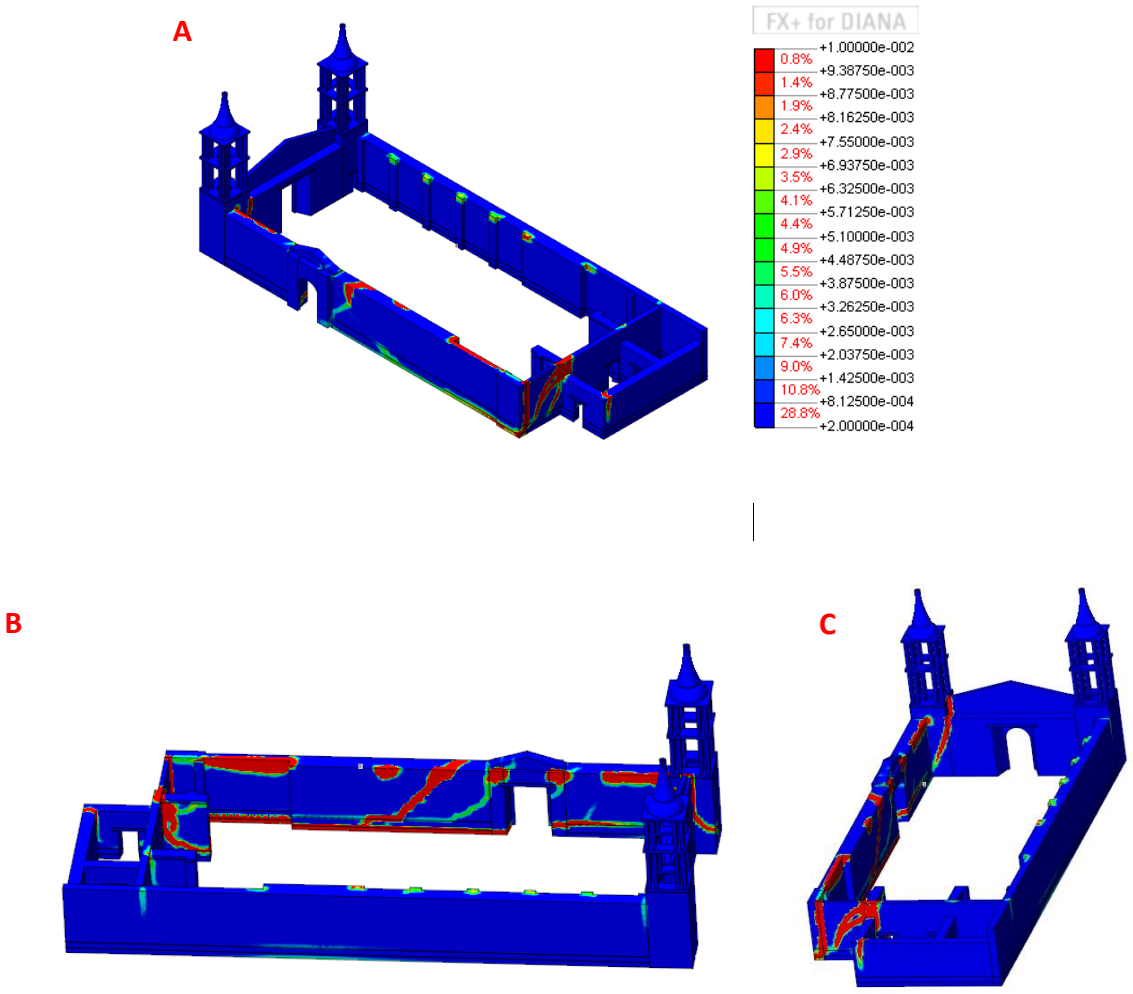

Figure 12. Crack pattern depicting the failure mechanism: A) global crack pattern and close up view of the tensile strains in B) inner face of longitudinal wall and C) in the proximity of the northern bell tower.

As the structure enters the post-peak part of the capacity curve, this longitudinal wall and the northern bell tower behave independently from the rest of the structure. This is verified by high values of incremental displacements observed in that part of the numerical model. Also tensile strains and correspondingly damages progress extensively in damaged regions.

The capacity of the combined numerical model of masonry and timber structures is presented in terms of the load displacement diagram in **Figure 13**. It can be observed that in this direction the numerical model of the combined structures presents an increase in the lateral load capacity to 0.28g from 0.22g obtained considering only the masonry envelope. Unlike the XX- direction, an appreciable decrease can be observed in the stiffness presented by the combined masonry and timber structure with respect to the timber and the masonry structures considered independently. In this case, it should be noted that the stiffness value obtained for TS_TR – i.e. for one node of the upper part of the main dome – is the most similar to that obtained from the combined model.

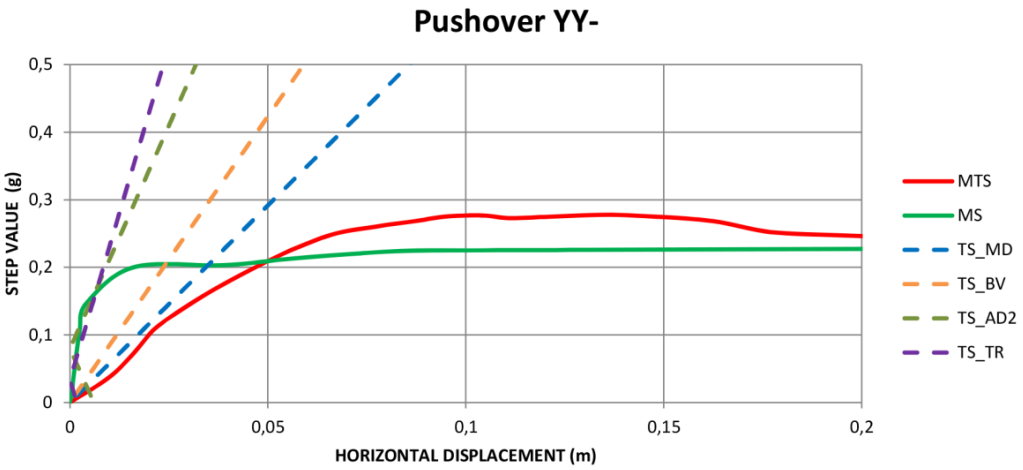

Figure 13. Comparison of the load displacement diagrams of the numerical models of the combined masonry and timber structures, the masonry envelope and various parts of the complete timber structure (YY– direction).

1.3.4 Nonlinear dynamic loading with time integration

The finite element model of the combined timber and masonry structures is also subjected to nonlinear dynamic loading with time integration. A similar analysis is carried out by Sharma (2015) on the masonry envelope and the parameters in terms of loading, damping of the system, time integration method used in this analysis are maintained to be the same. It is also to be noted that unlike the other nonlinear analyses mentioned in this section, the material properties of masonry

used in this analysis correspond to the values input to the numerical model before calibration with respect to ambient vibration tests was carried out. This facilitates in comparing the dynamic response of Ica Cathedral with and without the presence of the complex timber structure and with the same mechanical characterization of the masonry as in (Sharma, 2015).

Concerning the loading, the same artificially generated uncorrelated accelereograms used by Sharma (2015) are applied on the numerical model of the combined timber and masonry structures in the form of base excitation in two orthogonal directions. These accelerations correspond to a maximum peak ground acceleration of 0.4g (**Figure 14**).

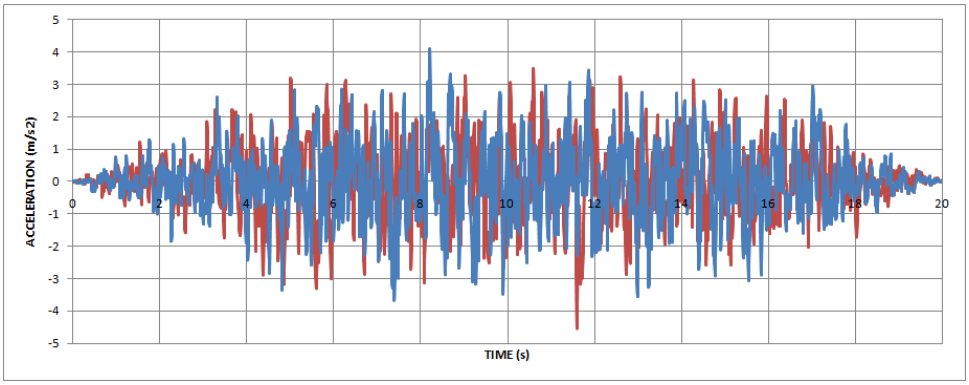

Figure 14. Acceleration – Time Histories applied on the numerical model of the combined structures.

Rayleigh viscous damping is also considered for the combined structure. The Rayleigh damping parameters for the combined structure are calculated as α = 0.389297260 and β = 0.0007876488. They are calculated considering the natural modes of this numerical model between which there is 80% cumulative mass participation of the structure.

The time-integration method used is the Hilber-Hughes-Taylor method or the HHT method. In particular, Δt adopted for this analysis is calculated as 0.0045s, corresponding to the highest time period of the natural mode of vibration considered.

The values of relative out of plane displacements along vertical alignments is studied in various regions of the structure. The north–western corner of the masonry envelope is identified as a very vulnerable region. In order to compare the out of plane movements with respect to the masonry envelope considered individually, the same results are collected for a vertical alignment in the same region of the model of the combined timber and masonry structures. As shown in **Figure 15**, the maximum out of plane displacement shown by the highest considered node along the vertical

alignment during the entire time history of loading is near 0.20 m while the same node shows a displacement of 0.14 m in (Sharma, 2015). Both of these are certainly unacceptable from a structural perspective and seem to indicate collapse.

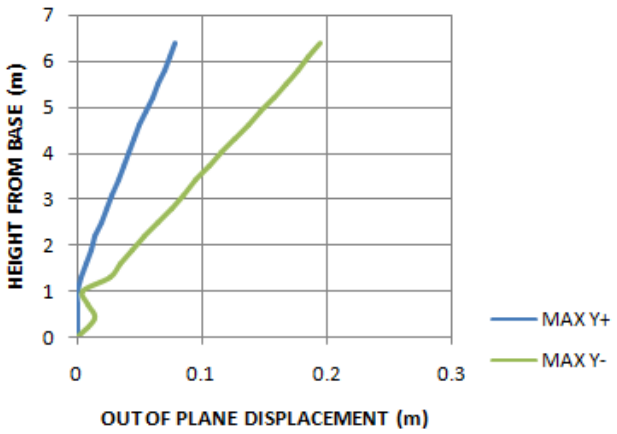

Figure 15. Relative out of plane displacements in elevation for a selected region of the structure.

The loading-unloading diagram plotted for the masonry of the combined model in the two orthogonal directions in which the accelerograms are applied are presented in **Figure 16**. These diagrams indicate that masonry loses its loading–unloading capacity entirely. This corresponds to severe damage to the structure under the applied dynamic loading.

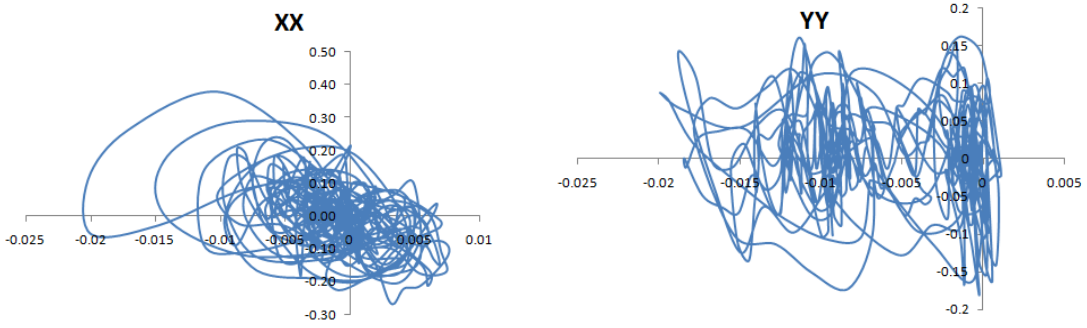

Figure 16. Load Factor – Horizontal displacement (m).

Critical cracks occurring in the structure are more well defined in the numerical model of the timber and masonry structure when subjected to nonlinear dynamic loading as compared to when only the numerical model of the masonry envelope is subjected to the same. This is illustrated in **Figure 17**.

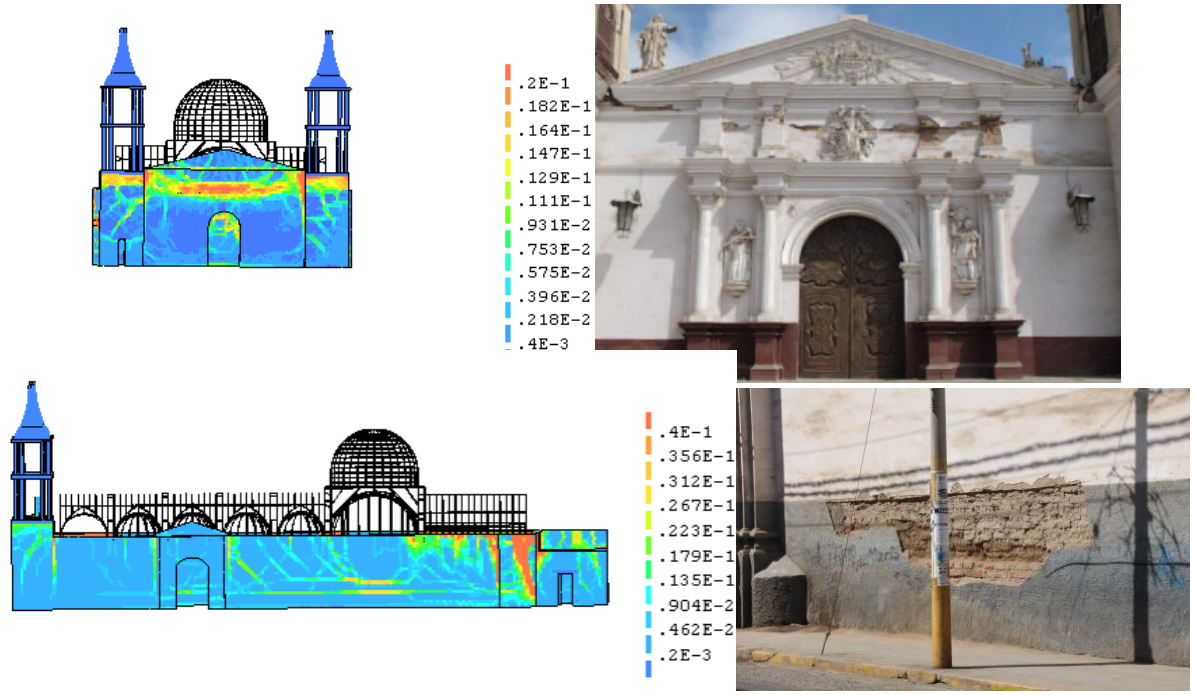

Figure 17. Crack correlation from time–history analysis.

1.4 Conclusion

On the basis of the results obtained from Ciocci (2015) and Sharma (2015), the numerical model of the combined timber and masonry structures was constructed. Linear and nonlinear analyses were performed in order to better understand the interaction of the two structural systems and how the global behaviour of Ica Cathedral is influenced by this interaction. The integration of the two structures in the combined model pointed out clearer co–relation between numerical and experimental dynamic response of the structures. Moreover, an increase in seismic capacity of about 25% was observed in both orthogonal directions considered with respect to only the masonry envelope.

Due to the limitation of time and significant computational effort involved in running each analysis on this numerical model, several areas that need to be addressed by further research have been identified. These include the following:

- The timber joints were assumed to be rigid in the numerical model of the combined structures, hence the less conservative model was considered. This was due to the

non-complete geometrical information and mechanical characterization of the most critical joints of the timber structure that did not allow to consider the semi–rigid behaviour of the timber connections (Ciocci, 2015). However, it should be mentioned that even with these information the introduction of the nonlinear behaviour for each timber connection could have been difficult to carry out in the complete timber structure considering their large number throughout the model. A simplified approach can be used considering reduction factors to decrease the linear elastic stiffness. In particular, this reduction factor can be assumed in accordance with the recommendations provided by *Eurocode* or resulting from numerical simulations of local parts of Ica Cathedral. Running structural analyses considering these reduction factors would be essential in understanding the upper and lower bound of the of the combined structure in terms of seismic capacity and elastic stiffness.

- A simple process of model updating has been performed in (Sharma, 2015) where the MOE of various materials in the model was updated such that the modal shapes and frequencies obtained numerically match the ones obtained experimentally. This was done using an optimised iterative procedure. It seems sensible to carry out the updating process on this model as both during the ambient vibration tests as well as during the post processing of the data from such tests, the timber structure was assumed to be present (even though in a much simpler form in the latter). Additionally, further dynamic identification tests with the location of more sensors on the timber structure would be even more accurate in this regard. Mass proportional lateral loading analyses carried out on the masonry envelope showed a 10-20% percent increase in the seismic capacity in each direction between the calibrated and un-calibrated models. It would be very interesting to observe the change in seismic capacity of the combined structure after the same process is carried out for this model.
- The damage in the beam elements representing the timber structure can also be studied in terms of principal tensile strains. However, the number of integration points in the cross section of the beam elements (2x2) present by default is not enough to capture their nonlinear behaviour. This needs to be increased in order to capture the damage pattern. Each integration point in elevation corresponds to a

surface while the top and bottom surfaces of the beam elements are defined by the local axes.

- It is certain that the timber structure is rather complex and the connections between the two structures play a relevant role in the response. Thus there is a need for calibrating and fine tuning the connection adopted in the numerical model between the two structures. Further research into the characterisation of this connection is thus of the utmost interest and importance.

References

Cancino, C., Lardinois, S., D'Ayala, D. & Ferreira, C. F., 2012. *Seismic Retrofitting Project : Assessment of Prototype Buildings,* Los Angeles: The Getty Conservation Institute.

Ciocci, M. P., 2015. *Structural Analysis of the Timber Structure of Ica Cathedral, Peru,* Guimaraes, Portugal: SAHC Masters Thesis.

Greco, F., Karanikoloudis, G., Lourenço, P. B. & Mendes, N., 2015. *Experimental in situ testing campaign on adobe historic structures in Peru, within the Getty SRP,* Guimarães: The Getty Conservation Institute.

Sharma, S., 2015. *Structural Analysis of the Masonry Envelope of Ica Cathedral, Peru,* Guimaraes, Portugal: SAHC Masters Thesis.

TNO DIANA, 2014. [Online] Available at: http://tnodiana.com/DIANA-manuals